TEMPERATURE AND RISE TIME EFFECTS ON DYNAMIC STRAIN MEASUREMENT WITH RESISTANCE STRAIN GAGES

Dissertation for the Degree of Ph. D.
MICHIGAN STATE UNIVERSITY
WILLIAM JAMES BAGARIA
1973

This is to certify that the

thesis entitled

TEMPERATURE AND RISE TIME EFFECTS
ON DYNAMIC STRAIN MEASUREMENT
WITH RESISTANCE STRAIN GAGES

presented by

William James Bagaria

has been accepted towards fulfillment
of the requirements for

Ph.D. degree in Mechanics

William N Sharpe Jr
Major professor

Date Aug 2, 1973

O-7639

ABSTRACT

TEMPERATURE AND RISE TIME EFFECTS
ON DYNAMIC STRAIN MEASUREMENT
WITH RESISTANCE STRAIN GAGES

by

William James Bagaria

Strain pulses in a test specimen were measured over a temperature range -100 to +300°F with foil and semi-conductor resistance strain gages. These tests were performed to determine if the gage-output rise time and amplitude change as a function of temperature. The existence of a constant that should be added to the theoretical rise times of resistance strain gages, as suggested by Koshiro Oi, was re-examined.

The foil gages were type ED-DY-031CF-350, manufactured by Micro-Measurements. The semi-conductor gages were type SPB3-06-12, manufactured by BLH Electronics, Inc. All gages were bonded to the test specimen with a large-temperature-range epoxy adhesive.

The test specimen was made from Ni-Span-C, Alloy 920® manufactured by The International Nickel Company, Inc. This alloy exhibited a constant long wave velocity over the temperature range -100 to +300°F. This characteristic was necessary in order to eliminate temperature

effects in the dispersion of the strain pulse.

"Long" rise time strain pulses were produced in the test specimen by a falling steel ball which impacted the end of the specimen. The rise times of these strain pulses were on the order of 7 μsec. and the strain amplitudes were approximately 65 μin/in. A new type of apparatus was designed and constructed that would generate "short" rise time strain pulses. The strain pulses were produced by impacting the end of the test specimen with a short pendulum-type hammer. The rise times were on the order of 0.13 to 2 μsec. The strain amplitudes were approximately 500 μin/in.

The results of the 7-μsec. rise-time tests showed that the rise time and amplitude of the gage output do not change appreciably as a function of temperature.

The results of the 2-μsec. rise-time tests showed that the amplitude of the gage output was relatively independent of the test temperature but did exhibit a hysteresis effect. The rise times remained constant up to a temperature of 200°F, then started to increase. The rise times at 300°F were approximately 100 per cent larger than at room temperature.

The results of the sub-microsecond rise time tests indicated that the theoretical rise time additive constant is 0.05 μsec. or less. This is one-half the value that Bickle arrived at by re-evaluating Oi's data. An analytical study was conducted on the sub-microsecond results using Taylor's theoretical work. From this analysis it was hypothesized that the output rise times of resistance strain gages do not require an additive constant.

TEMPERATURE AND RISE TIME EFFECTS ON DYNAMIC STRAIN MEASUREMENT WITH RESISTANCE STRAIN GAGES

by

William James Bagaria

A DISSERTATION

Submitted to
Michigan State University
in partial fulfillment of the requirements
for the degree of

DOCTOR OF PHILOSOPHY

Department of Metallurgy, Mechanics and Materials Science

1973

ACKNOWLEDGEMENTS

I wish to acknowledge the assistance given to me by Dr. William Sharpe, Jr. It was he, as my major advisor, who suggested the research problem and helped me in the data acquisition. Thanks are due to the rest of my guidance committee, Dr. D. J. Montgomery, Dr. D. H. Y. Yen and Dr. J. S. Frame.

My wife deserves special thanks for her continual encouragement and support; and my children, who had to share their father with his research.

TABLE OF CONTENTS

LIST OF TABLES

LIST OF FIGURES

LIST OF SYMBOLS

a	radius of bar
C_c	coupling capacitor
C_1	input capacitor
C_2	damping capacitor
C_2'	semi-conductor quadratic gage factor
c_g	sinusoidal wave group velocity
c_o	longitudinal long wave velocity
c_p	sinusoidal wave phase velocity
c_{pn}	phase velocity of n^{th} component in Fourier series
d	clearance between races of hammer bearings
E	modulus of elasticity
E_b	DC supply voltage
E_g	voltage across strain gage
E_o	output voltage
E_r	specimen reference density at temperature T_r
E_θ	voltage proportional to hammer angular position
E_ω	voltage proportional to hammer angular velocity
f_c	cut-off frequency
G_t	oscilloscope horizontal-amplifier gain (seconds/division)
G_ε	oscilloscope vertical-amplifier gain (volts/division)
GF	room temperature gage factor for foil strain gages
GF'	semi-conductor linear gage factor

GF_T test temperature gage factor for foil strain gages

I circuit current

K constant that relates ω to E_ω

L active gage length, length between hammer bearings

m mass of test specimen

R_b ballast resistor

R_f feed-back resistor

R_g strain gage resistance

R_o unbonded semi-conductor gage resistance measured at temperature T_o

R_{oo} unbonded semi-conductor gage resistance at 0°F

R_{oT} unbonded semi-conductor gage resistance at test temperature

T test temperature

T_o temperature at which R_o was measured

T_r reference temperature of ρ_r and E_r

t time

t_R rise time

u partical displacement in x direction of bar

V_r specimen reference volume at temperature T_r

V_2 thermal coefficient of resistance, linear term

V_3 thermal coefficient of resistance, quadratic term

x coordinate along longitudinal axis of bar

α linear coefficient of thermal expansion

β volume coefficient of thermal expansion

γ hammer shaft misalignment angle

Δ_ε strain-amplitude oscilloscope-trace deflection (divisions)

ΔR_B change in semi-conductor gage resistance due to bonding and thermal expansion

ΔR_g change in strain gage resistance

ΔR_t change in semi-conductor gage resistance due to bonding, thermal expansion and load

Δ_t strain-rise-time oscilloscope-trace deflections (divisions)

ε strain amplitude

ε_B bonding and thermal expansion strain

ε_t semi-conductor-gage strain due to bonding, thermal expansion and load

θ hammer angular position

Λ sinusoidal wave-length

ν Poisson's ratio

ρ bar/specimen density

ρ_r specimen reference density at temperature T_r

σ standard deviation

Ψ slope of the modulus of elasticity vs. temeprature curve

ω hammer angular velocity

ω_o frequency of fundamental Fourier component

CHAPTER 1

INTRODUCTION

1.1 General Comments and Purpose

Resistance strain gages are strain transducers consisting of a resistance element cemented to a backing material. The two most common types of resistance elements are made from metallic foils and from semi-conductors. These gages are commercially available in many shapes and sizes. The associated strain-gage instrumentation is well developed and readily available. The gages are easily bonded onto most specimens that are to be tested. The above features have led to the increasing application of resistance strain gages.

As the use of resistance strain gages becomes more wide-spread, the types of strain (static and dynamic) and the conditions under which they are measured are becoming more varied. Hence it is appropriate that research is conducted in the dynamic response of strain gages at room temperature. Before a gage can be used to measure dynamic strain, its dynamic response must be determined. The dynamic response of a gage is determined ideally by subjecting the gage to a step-function strain wave. Two parameters then define the dynamic response, the rise time and amplitude of the output signal. The rise time is the time it takes the output signal amplitude to rise from 10 to 90 per cent of its steady-state or first peak value. The greatest single factor that has been hindering

this research has been the generation of a strain pulse that approaches an ideal step-function.

Extensive research has been conducted on the application of strain gages for the measurement of static strain at various temperatures. It has been determined that there are two basic effects produced on a gage by a temperature change. First, the gage resistance and sensitivity (gage factor) will change. This is due to the non-zero coefficient of thermal resistivity of the gage element. Second, the gage will experience a strain due to thermal expansion. This "apparent" strain arises from different coefficients of thermal expansion for the gage element and the test specimen material. The dependence of gage sensitivity and apparent strain on temperature is supplied by the gage manufacture. The measured strain amplitude can thus be analytically corrected for temperature effects. The apparent strain can also be corrected for by appropriate instrumentation. Since these two temperature effects on gage output are independent of the type of strain being measured (static or dynamic), the same correction made for temperature effects under static strain conditions should be made under dynamic strain conditions.

One area that is becoming increasingly important is the measuring of dynamic strain at different test specimen temperatures. However, the effects of extreme environmental temperatures on the output of resistance strain gages when employed for the measurement of dynamic strain have not been investigated. When strain gages are to be used to measure dynamic strains at various specimen temperatures, two important parameters must be known: the rise time of the gage, and the effect of temperature on the gage output. Two additional problems arise which were not present when conducting dynamic tests at room temperature. First, the various test temperatures must not produce changes in the strain-generating

apparatus. If any changes occurred it would be difficult to separate the effects produced by changes in the test apparatus from those produced by any changes in the gage. Second, a test-specimen material must be chosen so that the material properties that affect a propagating wave do not change with temperature.

The purpose of this experiment was to determine the temperature effects on the rise time and output amplitude of foil and semi-conductor resistance strain gages. In order to accomplish this purpose the strain gages were mounted on a test specimen such that they could be subjected to a propagating strain wave. It was necessary that the strain-wave rise time be short and that the strain-wave shape be reproducible over the test-temperature range. It was not necessary that the wave have a specific shape. The wave fronts had rise times on the order of 1 to 2 microseconds. The tests were carried out at environmental temperatures ranging from -100 to +300°F.

1.2 Previous Studies of Strain Gage Dynamic Response

The first studies on the dynamic response of the resistance strain gage were conducted by De Forest (1939).* The resistance strain gages that he used had just been developed by the Hamilton Standard Propellor Company and the Massachusetts Institute of Technology. These gages consisted of a resistance strip, made from bakelite resin impregnated with graphite, sandwiched between layers of pure insulating bakelite. The gage length was one inch, the width was 0.25 inch, and the thickness was 0.015 inch. The amplifiers and oscillographs required to record the

---

* Surnames followed by dates in parenthesis refer to Bibliography.

resistance strain gage signal had been developed the previous year.

De Forest conducted tests on impacting bars. He compared his experimental results with the theoretical results computed by Sears (1908). From this investigation he concluded that "progress is being made in the measurement of stresses which are propagated at the speed of sound, and that impact strains need no longer remain in the realm of conjecture."

The magnetostrictive effects of wire strain gages were studied by Vigness (1956). This effect is the "self-generation" of a voltage by a ferromagnetic material. The magnetic domains in a ferromagnetic material can be aligned by repeated mechanical impact while the material is carrying a "large" electrical current. Once the domains are aligned, the material can self-generate a voltage when subjected to mechanical impact in the absense of an external voltage. Vigness "conditioned" strain gages made of various types of materials by subjecting them to different amplitude strain-pulses while they were carrying electrical currents of approximately 0.15 amp. This caused a preferential alignment of the gage material magnetic domains. When the gages without a supply current were subsequently subjected to dynamic strains they would generate a voltage. He found that gages made from strongly magnetostrictive materials, such as nickel, will self-generate voltages on the order of "several" millivolts. For materials such as isoelastic, which are "weakly" magnetostrictive, the self-generated voltages may be as large as one millivolt. Since typical outputs from strain-measuring systems range from 0.1 to 1000 millivolts, the above source of error can be appreciable for small-amplitude strain measurements.

A theoretical investigation was conducted by Taylor (1966) in order to study the effects that gage length has on measurement of strain-wave

rise-time and amplitude. His basic premise was that the output of a finite length strain gage will be the average value of the strain that is within the length of the gage. Then he computed the rise time and amplitude errors as a function of the length of the strain-pulse leading edge and the strain-gage length. From this he derived "application design charts" for use with resistance strain gages. With these charts, the rise time and amplitude outputs of the gage could be corrected. There are two limitations to the use of these charts. First, the experimental strain-pulses must be of a similar shape as compared to the theoretical ones upon which the charts are based. Second, since his approach was theoretical, he neglected effects such as instrumentation circuit capacitance and inductance, skin conduction, magnetostriction, gage backing and cement properties.

Oi (1966) devised a method by which an elastic step wave, that had a calculated rise time of 1.4 microseconds, could be produced in a test specimen. These step strain waves had rise times that were several times shorter than those used by previous investigators. For example, Cunningham and Goldsmith (1959) had reduced the rise time of strain waves to 7 microseconds and 10 microseconds in steel and aluminum bars respectively. Oi conducted tests on polyester-backed wire gages that had theoretical rise times of 0.16 and 0.48 microsecond. Linearly extrapolating his data and using the most conservative results, he determined that a gage has a rise time of less than

$$0.2\ \mu\text{sec} + 0.8\ L/c_o \quad ,$$

where L is the active gage length, and c_o is the long wave velocity of the test specimen material. The constant 0.8 arises from the definition of rise time. Oi felt it was "dangerous" to use the 0.2 microsecond value which was obtained by extrapolation of his data. His "moderate conclusion" was to estimate the rise time of a resistance strain gage as less than

$$0.5\ \mu\text{sec} + 0.8\ L/c_o \quad .$$

Dispersion, induced by Poisson's effect, will alter the rise time and amplitude of a propagating step wave and thus must be considered when using Oi's results. The rise time of the strain-wave in Oi's experiment was determined by a theoretical calculation based on crack-propagation theory. Then he compared the measured with the theoretical results. While he "supposed" that the amplitude differences of the experimental results compared to the theoretical were partially due to the dispersion, he apparently considered that the rise times were not affected. Because of dispersion, it seems likely that the strain-wave initially had a shorter rise time than the theoretical one. Subsequently, dispersion probably increased the rise time of the strain-wave by the time it reached the gage location. Consideration of dispersion effects would then seem to indicate that the original 0.2 additive constant arrived at by Oi might be conservative.

Oi's work was re-evaluated by Bickle (1970). He first considered the 0.5 microsecond additive constant. Bickle felt that a 0.3 microsecond "safety factor" should not have been added to the rise time, since 0.2 microsecond "represents actual experimental results." He examined the effect of Oi's instrumentation system on the measured rise time. Bickle

concluded that the rise time of a strain gage is less than:

$$0.1\ \mu\text{sec} + 0.8\ L/c_o \quad .$$

Next, Bickle considered the $0.8\ L/c_o$ term. By making a coordinate-system transformation, he derived a closed-form analytical expression which yielded the input to the resistance strain gage based on the output. The use of this analytical method for resistance strain gage data reduction eliminates the $0.8\ L/c_o$ term from the rise time expression. Bickle, then conducted an experiment which verified his analytical results.

1.3 An Investigation of Strain-Wave Generation Methods

1.3.1 Piezoelectric

Piezoelectric materials have been used to generate sinusoidal stress (strain) waves in various substances. For example, they have been used to generate sonar waves in water and resonate standing waves in the "horns" of ultrasonic welders and drills.

Stuetzer (1967) analyzed the transient behavior of thin piezoelectric elements. One of the many configurations and applications that he described was the use of a thin piezoelectric element as a mechanical pulse generator. The operating principle was as follows. A thin piezoelectric element was bonded between the ends of two "long" cylinders. A transient electrical voltage was applied across the faces of the piezoelectric element. When the voltage was applied by means of an "open-circuit operation," a stress wave traveled into each of the cylinders. The waves were identical rectangular stress pulses traveling in opposite directions.

This method of producing stress pulses appeared very attractive.

The pulses would be easily initiated by the application of a voltage across the piezoelectric element. The resulting stress pulse would have a step front. In studying this method two limitations were found. First, there was a maximum voltage that could be applied to the piezoelectric materials. This voltage limited the amplitude of the stress pulse to small values. Second, there were very few materials that exhibited piezoelectric properties over the temperature range selected for this testing. It was theoretically determined by this author that the generated pulse would have a maximum amplitude of approximately 9×10^{-9} in/in. This amplitude was too small to be measured by existing strain gage systems.

Mechanical amplification of the stress pulse as suggested by Rader and Mao (1972), could raise this amplitude to an acceptable level. With this technique a stress pulse was amplified as it traversed a tapered bar. However, the rise time of the pulse would rapidly increase due to dispersion effects, before the amplitude would be sufficient to measure with resistance strain gages. It was decided that this method would not be applicable to this testing.

1.3.2 Gas Pressure

Commerford and Whittier (1970) generated propagating waves by the use of a gas dynamic shock wave. The experiments were performed at the low-density shock-tube facility at The Aerospace Corporation. The working fluid was air and the driver gas was high-pressure helium. The shock tube had a driven section diameter of 17 inches. The shock wave traveled down the shock tube and impinged on the test sample. The desired strain pulse was thus produced in the sample. The shock wave parameters were approximately as follows: a rise time of 13 nanoseconds, an amplitude of 70 psi,

and a Mach number of 3.4. The shock wave produced strain pulses in the test sample that had rise times between 29 nanoseconds and 1 microsecond, depending on the sample material.

There were many advantages to this technique as a strain pulse generator: nanosecond rise times, amplitudes independent of sample material, uniform loading over the sample face, less critical sample alignment and flatness. The major limitation to this test system was lack of financing for the construction of such a facility.

Daniel and Marino (1971) produced stress waves in plastic models by the use of an explosive. They detonated a 50 mg charge of pentaerythritol tetranitrate (PETN) on a test model. The PETN explosive was held in a plexiglas cap and detonated by means of gold exploding-bridge-wire. A typical stress pulse produced by PETN had a rise time of less than one microsecond and mean width of 6 microseconds. Investigation of this technique revealed two major limitations. First, the commercial size of PETN was too coarse for ease of use in 50 mg quantities and had to be reduced. Second, a small variation in the weight of the charge and the use of the exploding-bridge-wire as a detonator produced large variations in the amplitude of the stress pulse. Both of these limitations seemed to preclude testing that would produce repeatable data.

In order to overcome the above limitations and still attain the desirable pulse properties of explosives, this author investigated the use of "hot" pistol primers as the stress pulse generator. The hot primer had the fastest rise time of the available primers. The primers used were manufactured by Omark Industries, (type CCI, Small Pistol Primers #500). They produced a repeatable pressure pulse with a 80 microsecond

rise time. This rise time was deemed much too long for this testing. Therefore, this technique was abandoned.

1.3.3 Pulsed Radiation

Peffley (1967) produced strain waves in a cylindrical rod with a linear accelerator. A high-energy transient pulsed-beam of electrons impinged on the test specimen. His test showed the feasibility of this method.

Percival (1967, 1969) used a pulsed ruby-rod laser to generate strain waves in aluminum rods. The laser output was approximately 5 joules in a 35-nanosecond pulse. Hartman and Forrestal (1970) used a pulsed neoydmium-doped glass laser to produce strain waves in a magnesium-fluoride (Irtran I) ring. The laser output was approximately 12 joules in a 30-nanosecond pulse. Both these methods produced strain pulses in the specimens with rise times on the order of 5 microseconds and amplitudes on the order of 1.5 microstrain.

There were two ruby-rod high-energy-output lasers available to this author. An investigation was undertaken to evaluate the use of these lasers as a strain pulse generator. It was determined that one of the lasers was not "Q-switched", therefore, its output was not regulated. Instead of the light energy being emitted in a single high-intensity pulse, it was released in a series of pulses. This "pulse train" was unsuitable for generating the desired strain wave. Furthermore, it was not feasible to convert the laser to a Q-switched type. The second laser, which was Q-switched, became inoperable shortly before its suitability could be investigated. Since these were the only two lasers available, this method of strain wave production was discarded.

1.3.4 Mechanical

An extensive study on the longitudinal impact of metal rods with round ends was conducted by Sears (1908). His work led to a great proliferation of stress(strain) pulse studies on impacting objects.

Cunningham and Goldsmith (1959) generated strain pulses in narrow rectangular bars by longitudinal impact of a 1/2-inch diameter steel ball. The ball produced plastic deformation in the end of the bar. Therefore, 1/4 inch of the bar end had to be removed and the bar end had to be reground between tests. The amplitude of the strain pulses were in the plastic range of the test-bar materials, and the rise times were on the order of 12 microseconds. Although the ball impact velocity could be reduced to produce elastic strains, the rise times produced by this system were not short enough for the proposed testing.

Chiddister (1961) conducted tests with round-ended rods and flat-ended rods that were not "precisely" aligned and produced pulses with rise times on the order of 20 microseconds.

Becker and Conway (1964) described an apparatus for precisely aligning and impacting a pair of plane-ended cylinders. The plane ends of both cylinders were lapped with the use of optical techniques, to within 10 seconds of arc deviation from the geometric plane. The bars were aligned by a three step procedure. First, coarse alignment was checked with spirit levels. Second, intermediate alignment was checked with carbon paper between the impacting ends of the cylinders. The third and final alignment was accomplished using an audio technique suggested by Sears (1908). It was observed that higher impact velocities produced shorter strain-pulse rise times. The rise times ranged between approximately 8 to 18 microseconds, depending on the impact velocity. These

rise times produced by this system were too long for this investigation.

Halpin et al. (1963) described the construction and use of an air gun to produce strain-pulses with sub-microsecond rise times in a test sample. An air gun was used to propel and guide a projectile against the test sample. The resulting strain-pulse rise times were on the order of 0.04 microsecond. The rise time was influenced by two parameters, the mis-alignment between the projectile and sample impact faces and the impact velocity. The rise time was proportional to the tangent of the angular mis-alignment between the faces and inversely proportional to the projectile velocity. For example, the 0.04 microsecond rise time was produced by an impact velocity of 1000 feet per second and an angular mis-alignment within 0.0002 radian.

A smaller version of this air gun was constructed to investigate its suitability to this experiment. The results were less useful than expected due to the lower projectile velocities that were required to produce elastic strains. At these low velocities the projectile-to-barrel friction would produce erratic strain-pulse amplitudes. Thereby, the repeatability of the device was severely impaired. If the projectile-to-barrel clearance was increased, to reduce the friction, then the projectile/specimen alignment could not be maintained. Erratic rise times resulted. Thus, the method of strain-pulse generation of Halpin et al. was deemed unsuitable.

Elastic step-waves were produced in wires by Oi (1966). He notched long pieces of music wire and heat-treated the notched area. By subjecting these wires to tensile load, they catastrophically fractured at the notch. This resulted in a step strain-wave that propagated along the wire. The strain-wave had a rise time of approximately one microsecond.

Thus, this method produces strain waves with properties that would meet the requirements for this experiment. However, the destruction of each sample would introduce many unwanted variables between tests. These variables arise because of the impossibility of constructing identical test samples. An assessment could not be made as to what effects the combination of unwanted and desirable variables would have on the output of the strain gage.

1.3.5 Hammer-Type Apparatus

It became apparent that the strain-wave generation devices currently in use were either unsuitable or too expensive to be usable in this experiment. It was decided to design and construct a new type of mechanical test apparatus. This device had a short pendulum (hammer) as the impact member. The hammer was mounted in a holder which also contained a torsional spring to drive the hammer. The test specimen was bonded into a holder with epoxy potting compound. The two holders were designed so that the holders, hammer and specimen could be machined and lapped to very precise tolerances. When mated, the two holders would position and align the hammer with the specimen. This apparatus was inexpensive to build, repeatable in its operation, produced strain-pulses with microsecond or sub-microsecond rise times and produced strain-pulses with amplitudes that could be varied within the elastic region of the test-specimen material. See Chapter 2 for a detailed discussion of this device.

1.4 Selection of Test Temperature Range

In order to select an appropriate test temperature range, it was necessary to review some of the areas in which the resistance strain gage is being used. The following are some typical dynamic tests and environmental temperatures.

Dynamic tests are performed on reciprocating-engine components, such as piston connecting rods. The normal connecting-rod operating temperatures on a summer day range from 200 to 240°F. Under extreme loading conditions these temperatures may reach 350°F.

The aircraft industry performs dynamic tests on aircraft structural components such as spars, stringers and stressed skins. In the stratosphere, these members are subjected to a temperature of -65°F.

Spacecraft tanks, which in some applications are also structural members, are dynamically tested. Liquid-oxygen tanks are at approximately -298°F; liquid-nitrogen, -320°F; liquid-hydrogen, -423°F.

The majority of dynamic testing is performed by the aircraft and automotive industries. Thus, it was felt that temperatures of -100 to +300°F would be a representative test range.

CHAPTER 2

TESTING APPARATUSES AND INSTRUMENTATION

2.1 Criteria for the Hammer-Type Apparatus

The following criteria were used in designing and constructing the hammer-type strain-pulse apparatus.

a) The strain-pulses should have rise times on the order of tenths of microseconds. This was necessary since the traverse time of "short" commercially available gages when mounted on "conventional" engineering materials was on the order of tenths of a microsecond.

b) The strain pulses should be repeatable. Statistical methods could then be used to reduce the test data.

c) The apparatus should have provisions that would enable the amplitude of the strain-pulse to be varied. This would allow the selection of appropriate test amplitudes.

d) The apparatus should be inexpensive to build.

e) The apparatus should be of a type that could be constructed by a "conventional" machine shop.

Criteria d and e would make the device available to experimenters who have neither unlimited funds nor "exotic" aero-space/governmental machine shop facilities available.

f) The apparatus should produce strain pulses by mechanical impact. This criterion was dictated by criteria d and e.

g) The faces of the impacting member of the device and the impacted face of the test specimen must meet the following criteria.

i) The impacting faces must have surface finishes of 5 rms microinches or less.

ii) The faces must be flat within 1/2 to 1 wave length of 6510 Å red light, as determined by conventional optical techniques.

iii) The mis-alignment of the faces upon impact must be less than 10 seconds of arc.

These limits were determined partly from other devices and partly from experiments conducted on the apparatus described in section 2.2.

h) The apparatus should have provisions to control the test specimen temperature between the limits of -100 to +300°F. This temperature range was based on section 1.4.

i) The apparatus should have a means of measuring the impact velocity.

It is necessary to determine the impact velocity, since the strain amplitude is a function of the impact velocity. Any variation in impact velocity would then produce an undesirable variation in the strain amplitude.

j) The apparatus should have means by which the recording instrumentation could be triggered.

2.2 Hammer-Type Apparatus

2.2.1 General Discussion

The hammer-type strain-pulse apparatus used in these experiments was comprised of two major assemblies: the test specimen assembly and the hammer assembly. The two primary parts of the specimen assembly were the

test specimen and the specimen holder. The specimen was bonded into the holder with epoxy potting compound. The two primary parts of the hammer assembly were the hammer (a short pendulum) and the hammer holder. The hammer was mounted into the holder by means of a shaft and two bearings. These assemblies were designed in a manner that would allow them to be separated for mechanical "lapping" operations. The lapping operations were necessary to produce the surface finish and flatness of the impacting faces as required in criteria g i) and g ii). The two assemblies, when joined together, were designed to meet the alignment requirement imposed on the impacting faces by criterion g iii).

There were two sub-assemblies which fasten to the hammer assembly. One was the transducer that was used in conjunction with appropriate instrumentation to determine the hammer impact velocity. The other was the hammer drive assembly.

There was a heating-cooling sub-assembly associated with the specimen assembly. The heating-cooling assembly, along with a system that provided a heated or cooled fluid, controlled the test specimen temperature.

The strain-pulse apparatus was mounted in a vacuum chamber. This eliminated a cushion of air between the hammer and specimen faces prior to impact. An air-cushion would have increased the strain-pulse rise time.

2.2.2 Detailed Description

The test specimen is shown in Figure 1a. The specimen was a cylinder with a solid and a hollow section. Impact occurred on the face of the solid end. Four strain gages were located at 90° intervals around the specimen.

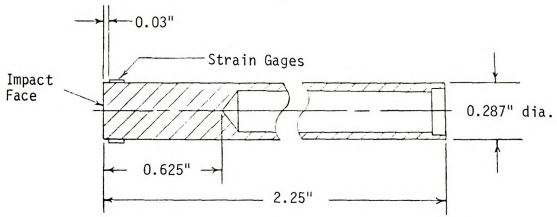

(a) Cross Section of Test Specimen

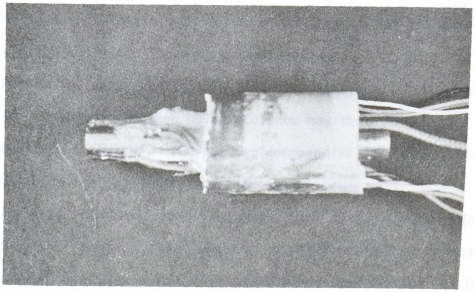

(b) Instrumented Test Specimen

Figure 1. Test Specimen

The gages were positioned with their active elements parallel to the cylindrical axis of the specimen. The leading edge of the active element of each gage was positioned 0.03 inch from the impact face of the specimen. Dispersion effects, as discussed in section 3.1.1, required the gage to be placed at the end of the specimen. The machining and lapping operations would remove some material from the end of the specimen. The 0.03-inch dimension was chosen as a compromise between these two requirements. An iron-constantan thermocouple was located between two of the gages.

The hollow portion of the specimen provided a passage for the heating-cooling fluid. The hollow section was terminated 5/8 inch from the impact face. This distance was chosen in order to allow the initial strain-pulse to reach its peak value at the gage locations, before the wave that would be reflected from the solid/hollow interface would reach the gage locations. In addition, this length was chosen in order to reduce the thermal gradients in the solid portion of the test specimen.

Figure 1b, shows the instrumented test specimen. This specimen was pressed out of the specimen holder to show how the specimen was supported by the potting compound. The potting compound is the large cylinder through which the gage-leads and thermocouple wire pass.

The test specimen assembly is shown in Figure 2. The specimen holder performed the following functions: a) provided a means of mounting and locating the test specimen, b) provided a locating surface for the hammer assembly, c) provided a lapping fixture for the test specimen, d) provided a means of mounting the heating-cooling assembly, and e) provided a means of mounting the entire test apparatus in the vacuum chamber.

After the specimen was instrumented it was bonded into the specimen holder with an epoxy potting compound. The potting compound must fulfill

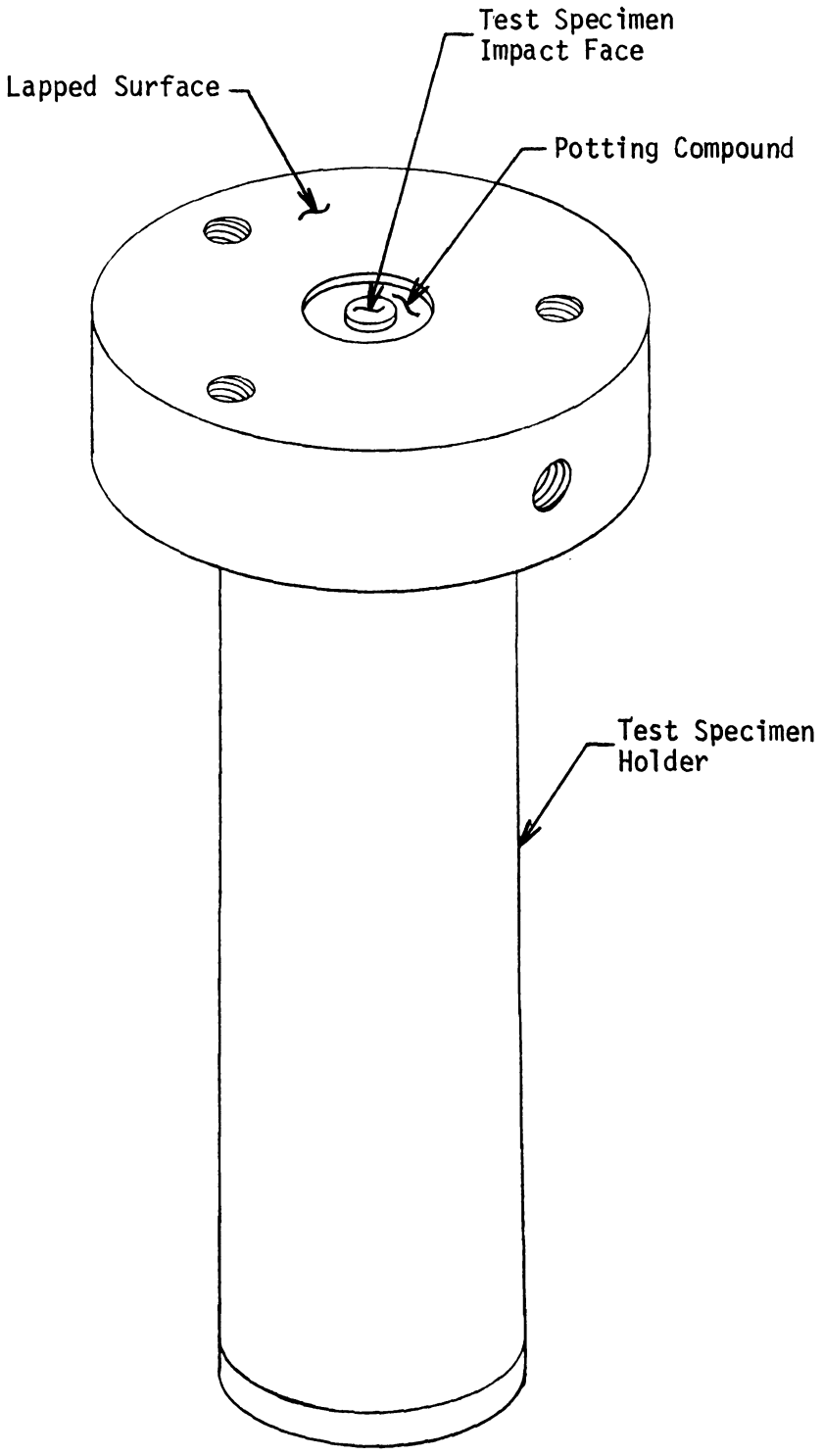

Figure 2. Test Specimen Assembly

two requirements. First, it must be rigid. This is to insure that the specimen does not move relative to the holder during lapping or testing. Second, its thermal conductivity should be low. This will reduce thermal gradients in the test specimen.

The potting compound was prepared from the follow ingredients:

Resin: Type DER 332, Dow Chemical Company,*

Filler: Type Vicron 15-15 (finest grade), Pfizer Corporation,

Hardener: Type H2-3561, Dexter Corporation.

The ingredients were measured by weight and mixed as follows:

Resin 50 parts

Filler 60 parts

Hardener 15 parts.

Curing time for the potting compound was 24 hours at room temperature.

After the specimen was bonded into the holder, the assembly was faced-off in a lathe to insure that the impact face of the specimen was coplanar with the large face of the holder. This machine surface was then lapped and polished. The resulting surface had a measured finish of 3 to 5 rms microinches, and a measured flatness within 1/2 to 1 wave length of 6510 Å red light.** The three inch diameter large end of the holder prevented the assembly from rocking during lapping. A rocking motion would have produced a convex surface. In addition, this large surface provided a precise means of locating the hammer assembly relative to the specimen. Figure 3 shows the specimen assembly after lapping.

The hammer assembly is shown in Figure 4. The hammer assembly

---

* See Appendix A for addresses of manufacturers.

** See Appendix B for lapping, polishing and surface-finish-measuring techniques.

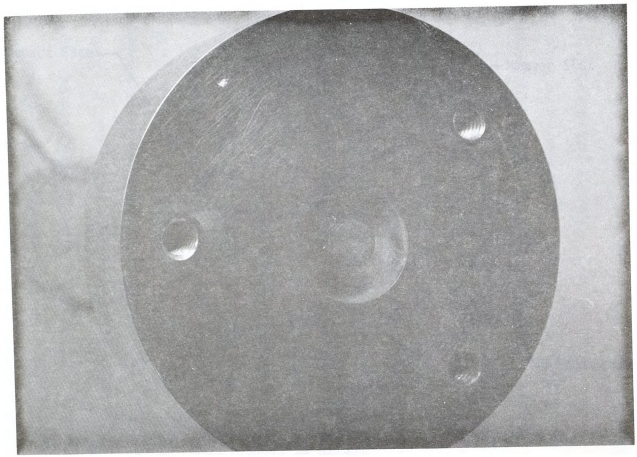

Figure 3. Lapped Specimen Assembly

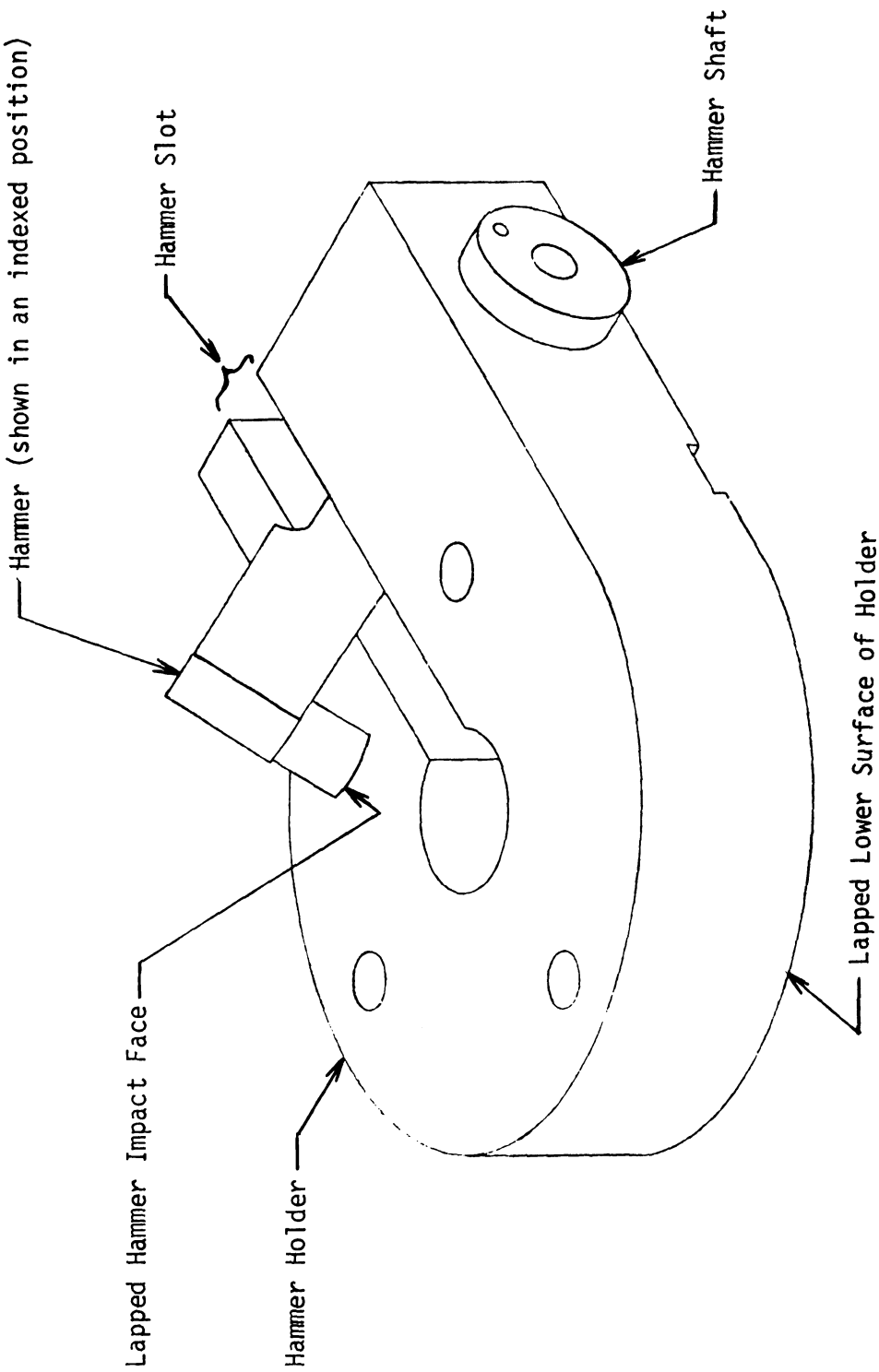

Figure 4. Hammer Assembly

served the following functions: a) provided a means of mounting the hammer, b) provided a means of precisely aligning the hammer with the specimen, c) provided a lapping fixture for the hammer, d) provided a means of mounting the transducer assembly, and e) provided a means of mounting the hammer drive assembly.

The hammer is a short pendulum semi-permanently assembled into the hammer holder. This design of the hammer assembly was a major departure from previous devices. The hammer assembly automatically accomplished and maintained the required alignment between the impacting face of the hammer and the impacted face of the specimen. Thus, the hammer assembly was the key factor that enabled this apparatus to produce repeatable, sub-microsecond rise-time strain-pulse, while being inexpensive to build.

Of the three parameters (surface finish, flatness and alignment) that influence rise time, alignment of the impacting faces was the most difficult to achieve. The required surface finish and flatness are routinely produced by commercially available lapping machines. The precise alignment of the impacting faces was directly dependent on the design of the apparatus. The following description of the hammer assembly will explain how the necessary alignment of the impacting faces was accomplished.

The hammer was installed into the holder as follows. Super-precision bearings were pressed into the holder, on either side of the hammer slot. The hammer shaft was pressed through the bearings and the hammer. The hammer was pinned to the shaft. The underside of the holder and the impact face of the hammer were faced-off in a lathe. This insured that the impact face of the hammer was coplanar with the underside of the holder. This machined surface, along with the impact face of the hammer was then lapped, polished and checked for surface finish and flatness. The hammer

assembly was then joined to the specimen assembly as shown in Figure 5.

The lapped surface of each assembly automatically accomplished and maintained the alignment between the hammer holder and specimen impact face. The press fit of the bearings in the holder maintained the position of the bearing outer races with respect to the hammer holder. Thus the position of the bearing outer races was maintained with respect to the specimen impact face. The press fit of the hammer shaft into the hammer and bearings maintained the position of the hammer impact face with respect to the inner race of the bearings. Thus, the clearance in the bearings is the only possible source of mis-alignment between the hammer impact face and the specimen impact face.

The hammer shaft mis-alignment due to bearing clearance is shown in Figure 6. The bearing clearance, which is required to allow rotation of the bearings, is shown as d. The distance between the bearings is shown as L. The angular mis-alignment of the hammer shaft center line from the center line of the bearings is the angle γ . Geometry then gives γ in terms of d and L as:

$$\gamma = \tan^{-1}(d/L) \quad .$$

The mis-alignment γ can then be minimized by reducing d or increasing L. To reduce the cost of the apparatus, inexpensive commercially-available super-precision bearings were used. This gave a minimum d at reasonable expense. Requiring γ to be 10 seconds of arc or less determined the lower limit on L. The lower limit on L was found to be approximately 2 inches. The dimensions of the lapped surfaces are governed by the size of the available lapping machine. The maximum surface diameter that the

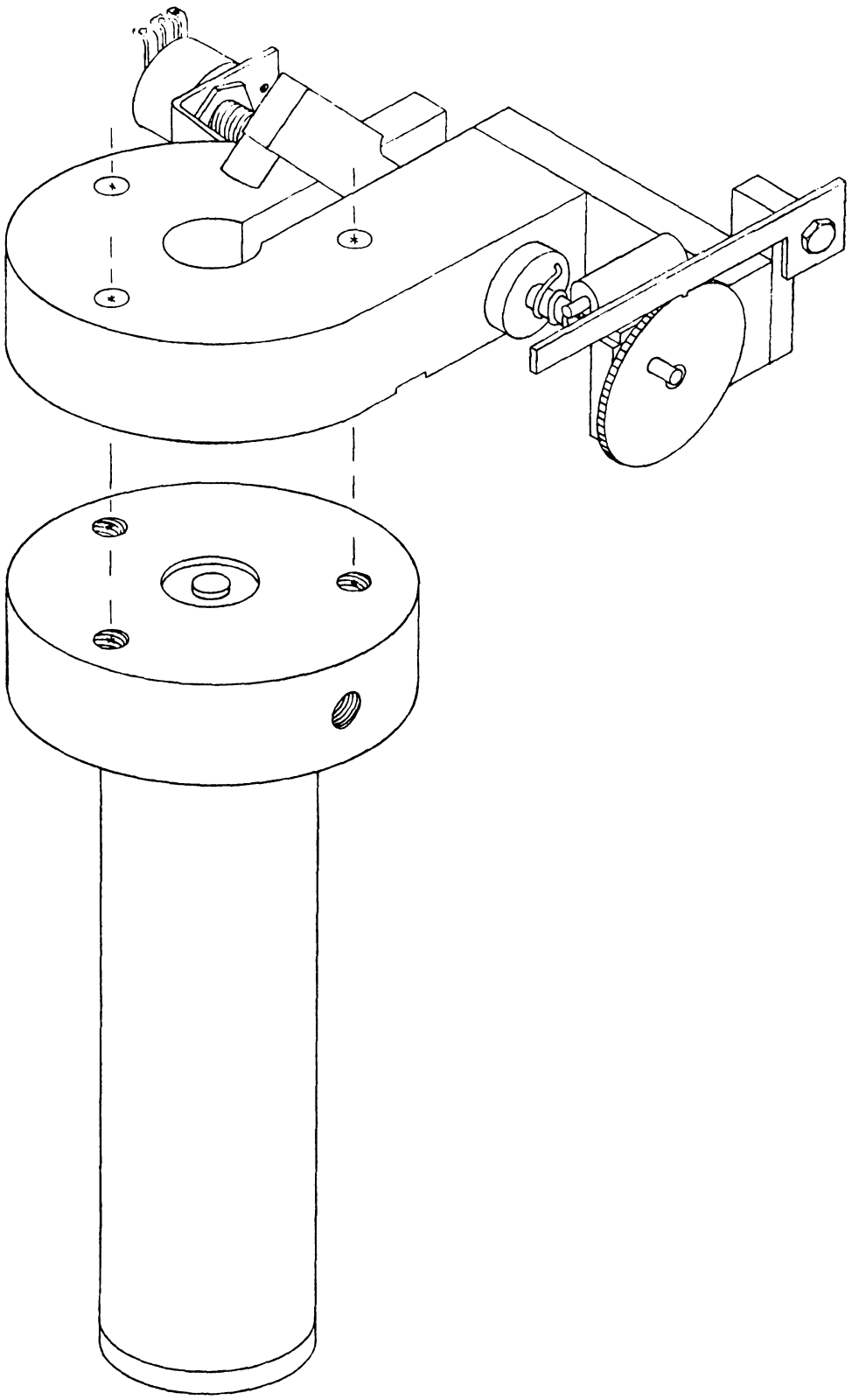

Figure 5. Specimen and Hammer Assemblies

Bearing Balls Omitted for Clarity

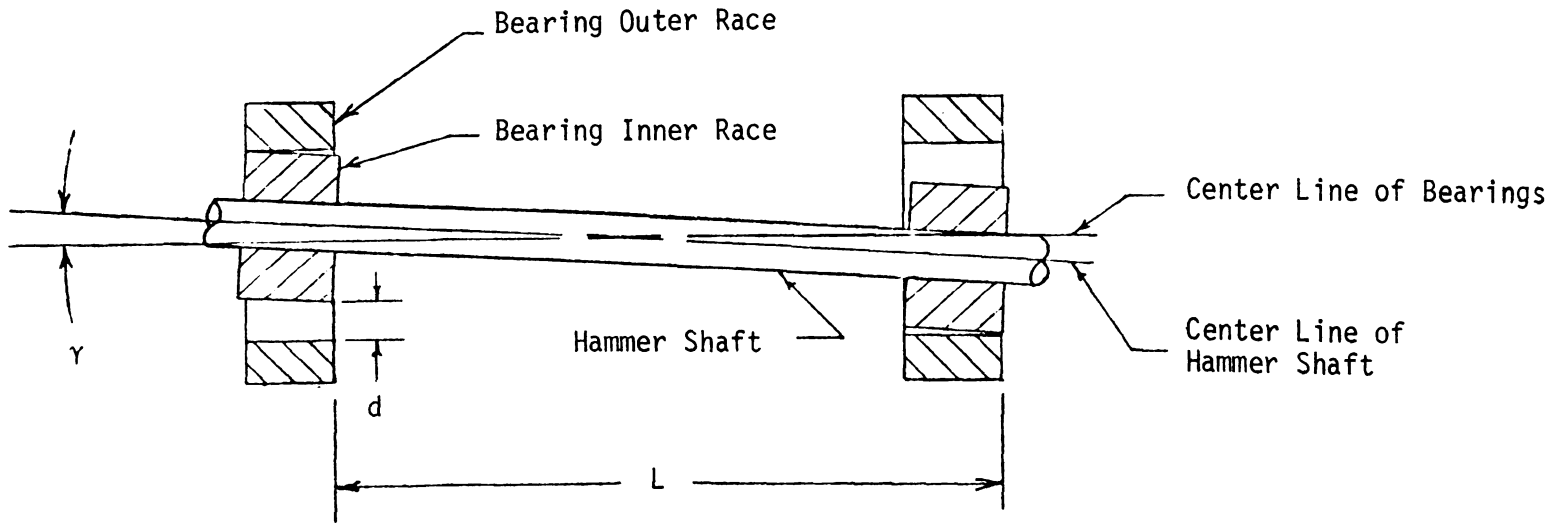

Figure 6. Hammer Shaft Mis-alingment Due to Bearing Clearance

lapping machine available for this experiment could accommodate was 4 3/32 inches. Therefore, the hammer holder could be sized to achieve the required L dimension and still fit into the lapping machine.

The design features of this strain-pulse apparatus permit the impacting face of the hammer and the impacted face of the specimen to meet the surface finish, surface flatness and alignment criteria.

The hammer drive assembly is shown in Figure 7. The hammer drive assembly fastened to the hammer assembly. The functions of the hammer drive assembly were as follows: a) provide a torsional reaction member for the torsional spring that drives the hammer, b) provide a means of indexing the hammer, c) provide a means of changing the torsional spring pre-load, and d) provide a means of releasing the hammer from the indexing position, thereby allowing the hammer to impact the specimen.

The hammer drive assembly was removed from the hammer holder assembly during the lapping operation. They were joined for test purposes.

An interconnecting shaft coupled the hammer shaft to the indexing gear. Rotating the index gear thus rotated the hammer. The rotation was accomplished by a rack and pinion drive installed in the vacuum chamber. The rack was operated from outside the chamber. This allowed the hammer to be indexed without releasing the vacuum. The hammer was held in the indexed position by the sear which engaged the indexing gear.

The interconnecting shaft passed through the torsional drive spring. This prevented distortion of the spring when the hammer was indexed. One end of the torsional drive spring was fastened to the hammer shaft. The other end was fastened to a worm wheel. The worm wheel was engaged with the worm gear. Rotation of the worm gear changed the pre-load on the drive assembly. By changing the indexing position and/or the spring

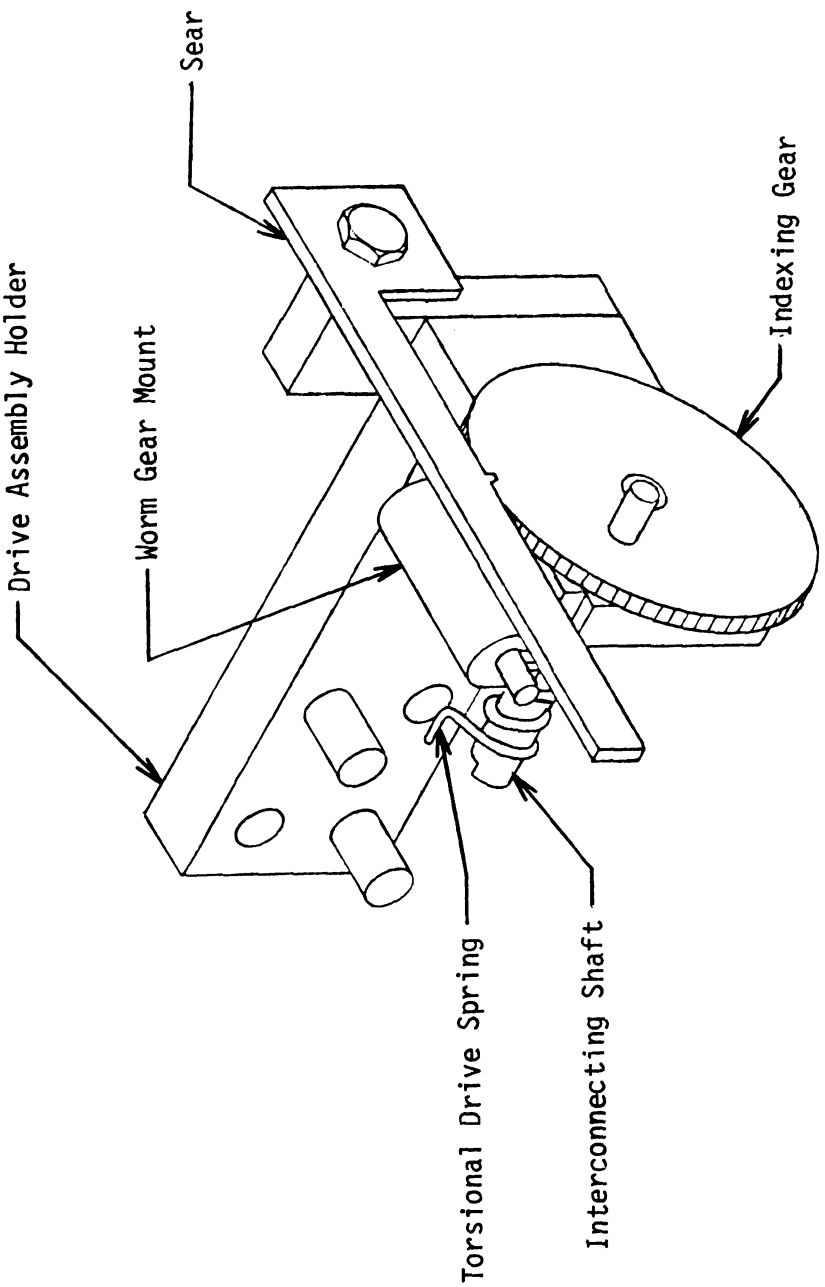

Figure 7. Hammer Drive Assembly

pre-load, the impact velocity of the hammer could be set to the desired value. The worm gear was rotated by a flexible shaft that passed through the vacuum chamber.

A plunger passed through the vacuum chamber. The plunger performed two functions. First, when it was pushed, it disengaged the sear from the index gear. This allowed the torsional spring to drive the hammer which resulted in the hammer impacting the specimen. Second, when the plunger contacted the sear, it completed an electrical circuit. This circuit provided the trigger for the hammer velocity recording instrumentation.

The transducer assembly is shown in Figure 8. This assembly mounted on the hammer assembly as shown in Figure 5. The transducer assembly coupled an angular potentiometer to the hammer shaft. The output of the potentiometer was a voltage proportional to the hammer angular position. This voltage was differentiated electronically, which resulted in a voltage proportional to the angular velocity of the hammer. This voltage was then recorded. A calibration constant along with the voltage record was used to determine the hammer angular impact velocity.

Figure 9 shows an exploded view of the hammer assembly, the hammer drive assembly, and the transducer assembly. Table 1 is a list of parts for Figure 9.

Figure 10 shows the hammer and specimen assemblies ready to be joined. A 0.01 x 0.25-inch slot on the underside of the hammer holder provided a path for a laser beam. The laser beam was directed into the vacuum chamber and through the slot. A photodiode was placed at the beam-exit-end of the slot. The diode was included in an electronic circuit with an operation amplifier (op-amp). With the hammer in a raised position the laser beam could illuminate the diode. This resulted in a voltage output

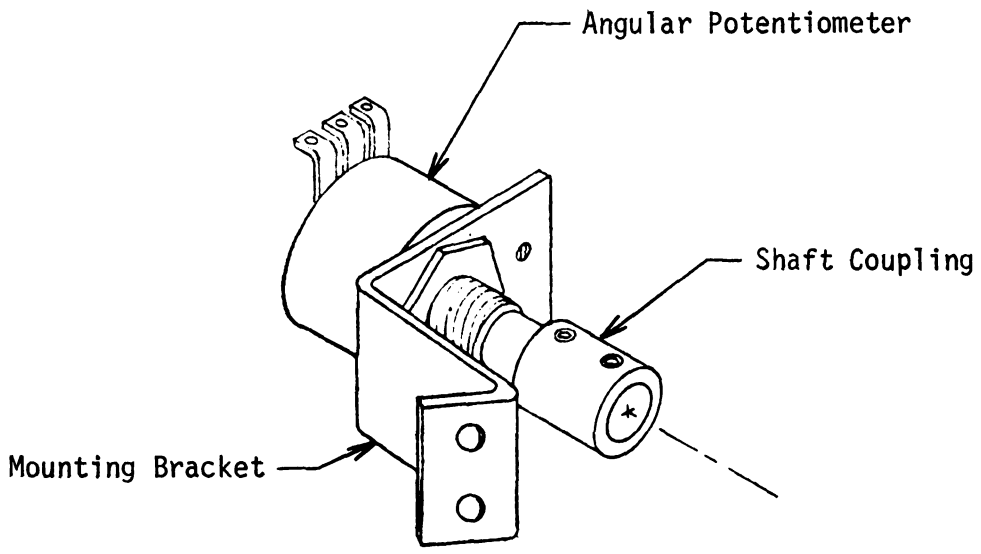

Figure 8. Transducer Assembly

Table 1. Parts List for Figure 9

Part Number	Part Name
1	Hammer Holder
2	Hammer
3	Hammer Shaft
4	Hammer Pin
5	Hammer Shaft Bearings
6	Coupling
7	Angular Potentiometer Mounting Bracket
8	Angular Potentiometer
9	Torsion Drive Spring
10	Interconnecting Shaft fastened to Indexing Gear
11	Interconnecting Shaft Bearings
12	Worm Wheel
13	Sleeve (acts as a bearing for the worm wheel and as a carrier for the interconnecting shaft bearings)
14	Sleeve Retainer Ring
15	Clamp (fastens torsional spring to worm wheel)
16	Worm Gear
17	Worm Gear Mount
18	Sear
19	Sear Mount
20	Drive Assembly Holder

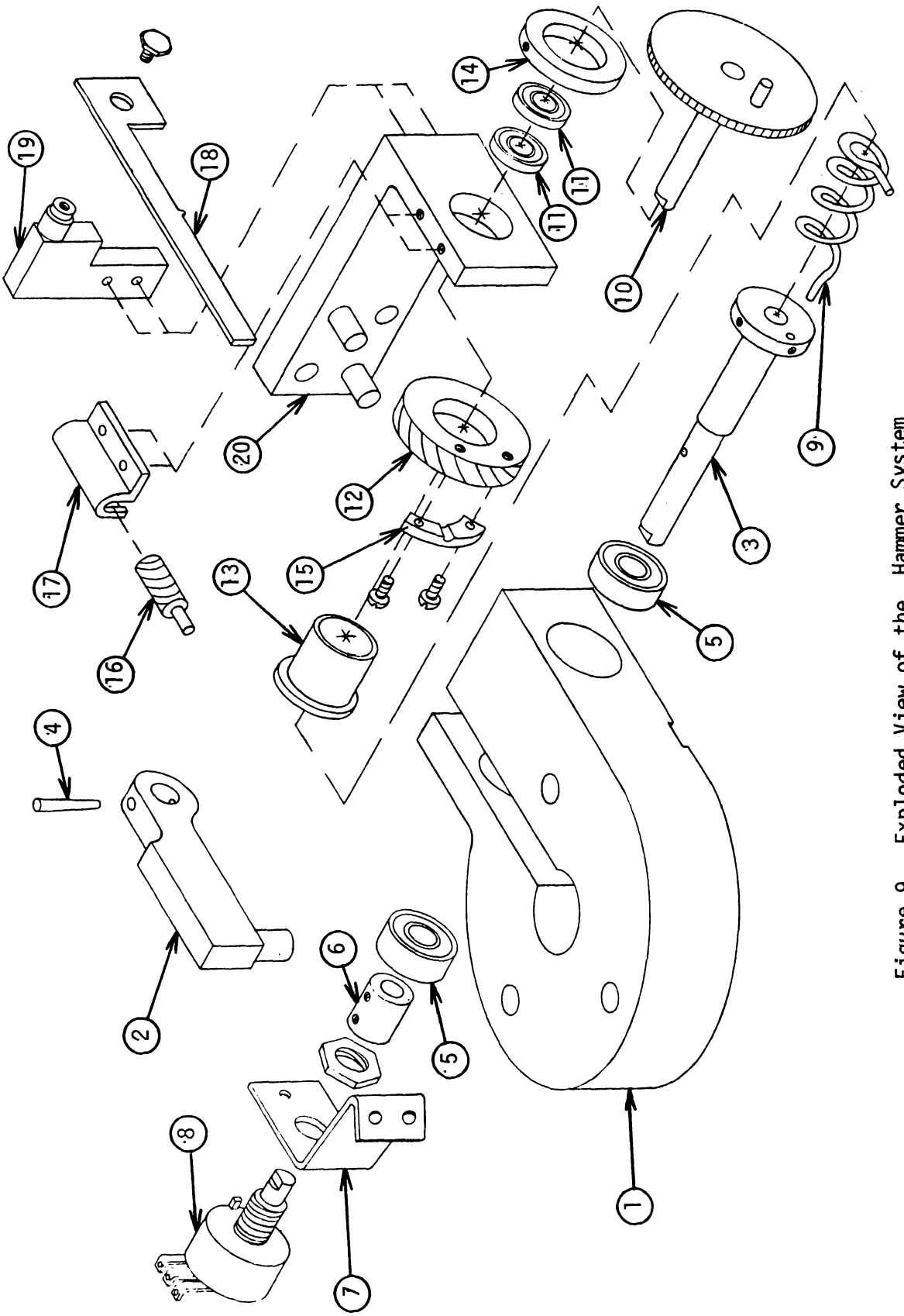

Figure 9. Exploded View of the Hammer System

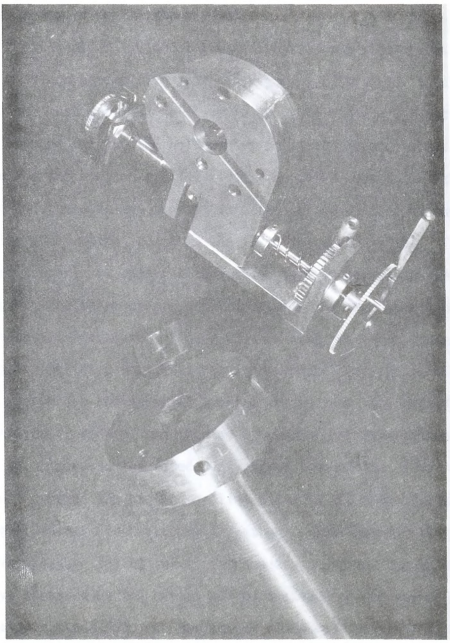

Figure 10. Hammer and Specimen Assemblies Showing Laser Beam Slot

from the op-amp. When the hammer contacted the specimen, the laser beam was interrupted. This resulted in a zero voltage output from the op-amp. The laser beam along with the diode circuit provided a trigger source for the strain recording instrumentation.

A cross sectional view of the heating-cooling assembly as it was fitted to the specimen assembly is shown in Figure 11. A hollow specimen support located the test specimen relative to the holder while the potting compound cured. During testing the hollow portion of the support acted as an exit passage for the heating-cooling fluid. An inlet tube passed through a tee-fitting and the specimen support into the hollow section of the test specimen. The tee-fitting separated the fluid inlet and outlet. The inlet tube, specimen support and specimen thus acted like a coaxial counter-flow heat-exchanger. The thermocouple determined when the test specimen was at the desired test temperature. Figure 12 shows the test specimen and heat-cooling assemblies. Note that the instrumented test specimen was pressed out of the holder and is still encased in the potting compound.

An overall view of the testing system and instrumentation is shown in Figure 13. A cruved insulated duct passed through the support tripod. This duct carried the heating-cooling fluid to the test apparatus. The heating fluid was air heated by a heat gun. The heat-gun fan provided a positive pressure to the inlet of the duct. A vacuum system provided a negative pressure at the outlet of the heating-cooling assembly. The air was heated by an electrical resistance element. The specimen temperature was controlled by varying the air flow rate and by cycling the heating element on and off.

Cold air could not be used for the cooling fluid. This was tried, but the water vapor in the air froze inside the heating-cooling assembly blocking the air flow.

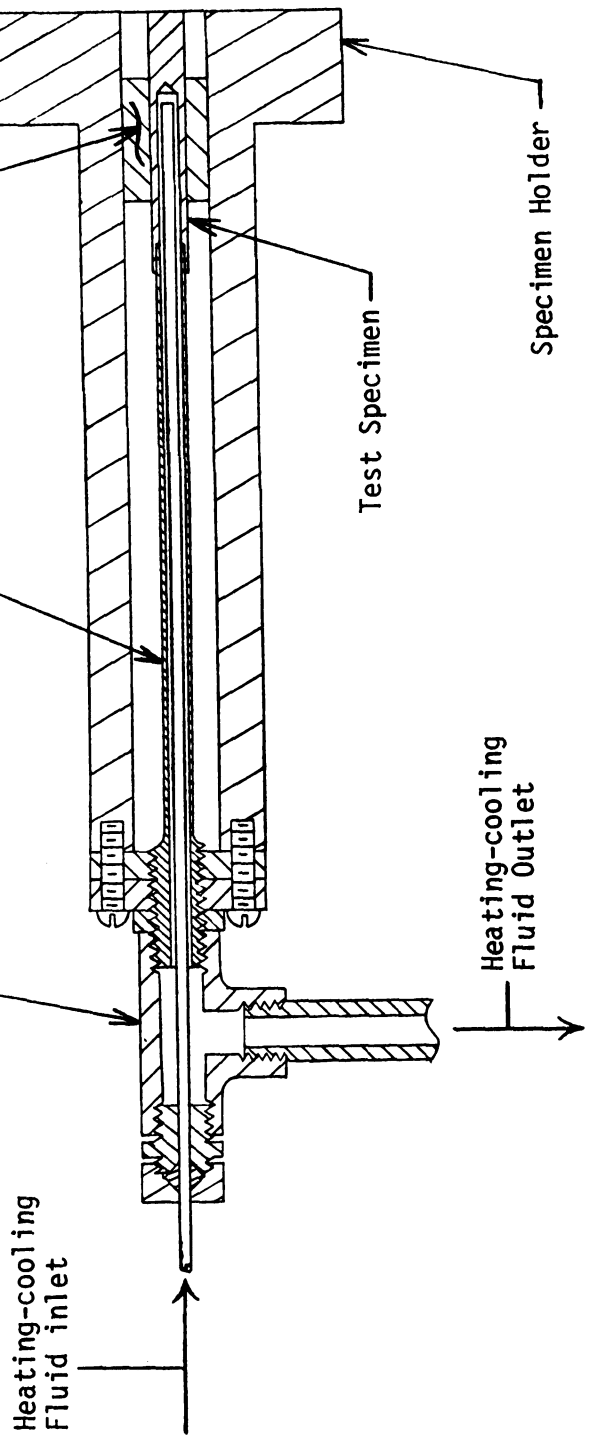

Figure 11. Cross-section, Heating-cooling and Specimen Assemblies

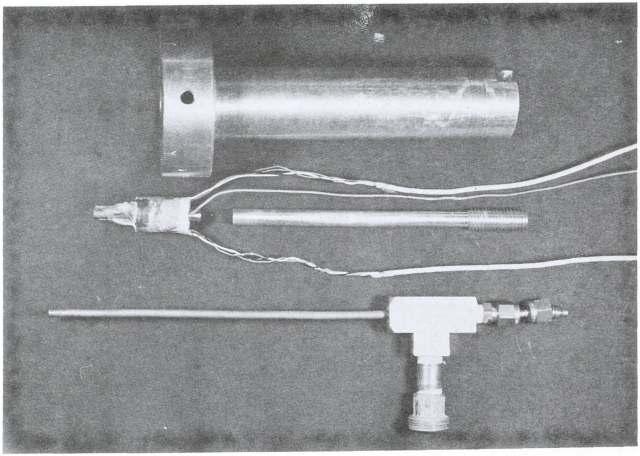

Figure 12. Heating-cooling and Test Specimen Assemblies

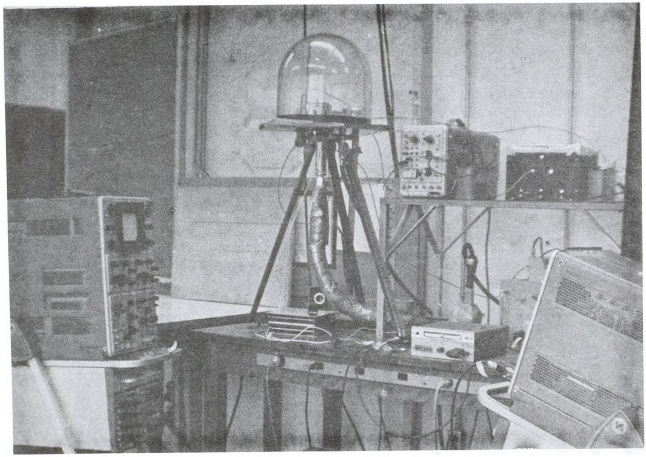

Figure 13. Overall View of Testing Equipment

Subsequently, cold nitrogen was used as the cooling fluid. This was supplied by a reservoir of liquid-nitrogen. The vacuum at the heating-cooling assembly outlet would cause gaseous nitrogen to boil off from the liquid-nitrogen. By adjusting the vacuum level, the boil-off rate was controlled. This resulted in an adjustable flow rate of cold nitrogen through the system. The flow rate then determined the specimen temperature.

Figure 14 shows the test apparatus as seen through the vacuum chamber.

Figure 15 shows a close-up view of the test apparatus. The vacuum bell-jar is removed for clarity.

2.2.3 Instrumentation

Resistance strain gages change resistance when they are subjected to a strain. A potentiometer circuit converted the resistance change into a voltage change. Calibration factors then determined the strain from the voltage change.

The potentiometer circuit is shown in Figure 16. A ballast resistor, R_b, is in series with the strain gage, R_g. For any fixed supply voltage, E_b, the maximum sensitivity of the circuit will occur when $R_b = R_g$. The coupling capacitor, C_c, prevents the passage of direct current to the recording instrument. Thus, this circuit will only respond to dynamic strains or the dynamic component of combined strains.

By Ohm's law the current in the circuit is

$$I = E_b/(R_b + R_g) \qquad (2\text{-}1)$$

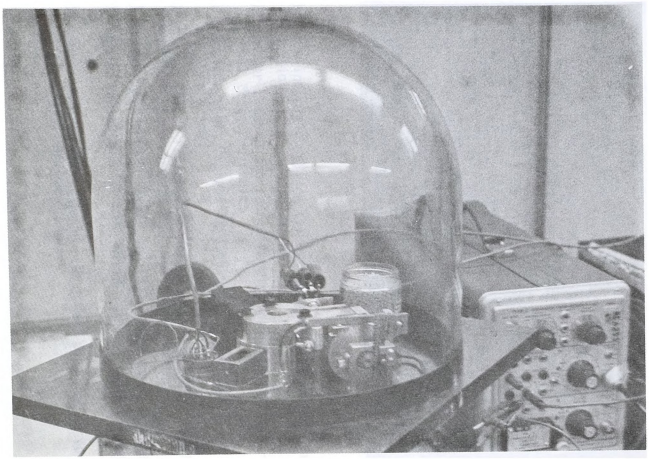

Figure 14. Test Apparatus Inside Vacuum Chamber

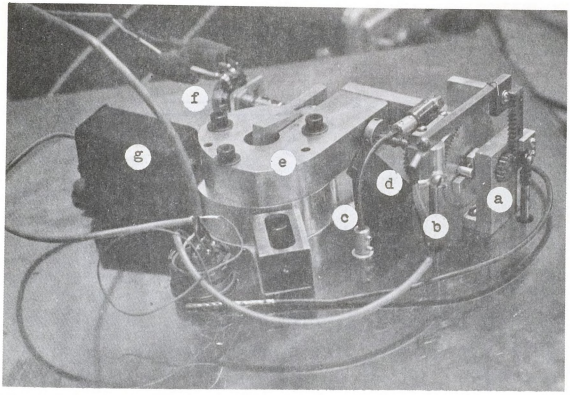

a) rack and pinion system for rotating the hammer to a raised position

b) plunger beneath the sear with wiring for the velocity-signal trigger-circuit

c) flexible shaft (curves through 90°) for adjusting the drive spring pre-load

d) mirror (black rectangular holder angled at 45°), to direct the laser beam through the slot in the hammer holder

e) hammer holder with hammer in a slightly raised position

f) angular potentiometer with wiring for the velocity signal circuit

g) photodiode (black rectangular housing) with wiring for the strain-signal trigger-circuit

Figure 15. Close-up View of the Test Apparatus

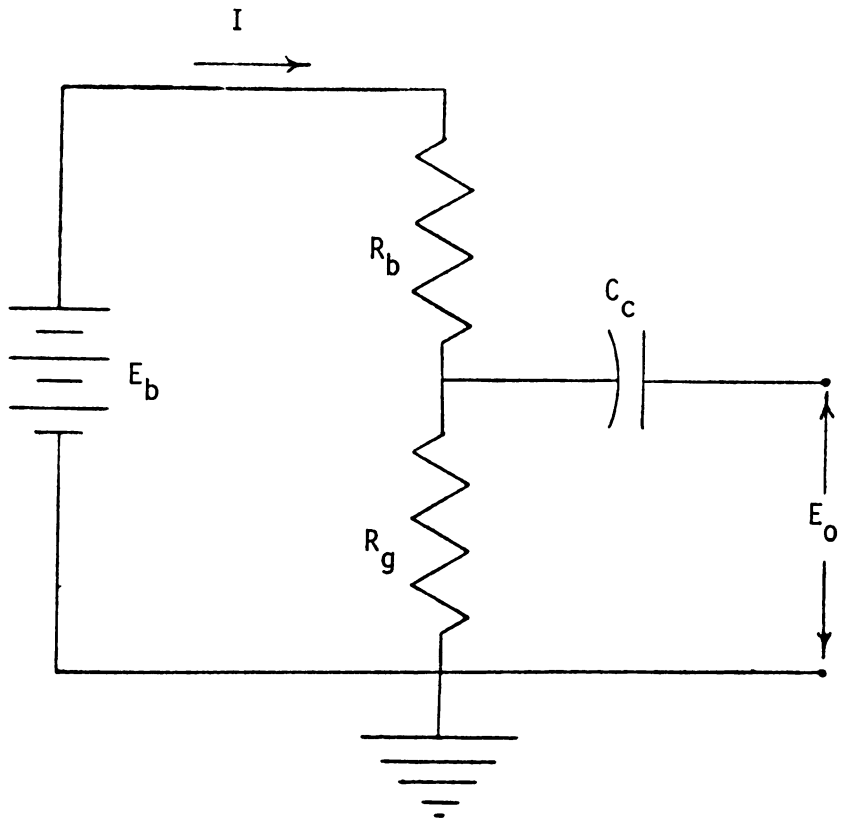

E_b : Circuit Supply Voltage (DC)

I : Circuit Current

R_b : Ballast Resistor

R_g : Strain Gage (Unstrained Resistance)

C_c : Coupling Capacitor

E_o : Output Voltage

Figure 16. Strain Gage Potentiometer Circuit

and the voltage across the gage is

$$E_g = IR_g \quad . \tag{2-2}$$

Substituting Eq. (2-1) into Eq. (2-2), gives the voltage across the strain gage as

$$E_g = E_b R_g/(R_b + R_g) \quad .$$

Applying a strain to the gage changes the gage resistance to $R_g + \Delta R_g$. The current then becomes

$$I = E_b/(R_b + R_g + \Delta R_g) \quad , \tag{2-3}$$

and the voltage across the gage becomes

$$E_g + \Delta E_g = I(R_g + \Delta R_g) \quad . \tag{2-4}$$

Substituting Eq. (2-3) into Eq. (2-4) gives the new voltage across the gage as

$$E_g + \Delta E_g = \frac{E_b(R_g + \Delta R_g)}{(R_b + R_g + \Delta R_g)} \quad . \tag{2-5}$$

Successive algebraic operations on Eq. (2-5) give

$$E_g + \Delta E_g = \frac{E_b R_g(1 + \Delta R_g/R_g)}{(R_b + R_g)(1 + \Delta R_g/(R_b + R_g))}$$

$$= \frac{E_b R_g(1 + \Delta R_g/R_g)}{R_b + R_g} \quad [1 - (\Delta R_g/(R_b + R_g))$$

$$+ (\Delta R_g/(R_b + R_g))^2 - (\Delta R_g/(R_b + R_g))^3 + \ldots]$$

$$= \frac{E_b R_g}{R_b + R_g} [1 + \Delta R_g R_b/R_g(R_b + R_g) - \Delta R_g{}^2 R_b/R_g(R_b + R_g)^2$$

$$+ \Delta R_g{}^3 R_b/R_g(R_b + R_g)^3 - \ldots] \quad . \qquad (2\text{-}6)$$

The first term on the right hand side of Eq. (2-6) is E_g which is the DC component of the voltage across R_g. The remaining terms are then the dynamic component of the voltage across the gage. Since the coupling capacitor will only pass the dynamic component of the voltage, we have as the circuit output voltage

$$E_o = \Delta E_g \quad . \qquad (2\text{-}7)$$

Thus Eqs. (2-6) and (2-7) give

$$E_o = \frac{E_b R_b \Delta R_g}{(R_b + R_g)^2} [1 - \Delta R_g/(R_b + R_g) + \Delta R_g{}^2/(R_b + R_g)^2 - \ldots] \quad . \qquad (2\text{-}8)$$

Typical foil strain gages subjected to elastic strains have the following values:

$R_g = 120\Omega$ or 350Ω

$\Delta R_g < 2\Omega$.

Therefore, the higher order terms in Eq. (2-8) can be neglected. This results in an error in E_o of less than one per cent. The output voltage for

foil gages is then

$$E_o = \frac{E_b R_b \Delta R_g}{(R_b + R_g)^2} \quad . \qquad (2\text{-}9)$$

Typical semi-conductor strain gages subjected to elastic strains have the following values:

$R_g = 120\Omega$ or 350Ω

$\Delta R_g < 10\Omega$.

Therefore, third-order and higher terms in Eq. (2-8) can be neglected. This results in an error in E_o of less than 1/5 per cent. The output voltage for semi-conductor gages is then

$$E_o = \frac{E_b R_b \Delta R_g}{(R_b + R_g)^2} [1 - \Delta R_g/(R_g + R_b)] \quad . \qquad (2\text{-}10)$$

The potentiometer circuit output voltage was displayed on a Tektronix, type 555, oscilloscope with a type 1A1 vertical amplifier. An oscilloscope camera provided a permanent record of the signal.

The input impedance of the oscilloscope was approximately one $M\Omega$. This value was much greater than the strain gage resistance. Therefore, the effect of the oscilloscope impedance on the output of the potentiometer circuit was negligible. The vertical gain of the oscilloscope was calibrated using a known amplitude square wave.

It was also necessary to determine the rise time of the total strain instrumentation system. The expected rise time of the strain-pulse was on the order of 0.1 microsecond. If the instrumentation system rise time was about 0.1 microsecond or larger, the recorded rise time would be of the

system and not of the strain gage. The rise time of the oscilloscope/ vertical amplifier combination was 0.01 microsecond. This value was obtained from the specific ations of the oscilloscope, Thus, the oscilloscope had the capability of measuring a voltage signal with a rise time of 0.1 microsecond.

A Tektronix, type 114, pulse generator was used as the source of a known rise time square-wave voltage. The rise time of the square wave was 0.01 μsec. The square wave was applied across the strain gage and displayed on the oscilloscope. The total strain instrumentation system rise time was found to be 0.02 microsecond. This value was sufficiently smaller than 0.1 microsecond to insure fidelity in the recording of a 0.1-microsecond rise-time output from the strain gage.

The angular potentiometer connected to the hammer shaft provides a voltage output, E_θ, proportional to the hammer angular displacement. An electronic circuit was designed and built in order to determine the hammer angular velocity. The output voltage, E_ω, of this circuit is proportional to the hammer angular velocity. This circuit is shown in Figure 17.

A six-volt battery supplied power to the potentiometer. The potentiometer output was the simultaneous input to two devices: the first channel of a dual-trace oscilloscope, and the differentiator circuit. The differentiator op-amp supply was a Model 5382, Dual Power Supply, ± 15VDC @ 100 ma, manufactured by Analog Devices, Inc. The output from the differentiator circuit was the input to a low-pass filter. The filter was a Model 335R, Variable Filter, manufactured by Krohn-Hite. The output from the low-pass filter was the input to the second channel of the dual-trace oscilloscope. The angular potentiometer and filter output voltages were recorded using a Tektronix, type 564, storage oscilloscope

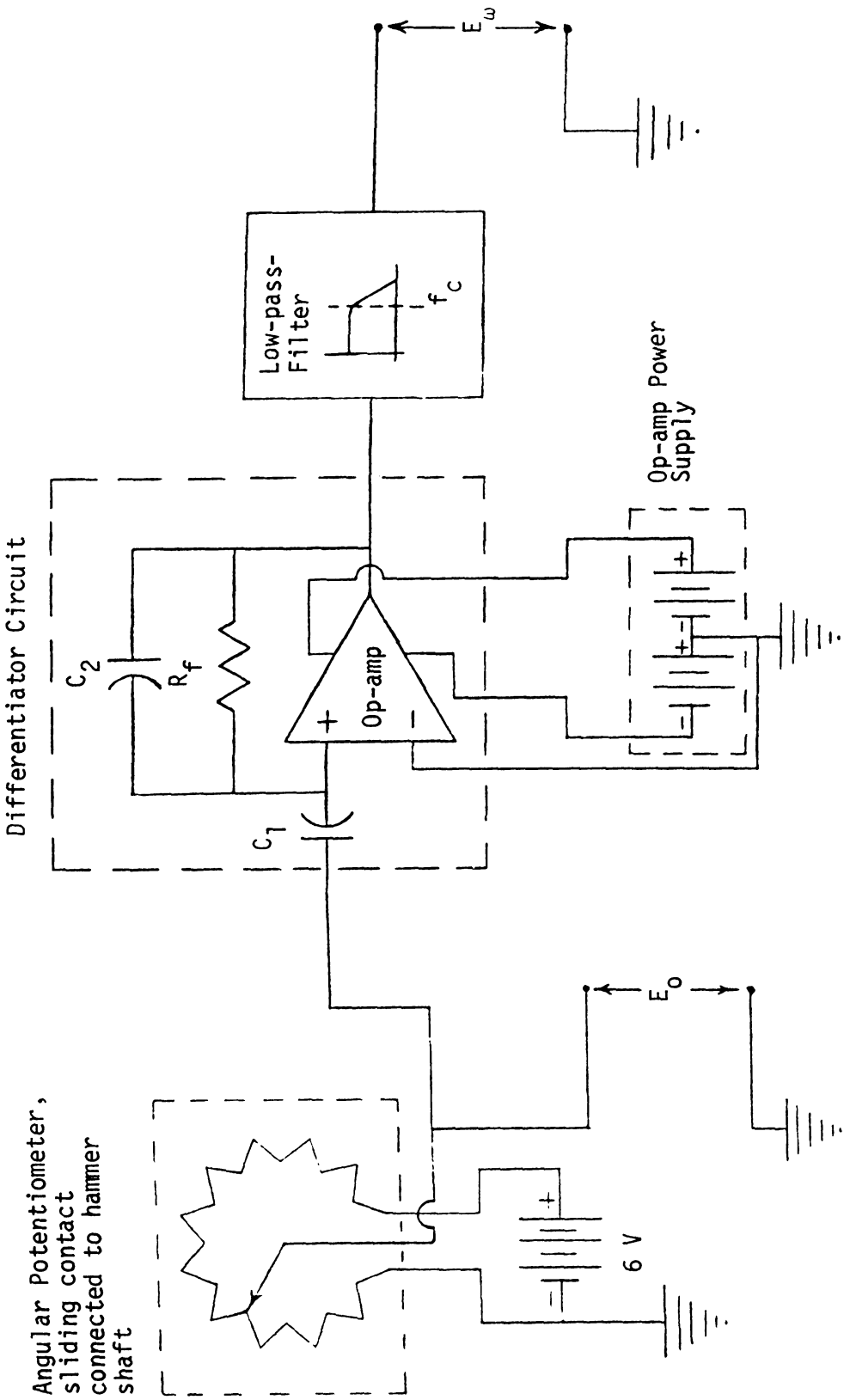

Figure 17. Hammer Velocity Circuit

and a Tektronix, type 3A3, dual-trace vertical-amplifier. An oscilloscope camera was used to provide permanent records of the signals.

It was necessary to determine the following velocity circuit parameters:

a) input capacitor, C_1,

b) feed-back resistor, R_f .

c) damping capacitor, C_2 ,

d) low-pass-filter cut-off frequency, f_c .

Standard practice when using a μA741 op-amp with a ± 15 VDC power supply is to choose R_f = 0.1 MΩ . Experimentally, C_1 was selected as 1μf. These values of R_f and C_1 enabled the op-amp to operate below its saturation level. This would assure that distortion of the output signal due to saturation would not occur.

The damping capacitor, C_2, is necessary to reduce the noise on the output of the differentiator. Caution must be exercised in selecting C_2. A large value would reduce the desired output signal along with the noise. The largest value found for C_2 that did not affect the output signal was 0.01μf. However, this value did not completely eliminate the noise.

The low-pass filter was used to further reduce the noise. As with the damping capacitor, the filter could also reduce the desired output signal. A cut-off frequency, f_c, of 200 Hz was experimentally selected.

The angular velocity, ω, of the hammer was determined from the equations of the differentiator circuit. The output voltage, E_ω, of the circuit as a function of the input voltage, E_θ, is

$$E_{\omega} = - R_f C_1 (dE_{\theta}/dt) \quad .$$

Rearranging gives

$$\frac{dE_{\theta}}{dt} = - E_{\omega}/R_f C_1 \quad .$$

Then the angular velocity of the hammer is

$$\omega = - KE_{\omega}/R_f C_1 \quad ,$$

where K is a constant to be determined. The impact velocity occurs when E_{ω} reaches a maximum value, since the hammer is continually accelerating until impact. Therefore,

$$\omega \Big|_{impact} = - KE_{\omega} \Big|_{max}/R_f C_1 \quad . \qquad (2\text{-}11)$$

Now, it is necessary to determine the constant K. When the hammer is in contact with the specimen, $E_{\theta} = - E_{\theta} \Big|_{max}$. When the hammer is indexed to a raised position, through an angle θ, $E_{\theta} = 0$. The resulting equation for K is

$$K = - \theta/E_{\theta} \Big|_{max} \quad .$$

For this experiment it was determined that

$$K = - 0.78 rad/volt \quad . \qquad (2\text{-}12)$$

Substituting Eq. (2-12) into Eq. (2-11) gives

$$\omega \Big|_{\text{impact}} = 0.78 E_{\omega} \Big|_{\text{max}} / R_f C_1 \quad . \tag{2-13}$$

The impact velocity is then calculated from the maximum recorded value of E_{ω} with the use of Eq. (2-13). A value of $\omega \Big|_{\text{impact}}$ calculated from Eq. (2-13) was compared with a value of $\omega \Big|_{\text{impact}}$ obtained by graphically differentiating a typical E_{ω} record. The agreement of these velocities showed that the values of C_2 and f_c were satisfactory.

Figure 18 shows typical E_{ω} and E_{θ} traces. The bottom trace, E_{θ}, showed that the hammer rotated from the indexed position to the impact position in approximately 15 milliseconds. The reversed portion of the curve, approximately 28 milliseconds in duration, shows the rebound of the hammer. After rebound the hammer remains at rest as shown by the straight remaining-poriton of the curve. The top trace, E_{ω}, reaches a maximum value at the same time that the E_{θ} trace shows that impact has occurred. After impact the E_{ω} trace becomes negative then positive showing the hammer rebound velocity. The hammer velocity then becomes zero as shown by the straight remaining-portion of the trace. It can be seen that the E_{ω} trace is not the precise differential of the E_{θ} trace after impact has occurred. This is due to three of the parameters of the velocity circuit: the op-amp "slew" rate; the damping capacitor, C_2; and the low-pass filter cut-off frequency, f_c. The combined effect of these three parameters was to reduce the rate at which the differentiator circuit can respond to its input signal. However, since the E_{θ} voltage changes slowly before impact in comparison with the reversal of velocity after impact, the differentiator does give the true value of $E_{\omega} \Big|_{\text{max}}$.

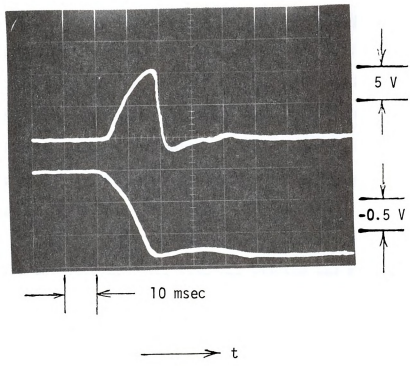

Top Trace: E_{ω} vs. time

Bottom Trace: E_{θ} vs. time

Figure 18. Typical E_{ω} and E_{θ} Traces

The circuit, which triggered the type 555 oscilloscope in order to record the strain signal, is shown in Figure 19. This circuit is based on one shown in the Silicon Photodetector Design Manual,* published by United Detector Technology. A laser beam from a continuous wave He - Ne, 4-milliwatt-output laser passed through the slot in the hammer holder and illuminated the photodiode. The photodiode was a type PIN-040A, manufactured by United Detector Technology. The op-amp was a Tektronix, type O. The values for R_f and E_b were experimentally determined. The values selected were R_f = 1MΩ and E_b = 6V. With the hammer in a raised position, the beam illuminated the diode and E_o = 70V. With the hammer in contact with the specimen, the beam was blocked and E_o = 0. The output voltage, E_o, was then used as the input to the type 555, oscilloscope, delayed-trigger, circuit. This allowed the starting time of the oscilloscope trace to be adjusted. The trace starting time could be set with ± 0.1 microsecond. This tolerance was necessary since the time period available for recording a tenths of microsecond rise time strain signal was about 0.6 microsecond.

The type 564 oscilloscope which recorded the hammer angle and velocity signals was triggered by the circuit shown in Figure 20. The sear engaged the indexing gear to hold the hammer in a raised position. When the plunger disengaged the sear from the indexing gear, the electrical circuit was completed. The resulting voltage, E_o, was then used as the input to the type 564, oscilloscope, trigger circuit.

The temperature was monitored on a standard thermocouple millivolt potentiometer.

---

* Manuals, Catalogs and Bulletins are listed in the Bibliography under manufacturer's name.

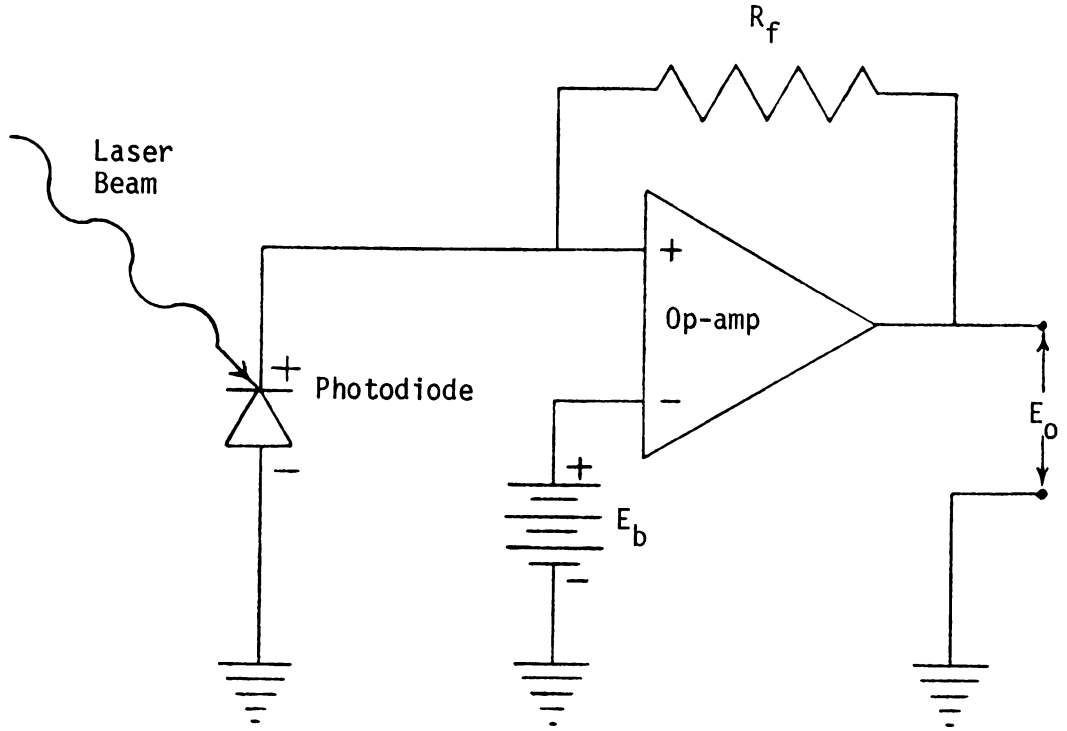

Figure 19. Strain Signal Trigger Circuit

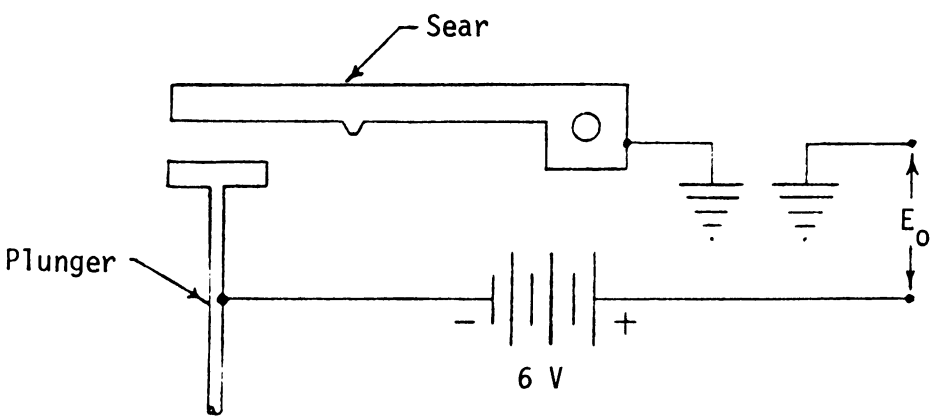

Figure 20. Hammer Velocity Trigger Circuit

2.3 Ball-Drop Apparatus

A ball-drop test fixture was constructed for the purpose of conducting two types of tests.

One test was to determine the strain gage output for less severe dynamic strain conditions. The strain-pulse amplitudes would be lower than the ones produced by the hammer-type apparatus. The strain pulse rise times would be on the order of 7 to 10 microseconds. The temperature range would be -100 to +300°F.

The second test was to verify the published test specimen material-properties data. The long wave velocity was measured in the temperature range of -100 to +300°F.

The ball-drop test fixture is shown in Figure 21. A 5/16-inch diameter ball dropped through a four-foot guide tube onto the end of the test specimen. The test specimen was 1/2 inch in diameter and 9 1/2 inches long. Two strain gages and one thermocouple were mounted on the specimen. The specimen was contained in an environmental chamber to control the specimen temperature. The trigger, strain and temperature instrumentation were the same as described in section 2.2.2.

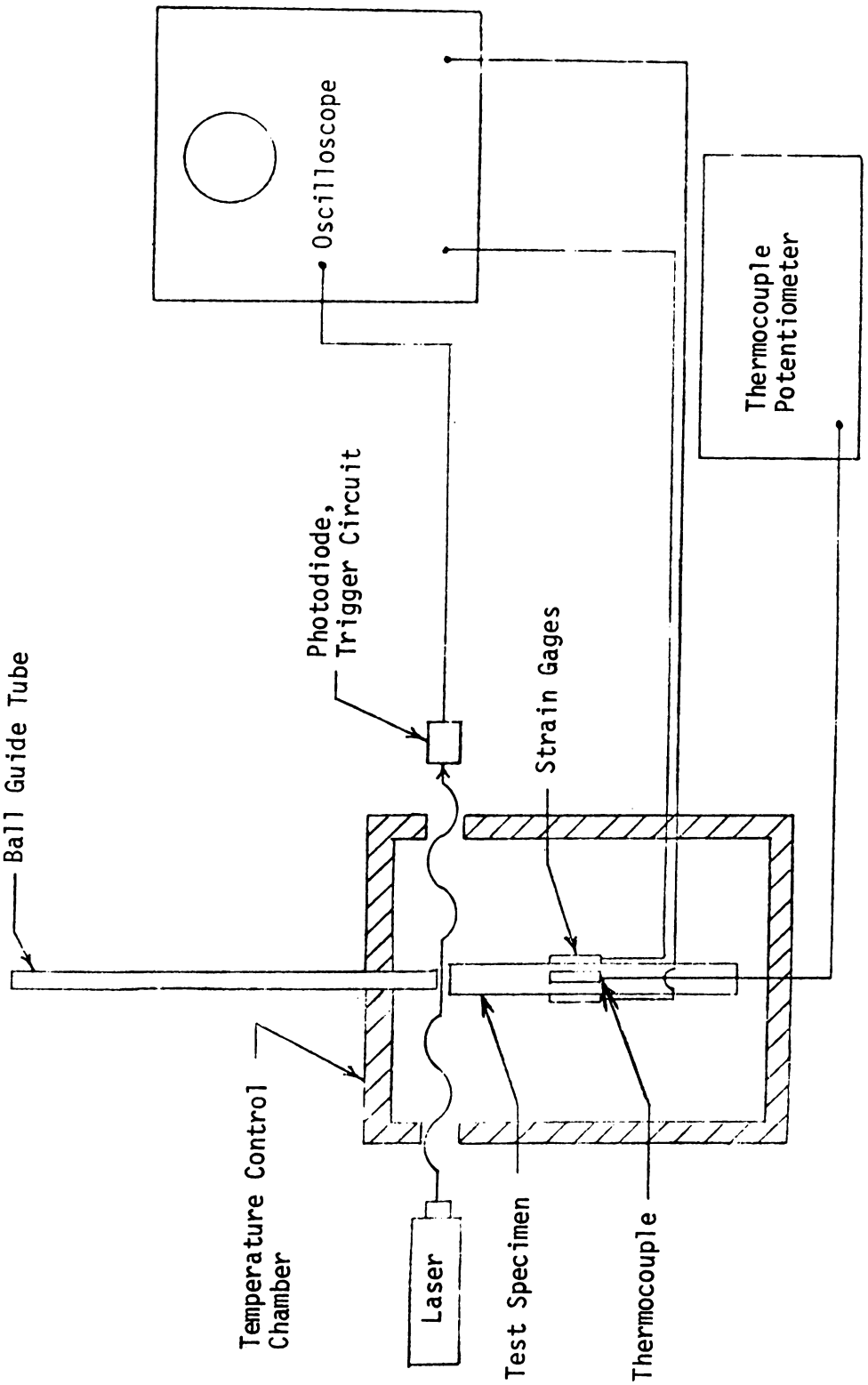

Figure 21. Ball Drop Test Apparatus

CHAPTER 3

SELECTION OF SPECIMEN MATERIAL AND STRAIN GAGES

3.1 Selection of Test Specimen Material

It has been noted that dispersion effects alter the rise time and amplitude of a step-wave as it travels along a specimen. If the dispersion effects are not recognized, this alteration of a step-wave might be attributed to the strain gage and/or the instrumentation system. In addition to a consideration of dispersion in a specimen, the effect that specimen temperature has on dispersion must be studied. When the effects of dispersion on traveling step-waves and the effects of temperature on dispersion are known, then a test specimen material can be chosen.

3.1.1 Dispersion and Temperature Effects

Davies (1948) thoroughly studied the Hopkinson pressure bar. He compared traveling wave properties as predicted by three theories. These were the elementary one-dimensional wave theory, the Pochhammer-Chree theory, and the Love theory. The Love theory will not be considered in this paper.

The elementary one-dimensional wave equation is

$$\frac{\partial^2 u(x,t)}{\partial t^2} = c_o^2 \frac{\partial^2 u(x,t)}{\partial x^2} \quad . \tag{3-1}$$

$$c_o = (E/\rho)^{1/2} \quad . \tag{3-2}$$

The only parameters considered in the one-dimensional theory are time, t, distance along the bar, x, partical displacement, u, bar density, ρ, and elastic modulus, E. This theory indicates that strain waves will travel along the bar at a velocity of c_o. This theory does not include any parameters related to the shape of the wave. This means that if a wave is composed of sine waves with various wave lengths, all of the waves will travel with the same velocity. Thus the phase velocity, c_p, and the group velocity c_g, between the sine waves are equal to c_o. Since these waves travel along the bar without shape change, they are called distortionless.

The general Pochhammer-Chree equations are exact for waves propagating in a circular cross section bar of infinite length. (see Love (1934), page 288, or Kolsky (1963), page 54). The boundary conditions at free ends of a finite length bar cannot be satisfied exactly for these equations, (see Love§201). Thus these equations cannot be solved in closed form for most test situations. This implies that specific dispersion effects cannot be determined for a particular test. Davies devised a method by which general dispersion effects could be studied. He

considered an infinite length bar that had a periodic initial displacement along its length. This allowed him to numerically solve for the first three roots of the Pochhammer-Chree frequency equations and to write the periodic initial-displacement in terms of a Fourier series. The frequence equations are given in Love, page 289, and Kolsky, page 57. The roots were then plotted with c_p/c_o as a function of a/Λ and $\nu = 0.29$. Here c_p is the phase velocity of sinusoidal waves traveling in the bar, a is the bar radius, Λ is the sinusoidal wave-length and ν is Poisson's ratio. The first root corresponds to the first longitudinal mode and is shown in Figure 22. The sinusoidal-wave group velocity, non-dimensionalized using c_o, is given by

$$\frac{c_g}{c_o} = \frac{c_p}{c_o} + \frac{a}{\Lambda} \frac{d(c_p/c_o)}{d(a/\Lambda)} \quad . \tag{3-3}$$

The curve of c_g/c_o as a function of a/Λ was calculated by differentiating the c_p/c_o curve and using Eq. (3-3). This curve is also shown in Figure 22.

It can be seen from Figure 22, that $c_p/c_o = 1$ and $c_g/c_o = 1$ only in the limit when a/Λ becomes zero (this is the reason that c_o is called the long wave velocity). Thus the general theory indicates that the propagation velocity of sinusoidal waves is a function of Λ, a, ν, E and ρ. Whereas according to the one-dimensional theory the propagation velocity of sinusoidal waves is only dependent on E and ρ. Therefore, the general

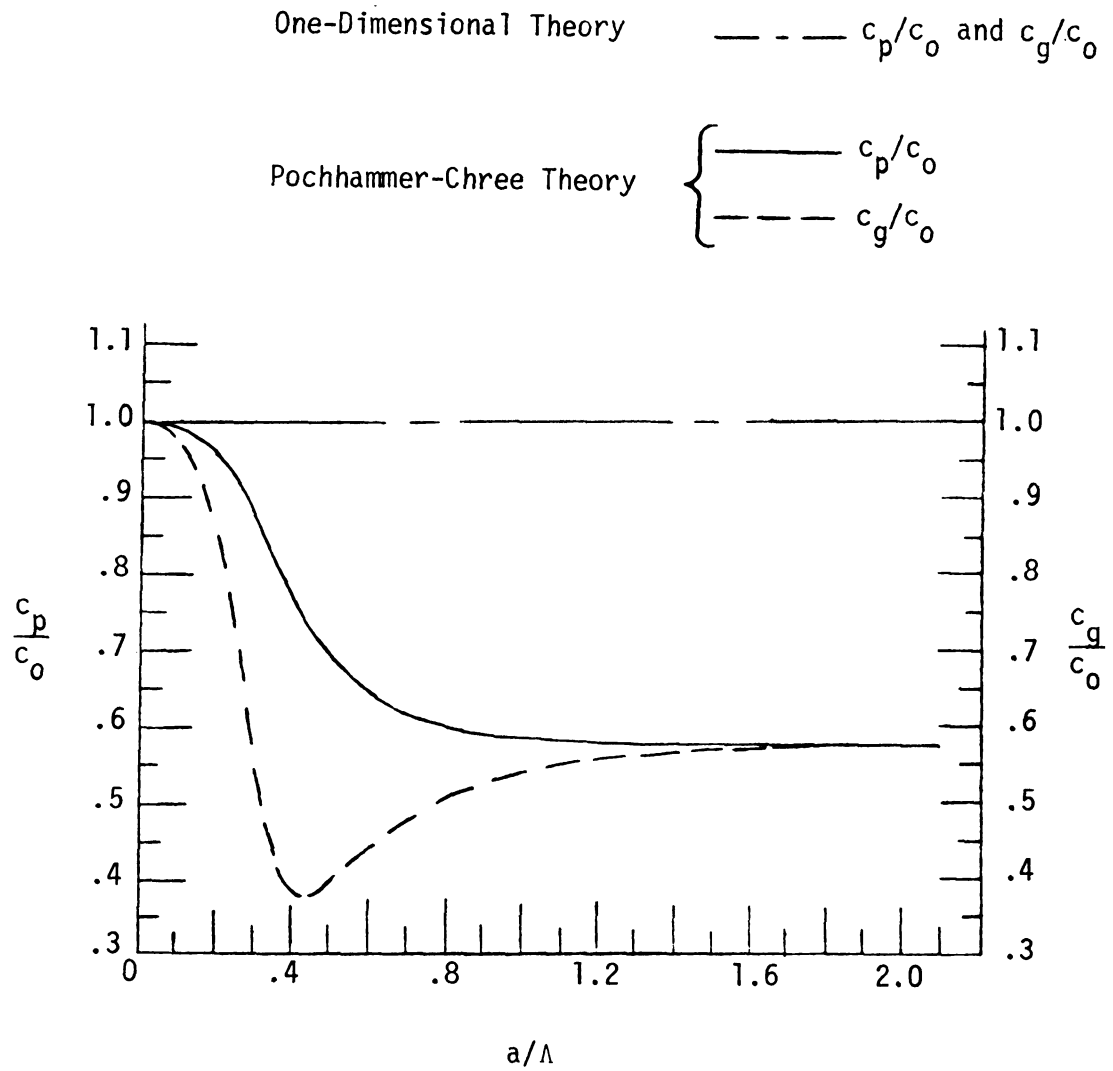

Figure 22. First Mode Phase and Group Velocities

equations imply that for any arbitrary wave that is resolvable into Fourier components, the relative phase of these components will vary with distance traveled. Dispersion will in general occur and any wave that is comprised of more than one sinusoidal component will suffer distortion as it travels along the bar.

Having determined the behavior of c_p/c_o and c_g/c_o, Davies then used the phase and group velocities along with Fourier's theorem to determine the dispersion effects on periodic waves. He considered a "trapezium-shaped" periodic wave and wrote the Fourier series for this wave. The n^{th} component of the Fourier series at a distance x from the origin was of the form

$$\beta_n \left\{ \begin{matrix} \text{Sin} \\ \text{Cos} \end{matrix} \right\} \left[n\omega_o (t - x/c_{pn}) - \phi_n \right] , \qquad (3\text{-}4)$$

where c_{pn} is the phase velocity of the n^{th} component and x/c_{pn} is the time it takes this component to travel the distance x. In order to evaluate the terms given by (3-4) it is necessary to evaluate the c_{pn} corresponding to the values of $n\omega_o$. From the relationship between frequency and wave length for sinusoidal waves, Davies derived the following equation.

$$\frac{an\omega_o}{c_o} = 2\pi \frac{c_{pn}}{c_o} \frac{a}{\Lambda} \quad . \qquad (3\text{-}5)$$

The quantity on the right hand side of this equation can be evaluated from Figure 22. Then a curve of c_{pn}/c_o as a function $an\omega_o/c_o$ can be plotted. This curve then gives the value of c_{pn} corresponding to a given

n when a and c_o are known. Thus using the curve of c_p/c_o as a function of $an\omega_o/c_o$ and the Fourier series, Davies determined the distortion of the "trapezium-shaped" wave as it traveled along the bar. These results are plotted in Figure 23, from Davies' paper. This plot shows, that as the "trapezium-shaped" wave traveled along the bar, the slope of the wave decreased, the amplitude increased, and superimposed sinusoidal-type oscillations appeared. Thus the rise time of a step-wave would increase, the amplitude would change and the shape would become distorted as the wave travels along the bar.

Davies concluded that two parameters greatly affect the distortion of a traveling wave: the radius of the bar and the distance that the wave travels. The assumption is made that the material property variables do not change along the bar. Therefore, when the dynamic response of a strain gage is to be studied by subjecting the gage to a traveling step-wave, the test specimen diameter should be as small as practical and the gage should be located as near to the source of the step-wave as possible.

The effects that test temperature have on dispersion can now be considered. The test specimen and apparatus were designed to minimize thermal gradients. Also the specimen temperature did not change during a test. Thus it can be assumed that temperature did not have a functional dependency on x or t. In Eq. (3-1), u is only a function of x and t with E and ρ considered as constants. The only way that temperature can be considered in this equation is to let E and ρ be functions of temperature, since the temperature is not a function of x or t. For these conditions, c_o is a constant for any given temperature. The temperature effect on the solutions of Eq. (3-1) can be seen to be only a change in the velocity c_o. Thus temperature changes do not affect the wave shapes which are

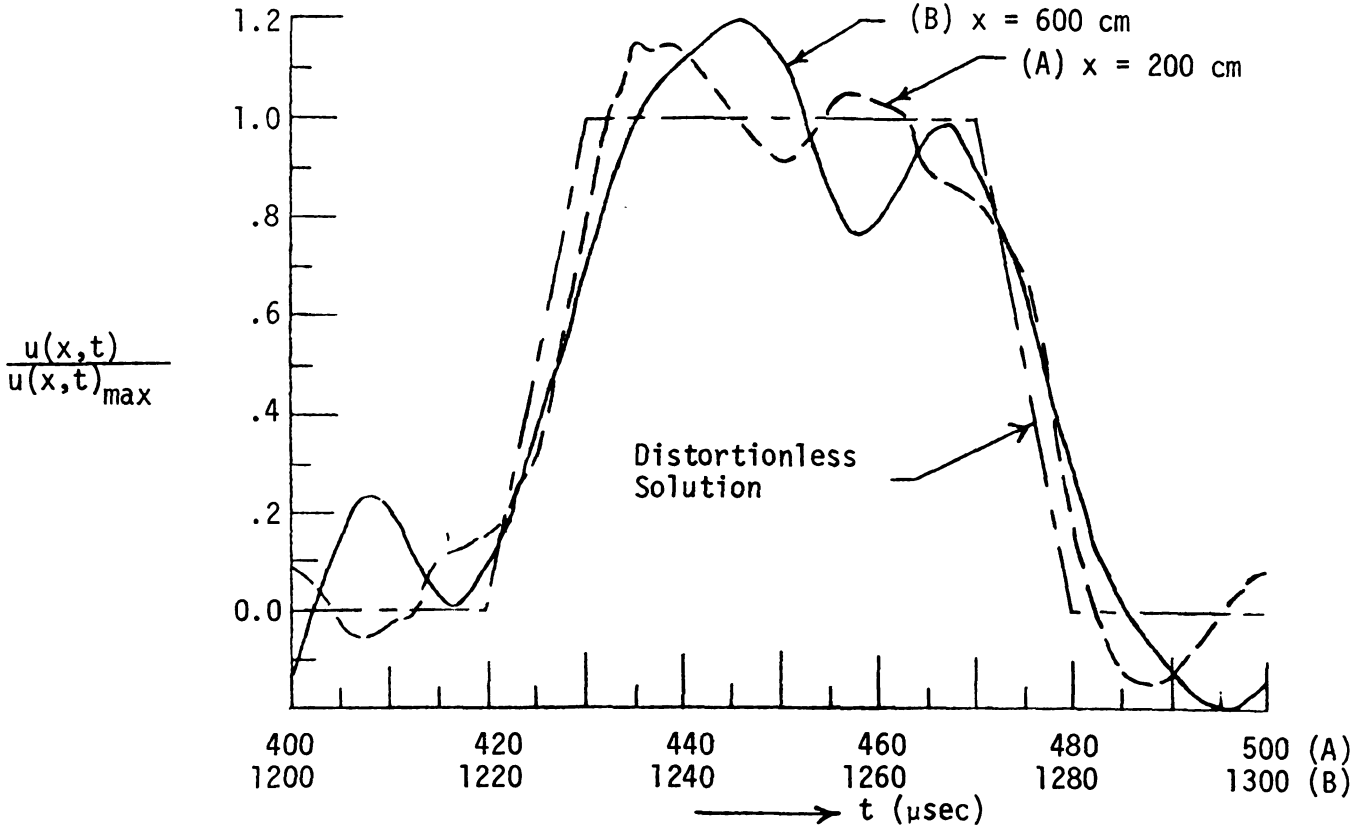

Figure 23. Distortion of Wave Shape Due to Dispersion

solutions to Eq. (3-1).

The Pochhammer-Chree equations, like the one-dimensional equation, do not have a functional dependency on temperature. However, if the bar temperature is not a function of x or t, we can introduce temperature effects into these equations by letting c_o be a function of temperature. Reviewing Figure 22, Eq. (3-5) and the n^{th} series component (3-4), we can determine the effect on distortion that a varying c_o produces.

The strain gages are bonded to the specimen, thus the value of x is fixed. Substituting a fixed value of x into the n^{th} component (3-4) and knowing c_{pn} then gives the time that it takes the n^{th} component to reach the fixed x position. Assuming that a is known, the curve of the relation between c_{pn}/c_o and $an\omega_o/c_o$ determines the c_{pn} values. Since this curve is based on the c_p/c_o curve in Figure 22 and Eq. (3-5), it is non-linear. Therefore, c_{pn} will be a non-linear function of c_o. This implies that the time it takes the n^{th} component to reach the fixed x location is a non-linear function of c_o. For a particular gage location therefore, the wave, which is the sum of the Fourier series components, will change its shape as c_o varies. In order to eliminate the temperature effect on a traveling step-wave, a material that has a constant c_o over the test temperature range must be selected.

3.1.2 Test Specimen Material

During the 1890's two iron-nickel alloys named Invar and Elinvar were developed by Charles E. Guillaume. Their thermoelastic coefficients were nearly zero over a wide temperature range. The thermoelastic coefficient is defined as the change in modulus of elasticity divided by the change in temperature. Since the discovery of Invar and Elinvar, many other

iron-nickel alloys of special thermoelastic properties have been developed. Specific thermoelastic coefficients in these alloys can be achieved by proper cold-working and heat-treating. One of these alloys named Ni-Span-C Alloy 902* or Elinvar Extra** was investigated in order to determine if its long wave velocity, c_o, could be maintained as a constant over the desired test temperature range.

The long wave velocity is given by $c_o = (E/\rho)^{1/2}$. Therefore, if c_o is to remain constant over the test temperature range, then E/ρ must also remain constant.

The thermal expansion and elastic modulus properties of Ni-Span-C, obtained from Bulletin T-31, International Nickel Co. Inc., 1963, are shown in Figures 24 and 25. Figure 24 shows the linear expansion characteristic. The linear coefficient of thermal expansion, α, is the slope of this curve. The volume coefficient of thermal expansion is given by

$$\beta \simeq 3\alpha \quad . \tag{3-6}$$

Equation (3-6) and Figure 24 show that β is a positive constant in the temperature range of -100 to +300°F. The volume of the test specimen at the test temperature is then given by

$$V = V_r[1 + \beta\,(T - T_r)] \quad , \tag{3-7}$$

---

* Registered Trade Mark, International Nickel Company,

** Registered Trade Mark, Hamilton Watch Company,

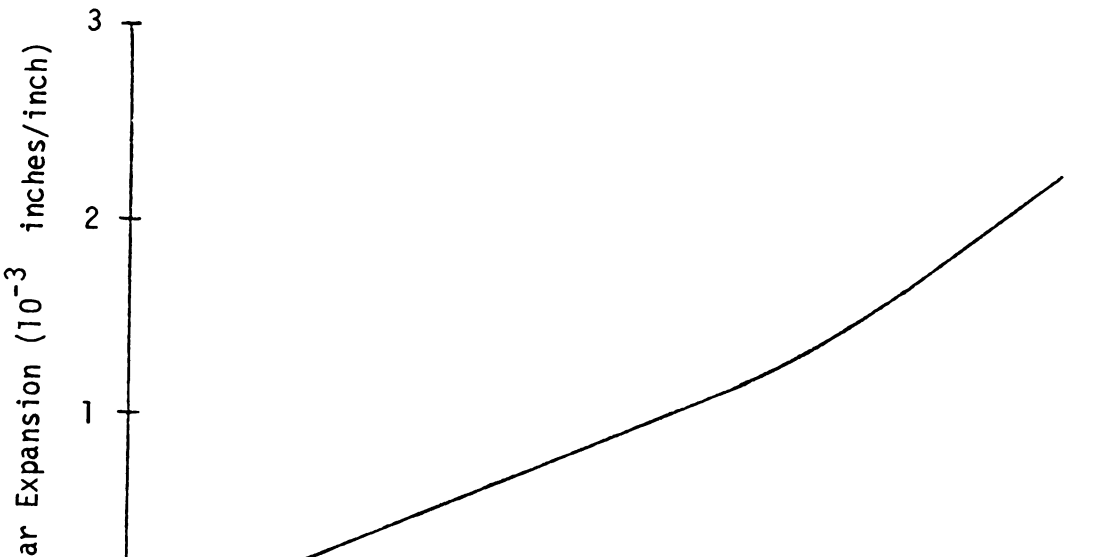

Figure 24. Thermal Expansion Characteristic

where V_r is the volume of the test specimen at the reference temperature T_r. The density of the specimen is then given by

$$\rho = m/V \quad , \tag{3-8}$$

where m is the mass of the test specimen. Substituting Eq. (3-7) into Eq. (3-8) gives the density of the test specimen at the test temperature as

$$\rho = \rho_r/[1 + \beta\,(T - T_r)] \quad , \tag{3-9}$$

where

$$\rho_r = m/V_r \quad .$$

Equation (3-9) shows that the specimen density will decrease with increasing temperature.

Figure 25 shows the effect that cold-working and heat-treating has on Ni-Span-C. The top graph shows that for a 50% cold-work and a heat-treatment of 900°F for 5 hours, the modulus of elasticity decreases with temperature up to 280°F. The middle graph shows that the modulus is almost a constant up to 280°F for a heat-treatment of 1000°F for 5 hours. The bottom graph shows that the modulus increases with temperature up to 280°F for a heat-treatment of 1300°F for 5 hours. The sharp rise and knee of these curves are due to the magnetic behavior of the material. As the Curie temperature is reached the material changes from ferromagnetic to paramagnetic behavior, causing the knee in the curves. Thus Figure 25

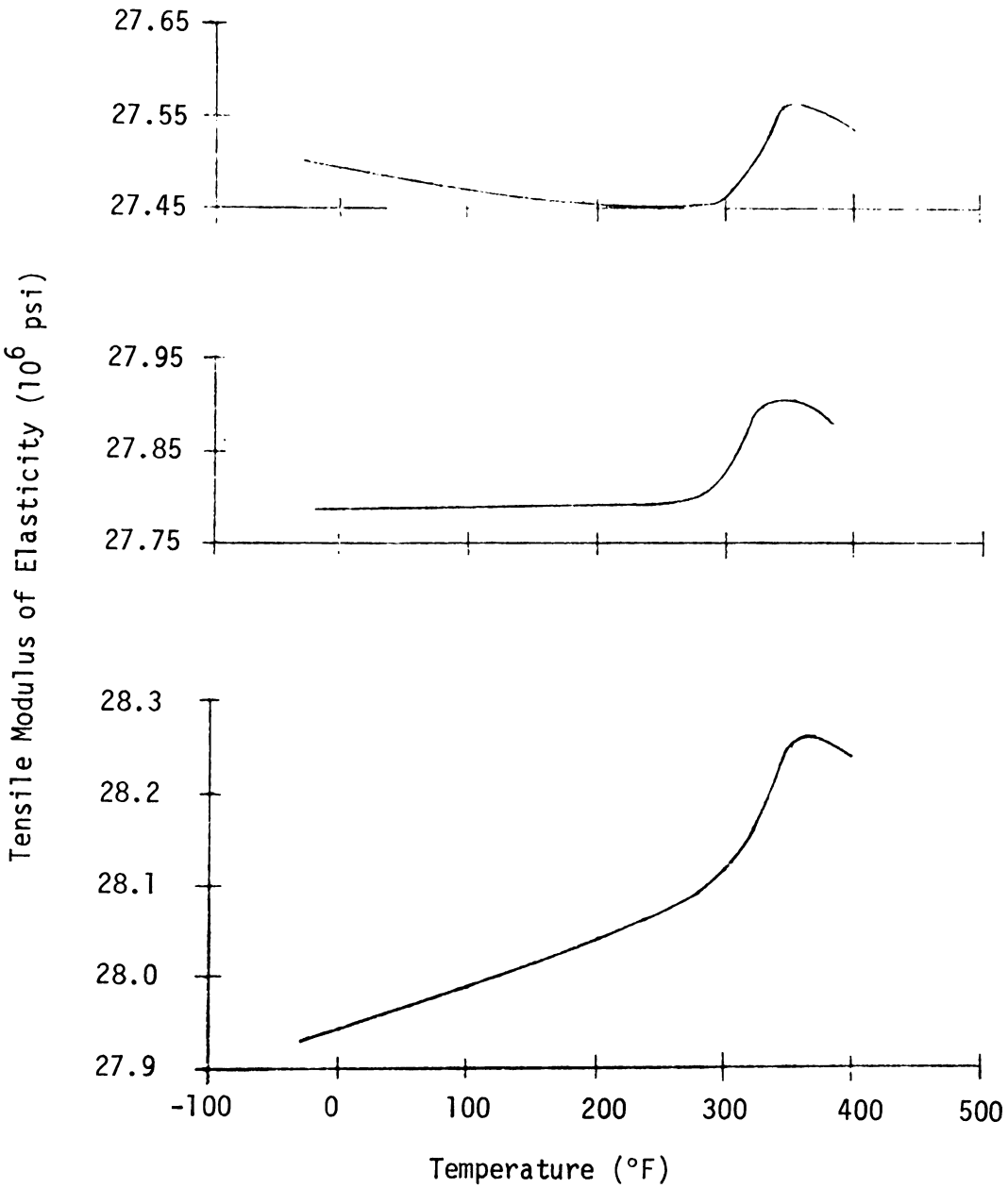

Material cold-worked 50% prior to heat treatment

Heat treatment

top : 900°F, 5 hours
middle : 1000°F, 5 hours
bottom : 1300°F, 5 hours

Figure 25. Effect of Heat Treatment on Modulus of Elasticity

indicates that the slope, ψ, of the modulus of elasticity versus temperature curve can be selected within a range of negative to positive values. The modulus of the test specimen at the test temperature can then be given by

$$E = E_r[1 + \psi\ (T - T_r)] \quad , \tag{3-10}$$

with

$$T < 280°F \quad ,$$

where E_r is the modulus measured at the reference temperature T_r. The long wave velocity can then be written in terms of Eq. (3-9) and Eq. (3-10) as

$$c_o = \sqrt{\frac{E_r}{\rho_r}}\,[1 + \psi(T - T_r) + \beta(T - T_r) + \psi\beta(T - T_r)^2]^{1/2} \quad . \tag{3-11}$$

If ψ is selected such that

$$\psi = - \beta \tag{3-12}$$

then Eq. (3-11) reduces to

$$c_o = \sqrt{\frac{E_r}{\rho_r}}\,[1 - \beta^2(T - T_r)^2]^{1/2} \quad . \tag{3-13}$$

From Figure 24 and Eq. (3-6), β can be determined as

$$\beta \simeq 12 \times 10^{-6}/°F \quad . \tag{3-14}$$

For these tests, $T_r = 75°F$, $T\,\big|_{max} = 300°F$ and $T\,\big|_{min} = -100°F$. Thus

$$(T - T_r)\,\big|_{max} = 225°F \quad . \tag{3-15}$$

The values of Eqs. (3-14) and (3-15) when substituted into Eq. (3-13) show that c_o will be essentially constant over the test temperature range if $\psi = - \beta$.

Table 2. Long Wave Velocity

Test Temperature (°F)	Average c_o (10^5 in/sec)	One σ Standard Deviation of c_o (10^5 in/sec)
-100	1.86	0.02
-40	1.85	0.01
0	1.86	0.02
52	1.86	0.03
70	1.85	0.02
100	1.85	0.02
150	1.85	0.02
200	1.85	0.05
250	1.84	0.03
300	1.85	0.02

Maximum variation from the average room temperature value is $\pm$ 0.54%.

The Ni-Span-C material used in this experiment was 50% cold-worked and in an annealed condition as-received from the manufacturer. For this condition ψ would be negative. The values of c_o were measured using the ball-drop test apparatus. The ball was dropped on the end of the test specimen. The time between successive reflections of the resulting strain pulse was recorded. The values of c_o were calculated using these times and the length of the test specimen. The results are shown in Table 2. The values of c_o as a function of temperature were acceptable when the

Ni-Span-C material was in the as-received condition. Therefore additional cold-working or heat-treating were not performed on the test specimen.

3.2 Selection of Strain Gages and Mounting Adhesive

Metal foil and semi-conductor strain gages are the two most widely used types of gages. Foil gages are commercially available in a wide variety of sizes and shapes. In addition these gages are inexpensive. The above characteristics enable this type of gage to be employed for the majority of strain measuring applications. Semi-conductor gages are more limited in available sizes and configurations. They are 10 to 20 times more expensive than foil gages. However, semi-conductor gages have sensitivities which are 50 to 70 times greater than those of foil gages. This greater sensitivity enables the semi-conductor gage to measure smaller strain than foil gages. Also, in certain applications where the strain can be measured by both types of gages, the higher sensitivity of the semi-conductor gage may allow the use of less expensive instrumentation. Thus, both types of gages were chosen to be tested.

The foil gage selected for this experiment was type ED-DY-031CF-350, manufactured by Micro-Measurements. The following explains the gage nomenclature code.

E: polyimide backing material

D: isoelastic foil alloy

DY: gage not available in self-temperature-compensated form

031: 0.031 inch active gage length

CF: grid and solder tab geometry

350: 350Ω unstrained resistance

This gage type was chosen for the following reasons.

The isoelastic foil, polyimide backed gage was designed for measuring dynamic strains. This gage can be used over a temperature range of -320 to +400°F. It has a usable strain range of $\pm$2% but becomes non-linear for strain levels over $\pm$0.5%. The 0.031 inch active gage length was chosen in order to measure sub-microsecond rise time strain-pulses. The CF grid and solder tab geometry has the tabs at one end of the gage. Thus, the strain-pulse will have traversed the active element of the gage before reaching the tabs. The 350Ω unstrained resistance was the standard resistance available for isoelastic alloy gages. This gage type was selected based on information given in Micro-Measurements Catalog 200. The suitability of this gage for the present experiment was confirmed by correspondence with application engineers at Micro-Measurements.

The semi-conductor gage selected for this experiment was type SPB3-06-12, manufactured by BLH Electronics, Inc. The following explains the gage nomenclature code.

S: silicon filament material

P: positive strain sensitivity

B: phenolic glass backing material

3: lead configuration

06: 0.06 inch active gage length

12: 120Ω nominal unstrained resistance

This type was chosen for the following reasons. The SPB series can be used to measure dynamic strains. The phenolic glass backing can be used over a temperature range of -423 to +500°F. It has a usable strain range up to +0.3%, and essentially without a negative limit. The number 3 lead configuration was chosen to facilitate mounting the gage on the specimen. The 0.06 inch active gage length was chosen because it was the

shortest length readily available. This type gage was selected based on information given in BLH Electronics Bulletin 102-2. The choice of this type was confirmed by a conversation with application engineers at BLH Electronics.

The mounting adhesive was M-Bond 610, manufactured by Micro-Measurements. This bonding material was chosen because it can be used over a temperature range of -452 to +450°F. The adhesive elongation capability ranges from 1% at -452°F to 3% at +450°F. This adhesive was also recommended for dynamic testing. This adhesive was selected based on information given in Micro-Measurements Instruction Bulletin B-130. The choice of this adhesive was confirmed by correspondence with application engineers at Micro-Measurements.

CHAPTER 4

EXPERIMENTAL PROCEDURE AND RESULTS

4.1 Experimental Procedure

4.1.1 Ball Drop Tests

The test specimen and ball guide tube were installed in the temperature control chamber. The vertical alignments of the specimen and guide tube were checked with a spirit level. The temperature control chamber was a low temperature electric furnace with thermostatic control. The laser beam, used to trigger the oscilloscope, passed through the furnace and between the ends of the guide tube and specimen. The oscilloscope, photodiode trigger circuit, thermocouple potentiometer and strain gage potentiometer circuit were turned on one-half hour before the tests were performed. This allowed the instrumentation to reach steady state operating condition.

The tests were performed using the following procedure.

a) The oscilloscope sweep speed was set at 10 microseconds per division for the strain gage tests and 0.1 millisecond per division for the long wave velocity tests. The oscilloscope sweep-trigger was set on delayed single sweep.

b) The gains of the two oscilloscope vertical amplifiers were set at values that were appropriate for each type of gage.

c) The temperature of the specimen was then raised or lowered to the

desired value. For the test temperatures above room temperature, the specimen was heated using the furnace and its thermostatic control. The specimen was heated at a rate of 150°F per hour until it reached the desired test temperature. The furnace and specimen were held at each test temperature until the desired number of tests were conducted. After the 300°F tests were completed, the furnace was allowed to cool at a rate of 150°F per hour. The furnace and specimen were again held at each test temperature and the tests were repeated.

For the test temperatures below room temperature, the furnace was filled and the specimen was surrounded with dry ice. The strain gages were shielded in order to prevent their direct contact with the dry ice. The dry ice cooled the specimen at a rate of 50°F per hour. After the test specimen reached -100°F, most of the dry ice was removed from the furnace. As the remaining dry ice sublimed, the specimen temperature increased at a rate of 50°F per hour. There was no means of stabilizing the specimen temperature at each cold test point. Thus the tests were started when the specimen was within 2°F of the test temperature and were completed before the temperature was 2°F beyond the test temperature. The test specimen temperature was monitored using the iron-constantan thermocouple.

d) The oscilloscope camera shutter was opened and held open until the ball impacted the specimen.

e) The ball was dropped down the guide tube.

f) When the ball broke the laser beam, the oscilloscope trace was delay triggered and the strain signal was recorded.

g) The ball was retrieved through the top end of the guide tube with a magnet-tipped rod. This prevented thermal gradients in the specimen that

would have been produced by opening the furnace door.

h) The bonded resistance, R_g, of the semi-conductor gage was measured at each test temperature. A precision resistance bridge was used to determine the gage and lead wire resistance within $\pm 0.1\Omega$. A jumper wire was placed across the gage solder tabs inorder to measure the lead wire resistance. A typical resistance valve of the lead wire was 1 Ω. The lead wire resistance was subtracted from the measured resistance in order to determine the actual gage resistance.

i) The gage type, test temperature, gage potentiometer circuit, supply-voltage, semi-conductor gage resistance and oscilloscope settings were recorded.

Strain pulse and long wave velocity tests were conducted at -100, -40, 0, 52, 70 to 75 (room temperature), 100, 150, 200, 250, and 300°F. At each test temperature 8 to 10 strain pulse and 4 to 6 long wave velocity tests were performed.

4.1.2 Hammer Tests

The test specimen and hammer assemblies were lapped, polished and checked for flatness. The two assemblies were then cleaned in an ultrasonic cleaner. The hammer and specimen assemblies were mated using three 3/16 inch cap bolts. The bolts were tightened to approximately 25 pound inches. The hammer drive and transducer assemblies were fastened to the hammer assembly. The entire test apparatus was then mounted to the base of the vacuum chamber. All electrical connections were made. The velocity-signal trigger-circuit, strain-signal trigger-circuit, and angular potentiometer circuit were checked for proper operation. The sear, rack and pinion, plunger and drive spring pre-load were also checked. The vacuum bell jar was placed over the system and a vacuum was drawn inside of the chamber. The two oscilloscopes, photodiode trigger circuit,

thermocouple potentiometer, strain gage potentiometer circuit, differentiator circuit and low-pass filter were turned on one-half hour before the tests were preformed. This allowed the instrumentation to reach steady state operating condition.

The tests were performed using the following procedure.

a) The horizontal sweep of the type 555 oscilloscope (which displayed the strain signal) was set at an appropriate value for the test being conducted. The oscilloscope sweep-trigger was set on delayed single sweep.

The horizontal sweep of the type 564 oscilloscope (which displayed the hammer angular position and velocity signals) was set at 10 milliseconds per division. The oscilloscope sweep-trigger was set on single sweep.

b) The gain of the vertical amplifier used in the type 555 oscilloscope was set at a value that was appropriate for the type of gage being used and for the test being conducted.

The gains of the dual-trace vertical amplifier used in the type 564 oscilloscope were set at 5 volts per division for the hammer angular velocity signal and 0.5 volt per division for the hammer angular position signal.

c) The temperature of the specimen was then raised or lowered to the desired value. For the test temperatures above room temperature, the specimen was heated using hot air supplied by the heat gun. The specimen was heated at a rate of approximately 200°F per hour until it reached the desired test temperature. The specimen temperature was held at the desired test point by controlling the flow rate of the heated air by the use of a valve. In addition, the heat gun heating element was cycled on and off. The specimen was kept at each test temperature until the desired number of

tests were conducted. After the 300°F tests were completed, the specimen temperature was reduced at a rate of about 200°F per hour. The specimen was again held at each test temperature and the tests were repeated.

For the test temperatures below room temperature, the specimen was cooled using cold gaseous nitrogen drawn from a reservoir of liquid-nitrogen. The specimen was cooled at a rate of approximately 150°F per hour until it reached the desired test temperature. The specimen temperature was held at the desired test point by controlling the boil-off rate and thus the flow rate of the gaseous nitrogen by means of a valve on a vacuum line. After the -100°F tests were completed, the specimen temperature was increased at a rate of 150°F per hour. The specimen was again held at each test temperature and the tests were repeated. The test specimen temperature was monitored using the iron-constatan thermocouple.

d) The sear was disengaged from the indexing gear by the use of the plunger. The hammer was rotated to an angle of 56.25° and the sear re-engaged with the indexing gear.

e) The shutter of each oscilloscope camera was opened and held open until the hammer impacted the specimen.

f) The plunger was operated which dis-engaged the sear from the indexing gear. This allowed the hammer to impact the specimen and also triggered the type 564 oscilloscope recording the hammer angular velocity and angular position signals.

g) When the hammer broke the laser beam, the type 555 oscilloscope trace was delay triggered and the strain signal was recorded.

h) The hammer was immediately re-indexed to the 56.25° position to prevent heat transfer from the specimen to the hammer.

i) The bonded resistance, R_g, of the semi-conductor gage was measured to

within $\pm 0.1\Omega$ at each test temperature. The lead wire resistance was subtracted from the measured resistance in order to determine the actual gage resistance.

j) The gage type, test temperature, gage potentiometer circuit supply-voltage, angular potentiometer supply-voltage, semi-conductor gage resistance and oscilloscope settings were recorded.

The microsecond strain-pulse tests were conducted at -100, -45, 0, 50, 72 to 75 (room temperature), 100, 150, 200, 250 and 300°F. At each test temperature 10 to 16 strain-pulse tests were preformed.

The sub-microsecond strain-pulse tests were conducted at 74°F. For each gage 6 to 8 strain-pulse tests were performed.

4.2 Data Reduction

4.2.1 Data Measurement

The photographic records of the strain pulses were projected onto a vertical drawing surface by the use of an opaque projector. The projections had grid line divisions of two inches compared to the one centimeter divisions on the photographic records. The oscilloscope trace of the strain pulse and the grid lines were copied onto plain paper. The strain-pulse amplitude and rise time were measured with a variable scale rule. The basic division on the rule was set to the grid line division of each copy. This eliminated any errors that might be produced by a variation in enlargement between copies. The enlarged grid lines were approximately 3/32 inch wide. Thus the grid divisons could be measured to within $\pm 1/40$ division. The enlarged trace widths were approximately 3/16 inch. Therefore, the data could be read to within $\pm 1/20$ division.

4.2.2 Foil-Gage Data-Reduction Equations

The relation between the change of resistance produced in a foil gage due to an applied strain is given by

$$\Delta R_g/R_g = \varepsilon GF_T \quad , \tag{4-1}$$

where GF_T is the test temperature gage factor and ε is the applied strain. The strain can be determined from the strain-gage potentiometer-circuit output-voltage by the use of Eq. (2-9) and (4-1). Multiplying the right hand side of Eq. (2-9) by R_g/R_g, setting $R_b = R_g$ and applying Eq. (4-1) we have

$$\varepsilon = 4E_o/E_b GF_T \quad . \tag{4-2}$$

The copies of the photographic records were used to determine the amplitude deflection of the strain-pulse trace. The value of E_o was then calculated with the following equation.

$$E_o = \Delta_\varepsilon G_\varepsilon \quad , \tag{4-3}$$

where Δ_ε is the trace deflection in divisions and G_ε is the oscilloscope vertical-amplifier gain in volts per division.

The gage factor variation as a function of temperature in the form of a graph was supplied by the gage manufacturer. An equation expressing the gage factor as a function of temperature was obtained by using the least-square technique to curve fit the graphical data. The resulting equation

was

$$GF_T = GF[0.99946 + 1.15 \times 10^{-4}(T) - 4.46 \times 10^{-7}(T)^2] \quad , \qquad (4\text{-}4)$$

where GF is the gage factor at room temperature.

The strain-pulse rise-time was calculated with the following equation.

$$t_R = \Delta_t G_t \quad . \qquad (4\text{-}5)$$

The copies of the photographic records were used to determine the rise-time deflection, Δ_t in divisions, of the strain pulse trace. The oscilloscope horizontal-amplifier gain was G_t in seconds per division.

The average values of the strain amplitude and rise-times at each test temperature were calculated with the equation

$$\bar{y} = \sum_{i=1}^{N} y_i/N \quad . \qquad (4\text{-}6)$$

The average value is $\bar{y}$ and the y_i are the values in a set of measurements. The number of measured values in the set is N. The standard deviation of the data at each test temperature was calculated using

$$\sigma = \left[\sum_{i=1}^{N} (y_i - \bar{y})^2/(N - 1)\right]^{1/2} \quad . \qquad (4\text{-}7)$$

4.2.3 Semi-conductor Data-Reduction Equations

Semi-conductor strain gages have a highly non-linear behavior with regard to strain amplitude and temperature. Thus the data reduction for semi-conductor gages is more complex than the data reduction for foil gages.

The 0°F unbonded gage resistance, R_{oo}, is determined from the equation

$$R_o/R_{oo} = 1 + V_2T_o + V_3T_o^2 \quad . \tag{4-8}$$

The unbonded gage resistance, R_o, is measured at a temperature T_o. The values of $R_o = 127.8\Omega \pm 1\%$, $T_o = 77 \pm 3°F$, $V_2 = -2.8 \times 10^{-6}$ and $V_3 = 2.3 \times 10^{-6}$ were supplied by the gage manufacturer. Then the test temperature unbonded gage resistance, R_{oT}, is given by

$$R_{oT} = R_{oo}(1 + V_2T + V_3T^2) \quad . \tag{4-9}$$

There are three sources of strain that act on a resistance strain gage sensing element. First, the element has a pre-strain due to bonding the gage onto the specimen. Second, the sensing element experiences a strain due to the different coefficients of thermal expansion of the element and the specimen. Third, the sensing element is strained due to the load applied to the specimen. The relation between the change of resistance produced in a semi-conductor gage due to all three strains is

$$\Delta R_t/R_{oT} = GF'(T_o/T)\varepsilon_t + C_2'(T_o/T)^2\varepsilon_t^2 \quad . \tag{4-10}$$

The values of T_o and T in Eq. (4-10) must be converted to absolute temperature. The total strain sensed by the element is ε_t. The values of GF' = 115.5 $\pm$ 2% and C_2' = 4500 $\pm$ 9% were supplied by the gage manufacturer. The change in gage resistance, ΔR_t, due to all three strains must be referenced to the unbonded resistance, R_{oT}. The change in resistance ΔR_t, is given by the equation

$$\Delta R_t = R_{oT} - (\Delta R_g + R_g) \quad . \tag{4-11}$$

The gage resistance, R_g, was measured at each test temperature. Thus R_g included the change in resistance due to bonding and thermal expansion. The change in resistance, ΔR_g, due to the strain pulse was determined from Eq. (2-10). Since the value of R_g changed by approximately 30% over the test temperature range, $R_b \neq R_g$. Thus solving Eq. (2-10) for ΔR_g gives

$$\Delta R_g = (1/2)(R_b + R_g)\left[1 - \sqrt{1 - 4E_o(R_b + R_g)/E_b R_g}\right] \quad . \tag{4-12}$$

It was required that $\Delta R_g = 0$ when $E_o = 0$, therefore, the negative radical sign was chosen. The value of E_o was calculated From Eq. (4-3). The ballast resistor, R_b, was fixed at 120Ω.

The relation between the change of resistance produced in the gage due to the bonding and thermal expansion strain is given by

$$\Delta R_B/R_{oT} = GF'(T_o/T)\varepsilon_B + C_2'(T_o/T)^2\varepsilon_B{}^2 \quad . \tag{4-13}$$

The bonding and thermal expansion strain is ε_B. The change in gage

resistance, ΔR_B, due to bonding and thermal expansion strain, must be referenced to the unbonded resistance R_{oT}. The change in resistance, ΔR_B is given by

$$\Delta R_B = R_{oT} - R_g \quad . \tag{4-14}$$

Equation (4-10) was solved for ε_t with the use of Eqs. (4-11) and (4-12). Equation (4-13) was solved for ε_B with Eq. (4-14). Since GF' was positive, the positive radical sign was used in solving for ε_t and ε_B. The amplitude of the strain pulse is then given by

$$\varepsilon = \varepsilon_t - \varepsilon_B \quad . \tag{4-15}$$

The strain pulse rise time was determined using Eq. (4-5). The mean value and the standard deviation of the strain pulse amplitude and rise time were determined using Eqs. (4-6) and (4-7).

The computer programs used for the data reduction are listed in Appendix C.

4.3 Ball Drop, Temperature-Test Results

The purpose of the ball drop tests was to determine the temperature effects on the strain gage output when the gages were subjected to "low" amplitude, "long" rise time strain pulses. The strain pulses for the tests had amplitudes of approximately 65 microinches per inch and rise times of approximately 7 microseconds.

One-dimensional wave propagation theory can be used to arrive at an approximate strain-pulse amplitude produced by a ball impacting the end of a rod. From this theory, the maximum amplitude of the initial strain pulse is given as

$$\varepsilon\,|_{max} = v/c_o \quad , \tag{4-16}$$

where v is the ball impact velocity. Assuming no losses, such as air friction, the velocity of a falling object is given by

$$v = (2gh)^{1/2} \quad . \tag{4-17}$$

Letting h be the ball drop height, Eq. (4-17) can then be substituted into Eq. (4-16) to give the maximum theoretical strain produced by the impacting ball as

$$\varepsilon\,|_{max} = (2gh)^{1/2}/c_o \quad . \tag{4-18}$$

For these experiments h = 48 inches and $c_o = 1.85 \times 10^5$ in/sec. Substituting these values and the value for g into Eq. (4-18) gives

$$\varepsilon\,|_{max} = 104\mu\text{in/in} \quad .$$

Due to losses, v will be smaller than given by Eq. (4-17); therefore, it would be expected that the experimental value of $\varepsilon\,|_{max}$ should be smaller than 104μin/in.

Typical records of oscilloscope traces for three test temperatures are shown in Figure 26. The upper trace on each record is the output from the foil strain gage. The lower traces are the outputs from the semi-conductor gage. The time scale reads from left to right. Thus the first upward going portion of the trace is the initial compression pulse

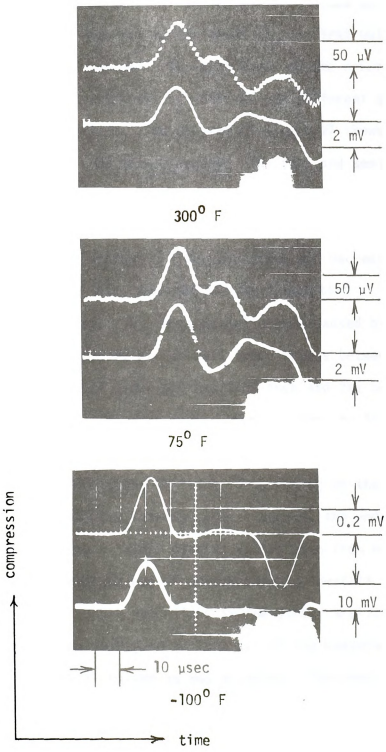

Figure 26. Ball Drop Test-Records

produced by the impacting ball. The downward going portion of the trace is the first reflected pulse. Since the ends of the specimen were free, the first reflected pulse is a tension pulse. It can be seen that no significant change occurred in the shape of the first pulse as the specimen temperature was changed. The amplitudes of the records cannot be compared because of different E_b voltages and different gage sensitivities at each temperature. The diagram of Figure 27 shows how the trace amplitude and rise time were measured. The foil and semi-conductor strain-pulse-amplitudes as a function of temperature are plotted in Figure 28. The curves are plotted separately for clarity. The plotted data points are the average of the increasing and decreasing temperature tests. The vertical bars show the standard deviation of the data at each test temperature. The large deviation was caused by two factors. First, the impact velocity of the ball would change between ball drops. The guide-tube-to-ball clearance was 3/32 inch and the ball was always dropped from a height of four feet. However, the air flow past the ball would cause the ball to intermittently graze the side of the tube. This resulted in an intermittent friction force acting on the ball that would change the ball velocity between tests. Second, the end of the test specimen experienced a slight plastic deformation from each impact. This caused the impacted end of the specimen to deviate from a smooth surface, thereby causing variations in the strain amplitudes.

It can be seen in Figure 28 that all of the measured amplitudes are below the theoretical values as was expected. The average strain amplitude as a function of temperature varied by about 35 per cent for the foil gage and by about 22 per cent for the semi-conductor gage. The maximum standard deviation was about $\pm$ 20 per cent for both types of gages.

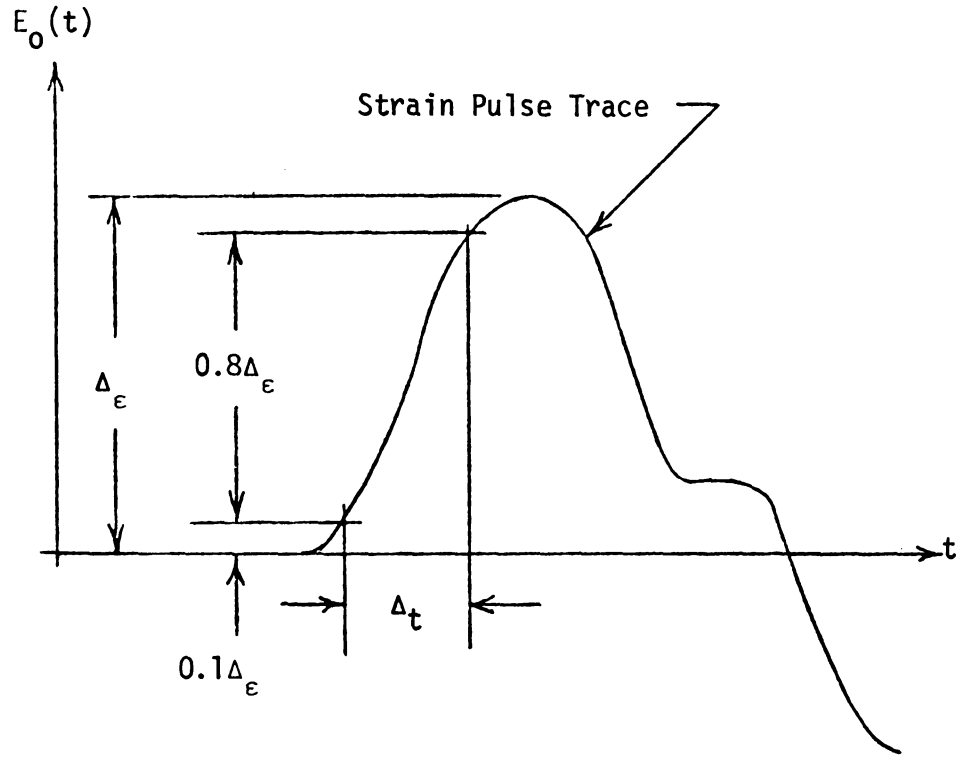

Figure 27. Measurement of Δ_ε and Δ_t for Ball-Drop Tests

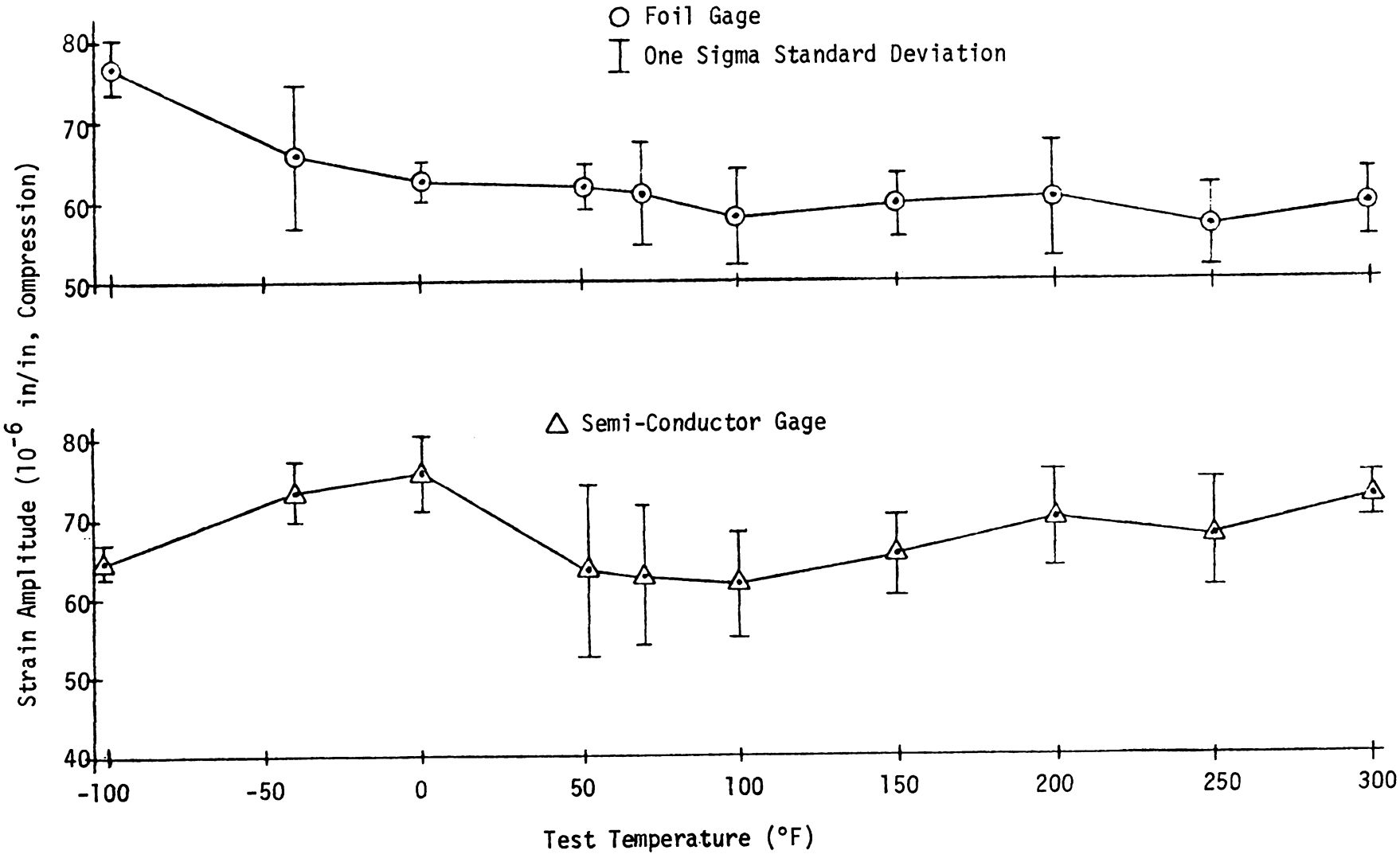

Figure 28. Strain - Temperature Curves, Ball Drop Tests

It appears that when the large deviations are considered, the measured strain-pulse amplitudes remain fairly constant over the temperature range.

The theoretical rise time of a resistance strain gage is given by

$$t_R = c_o/L \quad . \tag{4-19}$$

The length, L, of the foil gage was 0.031 inch and of the semi-conductor gage 0.06 inch. The long wave velocity, c_o, of the test specimen material was 1.85×10^5 inches per second. Thus the theoretical rise times for the foil and semi-conductor gages are

$$t_R \Big|_{foil} = 0.134 \text{ microsecond}$$

and

$$t_R \Big|_{semi\text{-}conductor} = 0.259 \text{ microsecond} \quad .$$

The foil and semi-conductor strain-pulse rise times as a function of temperature are plotted in Figure 29. The two curves are plotted separately for clarity. The plotted data points are the average of the increasing and decreasing temperature tests. The vertical bars indicate the standard deviation of the data at each test temperature. The large deviation was caused by slight plastic deformation of the test specimen from each impact. The average room temperature rise time of about 7 microseconds for both gages was about 35 times greater than the theoretical rise time . Thus there should not be any significant difference in the

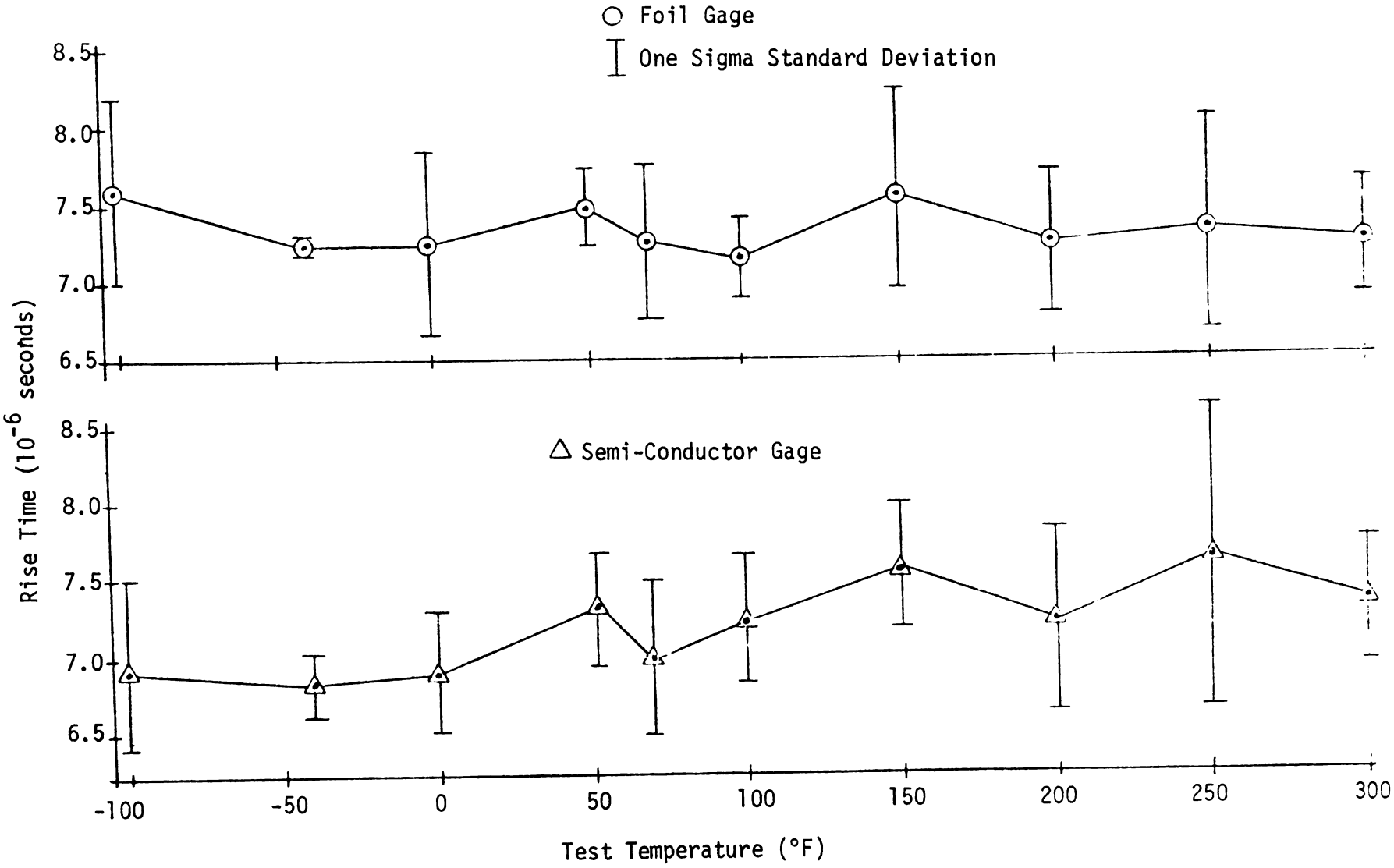

Figure 29. Rise Time - Temperature Curves, Ball-Drop Tests

measured rise times of the strain pulses due to the two different gage lengths. The average rise time as a function of temperature varied by about 10 per cent for the semi-conductor gage and by about 5 per cent for the foil gage. The maximum standard deviation was about $\pm$ 15 per cent for the semi-conductor gage and about $\pm$ 8 per cent for the foil gage. Within the deviation of the data, the measured strain-pulse rise times appear to remain constant over the test temperature range.

4.4 Hammer, Temperature-Test Results

The purpose of these hammer tests was to determine the temperature effects on the strain-gage output when the gages were subjected to "high" amplitude "short" rise time strain pulses. The strain pulses for these tests had amplitudes of approximately 450 microinches per inch and rise times of approximately 2 microseconds.

The amplitude of the strain pulse produced in the test specimen by the hammer impact could not be approximated by the one-dimensional wave propagation theory, due to the shor-pendulum geometry. The impact velocity was neither uniform across nor perpendicular to the specimen impact face, as can be seen by examining the impact velocity vector and the hammer geometry. The tangential velocity vector, $\bar{v}$, of a rotating object is

$$\bar{v} = \bar{\omega} \times \bar{r} \quad ,$$

where $\bar{\omega}$ is the angular velocity vector and $\bar{r}$ is the position vector to $\bar{v}$. If $\bar{\omega}\,|_{max}$, the angular velocity vector at impact, is substituted for $\bar{\omega}$, the $\bar{v}$ becomes the impact velocity vector, $\bar{v}\,|_{impact}$. The hammer geometry is shown in Figure 30. Also shown are the position vectors to the inside and outside of the specimen and their associated tangential velocity vectors $\bar{v}_i$ and $\bar{v}_o$. This figure shows that the position vector

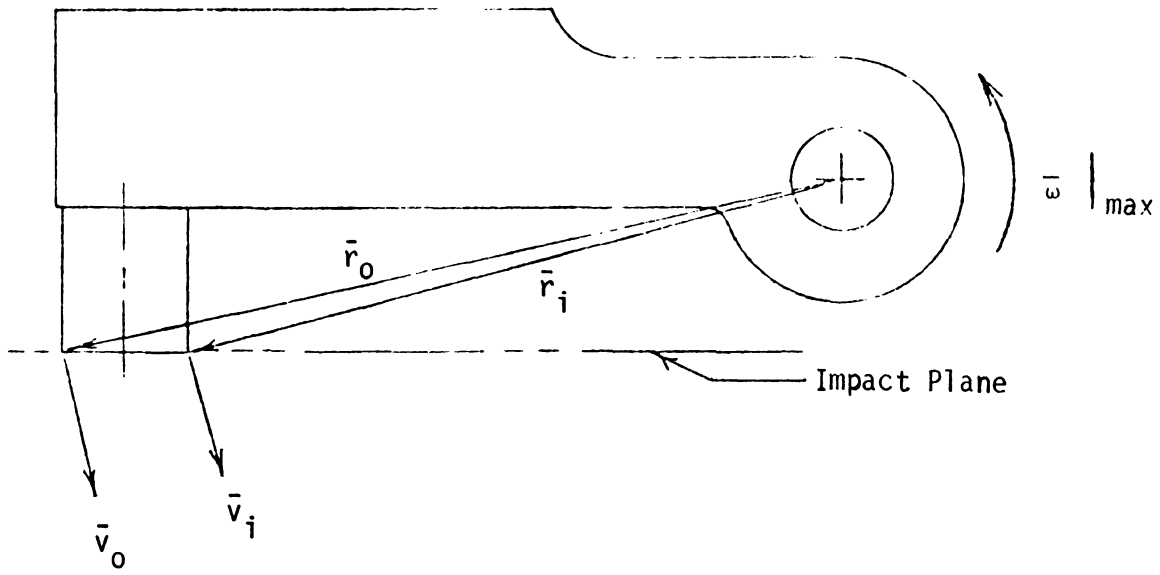

Figure 30. Non-Uniform Impact Velocity

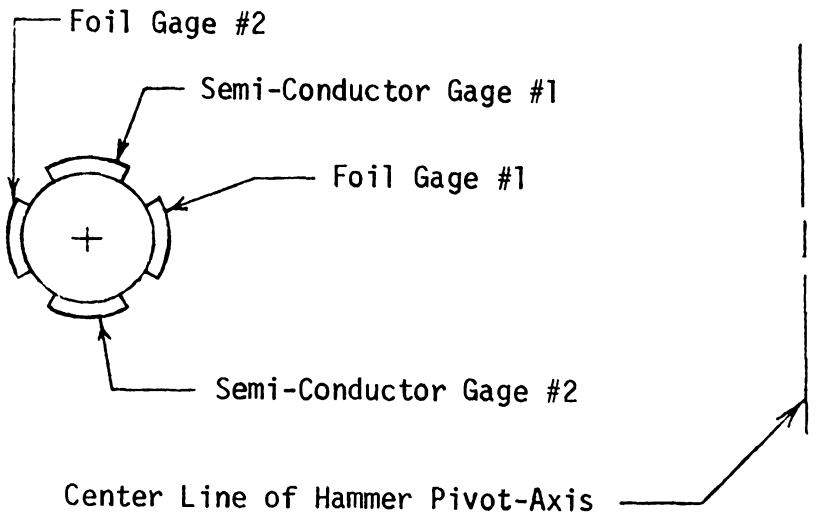

Figure 31. Strain Gage Location

$\bar{r}$ does not lie in the impact plane and does not have a uniform length across the specimen face. Therefore, $\bar{v}\,|_{impact}$ is not uniform across and not perpendicular to the specimen impact face. This results in a two-dimensional velocity initial condition. Thus the one-dimensional wave theory cannot be used to approximate the strain pulse amplitude for these tests.

Figure 31 shows an end view of the test specimen and the gage locations. Since each gage is on a different part of the specimen circumference and the impact velocity varies across the diameter of the specimen, each gage would experience a different strain amplitude and possibly a different wave shape. Another factor that would influence the strain amplitude around the specimen circumference is the mis-alignment between the hammer and specimen impact faces. The impact velocity would be the highest at the time when impact first occurs. The specimen and hammer would make contact at a certain point (due to mis-alignment) the deform until both faces were entirely in contact. As the area of contact increases the hammer velocity would decrease. Thus the impact velocity across the specimen would also vary due to the mis-alignment. This is another reason why the strain amplitude would not be uniform around the specimen circumference. The fact that each gage might not experience the same amplitude and shape strain pulse does not influence these tests. The only requirements imposed on the strain pulse by these tests are short rise times, elastic amplitudes and repeatability over the test temperature range. The repeatability criteria, however, does require that $\omega\,|_{max}$ be the same for all tests.

These tests were conducted using 2 microseconds rather than

sub-microsecond rise times because of an unexpected problem that arose. The test specimen was made from Ni-Span-C and the hammer was made from 7075T6 aluminum. Because of the ingot size and expense of Ni-Span-C, the hammer could not be made from this material. The test specimen was thermally isolated from the rest of the apparatus by the potting compound. This also caused the specimen to be electrically isolated. When the hammer impacted the specimen an electrical transient appeared on the strain signal. The transient was approximately 5 millivolts high and 0.1 microsecond long. It appeared approximately 0.2 microsecond before the strain signal. This would indicate that at the instant of hammer impact a voltage was being induced (possibly due to the dissimilar metals) across the specimen into the strain gage potentiometer circuit. The existence of a voltage potential between the hammer and specimen at impact was also indicated by the appearance of the hammer impact face after about 30 impacts. The face would lose its highly polished reflective surface and would become blackish-gray in color. Measurements taken of the discolored face indicated that the surface finish had deteriorated from 3-5 to 15-20 rms microinches. Thus it appeared that the hammer-impact-face surface finish was being degraded by an electrical arcing phenomenon. The specimen was then electrically grounded to the hammer. The electrical transient was no longer visible on the strain signal. However, the repolished hammer face still deteriorated to about 10-15 rms microinches surface finish. The surface finish would stabilize at this value after about 40 to 50 impacts. During the degradation of the surface finish the strain pulse rise time would increase from a sub-microsecond value to about 2 microseconds. Once the surface finish stabilized, the rise time also stabilized. Since the hammer would experience several hundred

impacts during the temperature tests, these tests were conducted after the rise times had stabilized at about 2 microseconds.

Another type of problem was encountered. When the foil strain gages were subjected to the short rise time strain pulses, the solder, which joined the lead wire to the gage solder tab, would unbond from the tab. In order to alleviate this problem, the minimum amount of solder for a good electrical/mechanical connection was used and the potentiometer circuit voltage, E_b, was reduced. The reduced voltage reduced the gage current, thus reducing the electrical-resistance heating of the gage and solder joint. The values of E_b finally chosen were 2 to 4 volts. At all temperatures, some tests were performed with E_b = 2 volts in order to compare the strain records as the tests were being conducted. The higher voltage was mainly used at the lower temperatures because of the improved heat transfer rate from the gage to the specimen. Even with these precautions the solder joint of foil gage number two (see Figure 31) failed at the 150°F tests. No problems were encountered with foil gage number one and this gage was used for all of the temperature tests. While the reduction in E_b did not influence the performance of the gage, just the solder joint, it did proportionally reduce the output, E_o, from the potentiometer circuit. This is one of the reasons that the amplitudes of the oscilloscope records for the foil gage are small (about two divisions). The other reason that these traces are small was due to the required band width on the oscilloscope vertical amplifier. In order for the amplifier to respond to a one microsecond rise time signal the band width had to be approximately 4 MHz or greater. This large band width reduces the gain available from any type of amplifier and thus the available oscilloscope trace deflection.

Two semi-conductor gages were bonded to the specimen so that there would be a "back-up" gage in the event that one gage failed. However, the semi-conductor gages did not experience any failure since the lead wires were welded to the gage by the manufacturer. All of the temperature tests were conducted using semi-conductor gage number one (see Figure 31). The average hammer angular velocity was 74.6 $\pm$ 3% radians per second for all tests. Thus the average magnitudes of $\bar{v}_o$ and $\bar{v}_i$ were 146.6 $\pm$ 3% and 138.3 $\pm$ 3% inches per second respectively.

Typical records of oscilloscope traces for three test temperatures are shown in Figures 32 and 33. The records in Figure 32 are for the foil gage and those in Figure 33 are for the semi-conductor gage. The time scale reads from left to right and compressive strain is indicated by a positive going trace. It can be seen that the wave shapes are different for each type of gage. This is attributed to the different locations of the gages on the specimen as discussed above. However, for each gage, the wave shape remained essentially the same as the test temperature was changed. The diagram of Figure 34 shows how the trace amplitude and rise time were measured. The foil and semi-conductor strain-pulse-amplitudes as a function of temperature are plotted in Figure 35. The curves are plotted separately and the vertical bars that indicate the standard deviation are omitted for clarity. The average value for the standard deviation at each test point was 16 microinches/inch for the foil gage and 7 microinches/inch for the semi-conductor gage. The arrowheads on the curves indicate the direction of temperature change between tests.

The room temperature amplitude for the foil gage was 520 microinches/inch and 444 microinches/inch for the semi-conductor gage. This

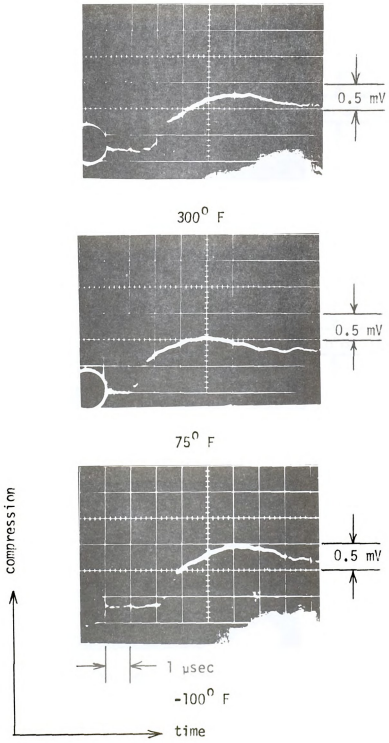

Figure 32. Foil Hammer-Test-Records

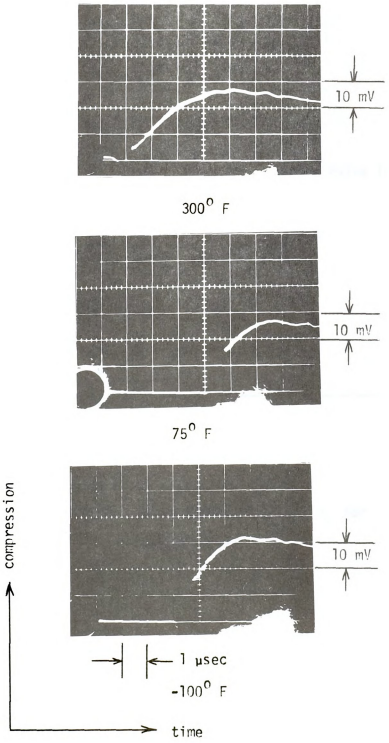

Figure 33. Semi-Conductor Hammer-Test-Records

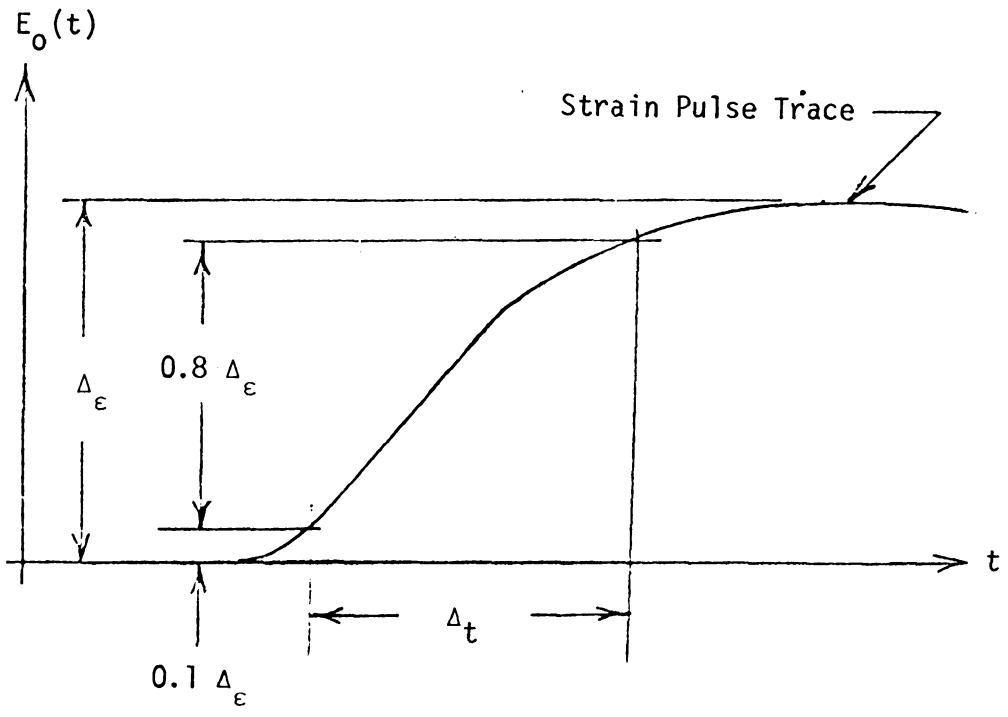

Figure 34. Measurement of Δ_ε and Δ_t for Hammer Tests

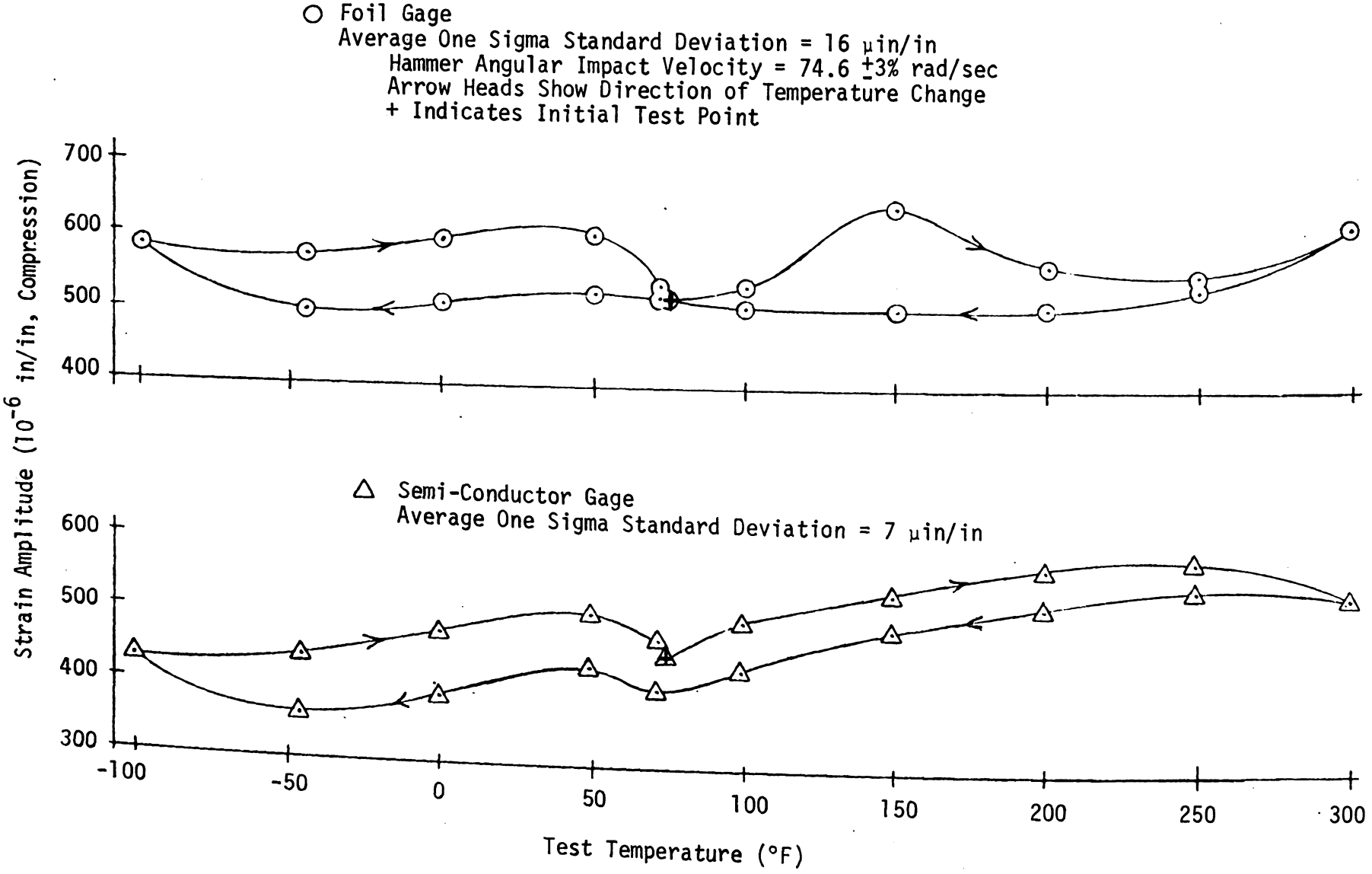

Figure 35. Strain - Temperature Curves, Hammer Tests

difference is attributed to the different locations of the gages on the specimen. Both curves exhibit a loop which is similar to the hysteresis effect seen in many types of instrumentation systems. This hysteresis effect is at times also seen when resistance strain gages are used to measure static strains at various temperatures. In static strain measurement this effect is due to a viscoelastic behavior of the gage backing material and the mounting adhesive. Since for these tests the standard deviation for each gage is not large enough to account for the amplitude differences at each temperature, it seems that the hysteresis effect must be attributed to the backing material and adhesive acting viscoelastically. Other than the hysteretic behavior, the strain amplitudes do not seem to deviate seriously from the room temperature values.

The foil and semi-conductor strain-pulse rise times as a function of temperature are plotted in Figure 36. The average values for the standard deviation at each test point was 0.6 microsecond for the foil gage and 0.1 microsecond for the semi-conductor gage. Since the rise time did not exhibit a hysteresis effect larger than the standard deviation, the plotted data points are the average of the increasing and decreasing temperature tests. The average room temperature rise times of about 2 microseconds is approximately 14 times greater than the theoretical rise time of the foil gage and about 7 times greater than the theoretical rise time of the semi-conductor gage. Thus a difference of about 14 per cent might be expected between the rise times of the foil and semi-conductor gages. However, the standard deviations of the data apparently masks this difference.

It can be seen in Figure 36 that the rise times of both gage outputs

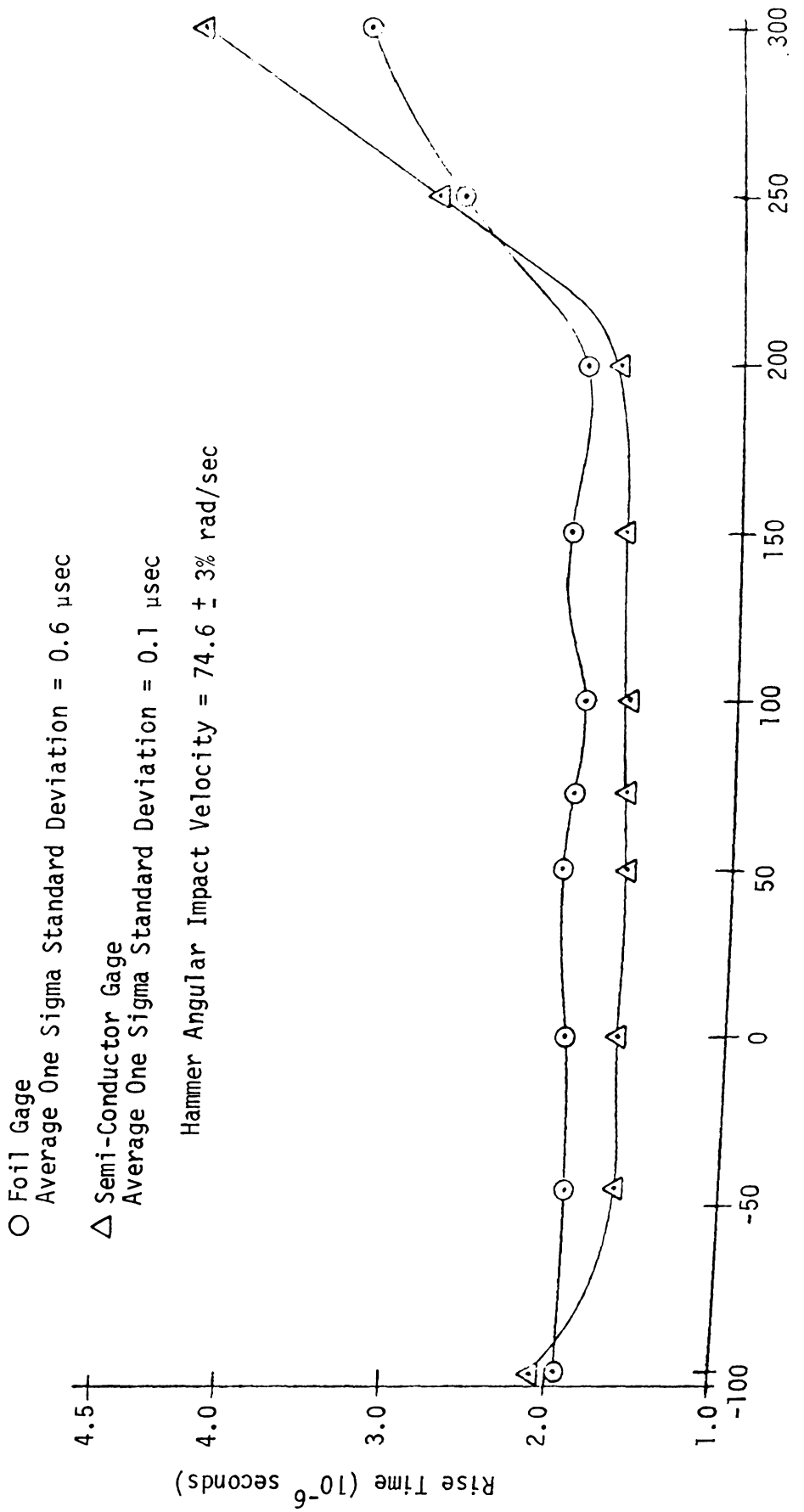

Figure 36. Rise Time - Temperature Curves, Hammer Tests

exhibit a sharp increase above a temperature of 200°F. This characteristic could also be attributed to a viscoelastic behavior of the gage backing and adhesive materials. Since the pulse duration of approximately 20 microseconds was much longer than the pulse rise time, the backing and adhesive materials would have enough time in order to attain and transmit to the gage element the maximum amplitude of the strain pulse. This behavior would have to be taken into account when resistance strain gages are used to measure microsecond rise time strain pulses at specimen temperatures above 200°F.

4.5 Hammer, Sub-Microsecond Rise-Time-Test Results

The ability of the hammer apparatus to produce sub-microsecond rise time strain pulses was used to investigate whether the rise time of a resistance strain gage includes an additive constant.

New gages (two 0.031 inch long foil and one 0.06 inch long semiconductor types) were mounted on a test specimen. This was done because it was felt that the gages used in the temperature tests might have changed their room temperature properties due to being subjected to various temperatures and to large numbers of strain pulses. The hammer and specimen holder surfaces were refinished and the apparatus reassembled. The test specimen was subjected to 26 impacts.

Two of the oscilloscope records are shown in Figure 37. The oscilloscope traces were dim because the trace was swept across the screen at a rate of 0.1 microsecond per division. Therefore, the oscilloscope records had to be rephotographed in order to enhance the traces.

The average measured rise time for the 0.031 inch long foil gages was 0.18 microsecond. This was 0.046 microsecond greater than the 0.134

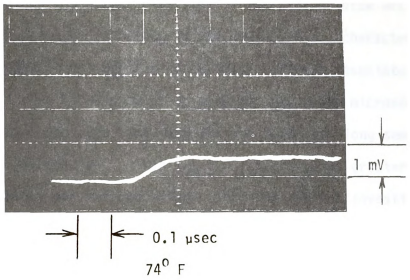

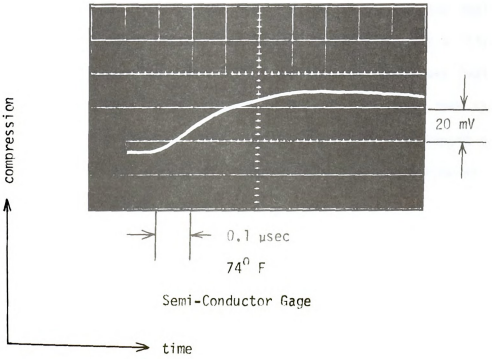

Figure 37. Foil and Semi-Conductor Sub-Microsecond Rise Time Test-Results

microsecond theoretical value. It was 0.054 microsecond less than the 0.1 microsecond additive constant Bickel arrived at by re-evaluating Oi's data. Since the actual rise time of the strain pulse was unknown, the 0.046 microsecond difference is not necessarily a characteristic of the gage. However, if there is an additive constant associated with foil gages, it can be said to be no greater than 0.046 microsecond .

The average measured rise time for the 0.06 inch long semi-conductor gage was 0.31 microsecond. This was 0.051 microsecond greater than the 0.259 microsecond theoretical value. Since Oi did not investigate semi-conductor gages, the 0.051 microsecond difference cannot be compared to the 0.1 microsecond additive constant arrived at by Bickel. As above the 0.051 microsecond difference is not necessarily a characteristic of the gage.

A hypothesis about the rise time additive constant may be formulated by considering the results from the theoretical study by Taylor (1966) and the combined results from the foil and semi-conductor tests. One of the strain pulse shapes that Taylor investigated was a "linear ramp rise" up to a constant level, then the constant level was "maintained indefinitely relative to the time of rise." This wave form is shown in Figure 38. The constant level amplitude is A and the length of the rise portion is b. For a gage of length L the output amplitude of the gage is S where $S = \Delta R_g/R_g$ and is given by Taylor as

$$S = x_t^2 A(GF)/2Lb \quad , 0 \leq x_t \leq L \tag{4-21}$$

and

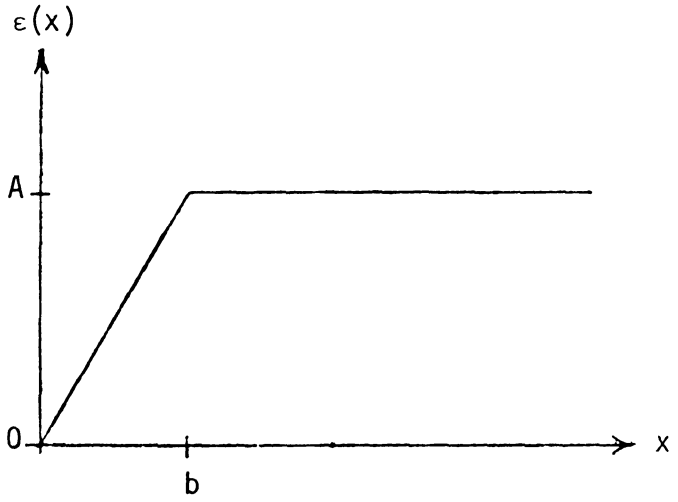

Figure 38. Wave-Form Studied by Taylor

$$S = \frac{A(GF)}{2Lb}\ [2x_t(b + L) - x_t^2 - b^2 - L^2] \quad , b \leq x_t \leq b + L \quad . \qquad (4\text{-}22)$$

In this equation, x_t is the "distance of progression of the impressed strain wave form into the gage length." The 10 per cent amplitude of the gage output is then found by multiplying Eq. (4-21) by 0.1 and the 90 per cent value by multiplying Eq. (4-22) by 0.9. Performing these operations gives

$$x_t \Big|_{10\%} = 0.447\ (bL)^{1/2} \qquad (4\text{-}23)$$

and

$$x_t \Big|_{90\%} = (b + L) - 0.446\ (bL)^{1/2} \quad . \qquad (4\text{-}24)$$

In arriving at Eqs. (4-22) and (4-23) it is noted that

$$S/A(GF) = 1 \quad .$$

The 10 to 90 per cent rise time of the gage output signal is then given by

$$t_R = (x_t \Big|_{90\%} - x_t \Big|_{10\%})/c_o \quad . \qquad (4\text{-}25)$$

Substituting Eqs. (4-23) and (4-24) into Eq. (4-25) gives

$$t_R = [b + L - 0.894\ (bL)^{1/2}]/c_o \quad . \qquad (4\text{-}26)$$

Now if it is assumed that the strain pulse produced by the hammer apparatus has the same shape as the one shown in Figure 38, then Eq. (4-26) can be solved in terms of b by using the foil gage data. This is done by letting

$$t_R = 0.18 \text{ microsecond}$$
$$L = 0.031 \text{ inch}$$
$$\text{and } c_o = 1.85 \times 10^5 \text{ inches/second} \quad .$$

The result is

$$b = 0.292 \text{ inch} \quad .$$

The theoretical rise time of the strain pulse based on the rise time of the foil gage output can then be determined from Figure 9 in Taylor's paper. In order to use this figure the value of $\alpha = b/L$ must be calculated. For the foil gage, L = 0.031 inch; thus

$$\alpha \Big|_{\text{foil}} = 0.934 \quad .$$

Then theoretical rise time of the strain pulse was then determined to be

$$t_i = 0.127 \text{ microsecond} \quad . \qquad (4\text{-}27)$$

The theoretical output of the semi-conductor gage to this strain pulse can now be determined. For the semi-conductor gage we have L = 0.06 inch thus

$$\alpha \Big|_{\text{semi-conductor}} = 0.482 \quad . \tag{4-28}$$

Using Eqs. (4-27) and (4-28) and Taylor's Figure 9, the theoretical rise time of the semi-conductor gage output for the type of strain pulse shown in Figure 38 is found to be

$$t_R = 0.28 \text{ microsecond} \quad . \tag{4-29}$$

The theoretical rise time of the semi-conductor gage as given in Eq. (4-29) compares reasonably well with the measured rise time of 0.31 microsecond. Better agreement might have been achieved if the leading edge of the theoretical strain pulse had less abrupt slope changes as probably occurred in the tests. Also the semi-conductor gage might have been subjected to a slightly different rise time due to its being located at a different position on the specimen than the foil gage.

The above calculations are based on a gage rise time given by

$$t_R = 0.8L/c_o \quad .$$

Since these theoretical calculations did not include an additive constant and they agreed well with the experimental results, it may be hypothesized that there is no additive constant associated with the rise time of resistance strain gages.

CHAPTER 5

CONCLUSIONS

Foil and semi-conductor resistance strain gages were subjected to strain pulses over a temperature range of -100 to +300°F. The foil gages were type ED-DY-031CF-350, manufactured by Micro-Measurements. The semi-conductor gages were type SPB3-06-12, manufactured by BLH Electronics, Inc. The gage elements were made of isoelastic and P-type silicon. Two types of strain pulses were used for these tests. One type of pulse was approximately a half-sine wave with a peak amplitude of 65 microinches/inch and a rise time of 7 microseconds. The second type of pulse was approximately a ramp function. The maximum amplitude of this pulse was 450 microinches/inch with a 2 microseconds rise time.

The rise times and amplitudes of the gage outputs were unaffected by temperature for the tests using the longer type pulse.

When the gages were subjected to the shorter ramp type pulse, the output amplitudes were essentially unaffected by temperature. However, the output amplitudes did exhibit a hysteresis loop. This hysteresis effect is attributed to a viscoelastic behavior of the gage backing and bonding materials. The rise time of the output remained independent of temperature up to a value of 200°F. Above this temperature, the rise time showed a marked increase. The rise time at 300°F was 100 per cent greater than the room temperature value. This increase at the high

temperatures is also attributed to a viscoelastic behavior of the gage backing and bonding materials. This increase in the rise time of the output with increasing temperature would have to be taken into account when using resistance strain gages above 200°F.

It was found that the gage circuit supply voltage had to be reduced when the foil gages were subjected to the 2 microseconds rise time pulse. This was to prevent the solder joints, which attached the lead wires to the gage solder tabs, from unbonding.

The constant added to the rise time of the gage output which was suggested by Oi was re-examined. Since the rise time of the strain pulse was not known, the conclusion reached was that the additive constant is 0.05 microsecond or less. However, using the theoretical work of Taylor it was hypothesized that there is no additive constant associated with the rise time of the output from resistance strain gages.

APPENDICES

APPENDIX A

LIST OF MANUFACTURER'S ADDRESSES

1. Analog Devices, Inc., Cambridge, Massachusetts.
2. Bendix, Industrial Metrology Division, Dayton, Ohio.
3. BLH Electronics, Inc., Subsidiary of Baldwin-Lima-Hamilton Corporation, Waltham, Massachusetts 02154.
4. Crane Packing Company, Lapmaster Division, 6400 Oakton Street, Morton Grove, Illinois.
5. Dexter Corporation, Hysol Division, Orlean, New York & Los Angeles, California.
6. Dow Chemical Company, Midland, Michigan 48640.
7. Hamilton Watch Company, Precision Metals Division, Lancaster, Pennsylvania 17604.
8. International Nickel Company, Huntington Alloy Products Division, Huntington, West Virginia 25720.
9. Krohn-Hite, Cambridge, Massachusetts.
10. Micro-Measurements, a division of Vishay Intertechnology Inc., 38905 Chase Road, Romulus, Michigan 48174.
11. Pfizer and Company, Inc., Minerals, Pigments, and Metals Division, 260 Columbia Street, Adams, Massachusetts 01220.
12. Poly-Paks Inc., South Lynnfield, Massachusetts 01940.
13. Tektronix, Inc., P.O. Box 500, Beaverton, Oregon 97005
14. United Dector Technology, 1732 21st Street, Santa Monica, California 90404.

APPENDIX B

LAPPING, POLISHING AND SURFACE MEASUREMENT TECHNIQUES

The specimen in the specimen holder and the hammer in the hammer holder were lapped with a Lapmaster® 12 lapping machine manufactured by Crane Packing Company. This machine had a 12 inches in diameter cast iron lap. Up to three parts could be lapped simultaneously. The lapping abrasive was Lapmaster #1800. The abrasive consisted of aluminum oxide particles. The average particle size was 18.5 microns. The oil-based abrasive-vehicle was Lapmaster #5-001-0-0009. An oil based vehicle was necessary for two reasons. First, water would rust the lap. Second, aluminum oxide in water will react with aluminum. This would have prevented the achievement of a smooth surface. Weights were placed on the parts during lapping. The weights were sized in order to exert a pressure of approximately 0.35 pound per square inch over the surface being lapped. This resulted in a material removal rate of approximately 24 microinches per minute.

The lapping operation was followed by two hand polishing operations. First, the parts were polished with a one micron particle size aluminum oxide abrasive in the oil based vehicle. A cast iron hand lap plate covered with a polishing cloth made from a denim type material was used for this operation. Second, the parts were polished with a 1/3 micron particle size aluminum oxide abrasive in the oil based vehicle. For this

operation the hand lap plate was covered with a polishing cloth made from a synthetic velvet-type material. After final polishing the parts were cleaned in a ultrasonic cleaner.

The finished surfaces of the parts were checked for flatness by an optical technique. A Lapmaster optical flat was placed on the polished surface. A 6510 Å wave length red light was used to illuminate the polished surface through the optical flat. Interference fringes are thus produced by the polished surface and the optical flat. The curvature of these fringes was used to determine the flatness of the part. For a detailed description of this method see the Crane Packing Company Bulletin No. L-404-6. If the surfaces were not flat within one-half wave length, the lapping, polishing and cleaning operations were repeated.

The surface finish was measured using a profilometer. This is a device which moves a "tracing head" over the surface to be measured and automatically gives a readout in rms microinches. The profilometer, type QB Model 18, and tracing head, type MA, were manufactured by Bendix, Industrial Metrology Division.

APPENDIX C

COMPUTER PROGRAMS

This appendix contains the print-outs of the four principal computer programs used for reduction of the test data. The programing language was Time Sharing Fortran IV. The programs were run on an IBM 360 computer. The use of individual programs is shown by the comment statement on line 2 of each program. The line numbers are indicated by a L followed by a number on the left hand side of the print-out.

```
L.ØØØ1   /JOB GO
L.ØØØ2   C       SEMI-COND BALL DROP DATA REDUCTION
L.ØØØ3          DIMENSION DST(5Ø),GST(5Ø),EBG(5Ø),DPT(5Ø),GT(5Ø)
L.ØØØ4         1,E(5Ø),RT(5Ø)
L.ØØØ5          WRITE(6,6ØØ)
L.ØØØ6     6ØØ FORMAT('TEST TEMPERATURE (DEG F)')
L.ØØØ7          WRITE(6,61Ø)
L.ØØØ8     61Ø FORMAT(1X,'AVG  STRAIN',4X,'ONE SIGMA  AVG',
L.ØØØ9         11X,'RISE TIME  ONE  SIGMA')
L.ØØ1Ø          WRITE(6,62Ø)
L.ØØ11     62Ø FORMAT(3X,'(IN/IN)',8X,'STRAIN',6X,'(SEC)',
L.ØØ12         17X,'RISE TIME'//)
L.ØØ13      1Ø READ(5) N,TEMP,GF,C2,RO,TO,RG
L.ØØ14          IF(N)999,999,2Ø
L.ØØ15      2Ø DO 3Ø I=1,N
L.ØØ16          READ(5) DST(I),GST(I),EBG(I),DPT(I),GT(I)
L.ØØ17      3Ø CONTINUE
L.ØØ18          EN=N
L.ØØ19          SUME=Ø.Ø
L.ØØ2Ø          SUMRT=Ø.Ø
L.ØØ21          SSDE=Ø.Ø
L.ØØ22          SSDRT=Ø.Ø
L.ØØ23          X=1.Ø-Ø.ØØØØØ28*TO+Ø.ØØØØØ23*TO**2
L.ØØ24          ROO=RO/X
L.ØØ25          ROTT=ROO*(1.Ø-Ø.ØØØØØ28*TEMP+Ø.ØØØØØ23*TEMP**2)
L.ØØ26          TOR=TO+459.65
L.ØØ27          TTR=TEMP+459.65
L.ØØ28          AS=ROTT*C2*(TOR/TTR)**2
L.ØØ29          BS=ROTT*GF*(TOR/TTR)
L.ØØ3Ø          CS=ROTT-RG
L.ØØ31          RADS=SQRT(BS**2-4.Ø*AS*CS)
L.ØØ32          ES=(-BS+RADS)/(2.Ø*AS)
L.ØØ33          A=ROTT*C2*(TOR/TTR)**2
L.ØØ34          B=ROTT*GF*(TOR/TTR)
L.ØØ35          DO 5ØØ I=1,N
L.ØØ36          DEG=-DST(I)*GST(I)
L.ØØ37          AR=(EBG(I)*12Ø.Ø)/((12Ø.Ø+RG)**3)
L.ØØ38          BR=-(EBG(I)*12Ø.Ø)/((12Ø.Ø+RG)**2)
L.ØØ39          CR=DEG
L.ØØ4Ø          RADR=SQRT(BR**2-4.Ø*AR*CR)
L.ØØ41          DR=(-BR-RADR)/(2.Ø*AR)
L.ØØ42          C=ROTT-(DR+RG)
L.ØØ43          RAD=SQRT(B**2-4.Ø*A*C)
L.ØØ44          ET=(-B+RAD)/(2.Ø*A)
L.ØØ45          E(I)=ET-ES
L.ØØ46          SUME=SUME+E(I)
L.ØØ47          AVGE=SUME/EN
```

```
L.ØØ48          RT(I)=DPT(I)**GT(I)
L.ØØ49          SUMRT=SUMRT+RT(I)
L.ØØ5Ø          AVGRT=SUMPT/EN
L.ØØ51      5ØØ CONTINUE
L.ØØ52          DO 55Ø I=1,N
L.ØØ53          DEE=(E(I)-AVGE)**2
L.ØØ54          SSDE=SSDE+DEE
L.ØØ55          SDE=SQRT(SSDE/EN)
L.ØØ56          DERT=(RT(I)-AVGRT)**2
L.ØØ57          SSDRT=SSDRT+DERT
L.ØØ58          SDRT=SQRT(SSDRT/EN)
L.ØØ59      55Ø CONTINUE
L.ØØ6Ø          WRITE(6,63Ø) TEMP
L.ØØ61      63Ø FORMAT(1X,E13.5)
L.ØØ62          WRITE(6,64Ø) AVGE,SDE,AVGRT,SDRT
L.ØØ63      64Ø FORMAT(1X,4E13.5/)
L.ØØ64          GO TO 1Ø
L.ØØ65      999 STOP
L.ØØ66          END
L.ØØ67    /DATA
L.ØØ68    /END
```

```
L.ØØØ1   /JOB GO
L.ØØØ2   C      SEMI-COND HAMMER-DATA REDUCTION
L.ØØØ3          DIMENSION DST(5Ø),GST(5Ø),EBG(5Ø),DRT(5Ø)
L.ØØØ4         1,GT(5Ø),DW(5Ø),GST(5Ø),EBG(5Ø),DRT(5Ø)
L.ØØØ5         2,W(5Ø),V(5Ø)
L.ØØØ6          WRITE(6,6ØØ)
L.ØØØ7     6ØØ FORMAT('TEST TEMPERATURE (DEG F)')
L.ØØØ8          WRITE(6,61Ø)
L.ØØØ9     61Ø FORMAT(1X,'AVG  STRAIN    ONE SIGMA  AVG RISE'
L.ØØ1Ø        1,1X,'TIME  ONE SIGMA   AVG IMP VEL   ONE',1X,
L.ØØ11        2'SIGMA   MEAN IMP VEL')
L.ØØ12          WRITE(6,62Ø)
L.ØØ13     62Ø FORMAT(3X,'(IN/IN)',8X,'STRAIN',6X,'(SEC)',7X,
L.ØØ14        1'RISE TIME    (RAD/SEC)      IMP VEL',5X,
L.ØØ15        2'(IN/SEC)'//)
L.ØØ16      1Ø READ(5) N,TEMP,GF,C2,RO,TO,RG
L.ØØ17          IF(N)999,999,2Ø
L.ØØ18      2Ø DO 3Ø I=1,N
L.ØØ19          READ(5) DST(I),GST(I),EBG(I),DRT(I)
L.ØØ2Ø          READ(5) GT(I),DW(I),GW(I)
L.ØØ21      3Ø CONTINUE
L.ØØ22          EN=N
L.ØØ23          SUME=Ø.Ø
L.ØØ24          SUMRT=Ø.Ø
L.ØØ25          SUMW=Ø.Ø
L.ØØ26          SSDE=Ø.Ø
L.ØØ27          SSDRT=Ø.Ø
L.ØØ28          SSDV=Ø.Ø
L.ØØ29          X=1.Ø-Ø.ØØØØØ28*TO+Ø.ØØØØØ23*TO**2
L.ØØ3Ø          ROO=RO/X
L.ØØ31          ROTT=ROO*(1.Ø-Ø.ØØØØØ28*TEMP+Ø.ØØØØØ23*TEMP**2)
L.ØØ32          TOR=TO+459.65
L.ØØ33          TTR=TEMP+459.65
L.ØØ34          AS=ROTT*C2*(TOR/TTR)**2
L.ØØ35          BS=ROTT*GF*(TOR/TTR)
L.ØØ36          CS=ROTT-RG
L.ØØ37          RADS=SQRT(BS**2-4.Ø*AS*CS)
L.ØØ38          ES=(-BS+RADS)/(2.Ø*AS)
L.ØØ39          A=ROTT*C2*(TOR/TTR)**2
L.ØØ4Ø          B=ROTT*GF*(TOR/TTR)
L.ØØ41          DO 5ØØ I=1,N
L.ØØ42          DEG=-DST(I)*GST(I)
L.ØØ43          AR=(EBG(I)*12Ø.Ø)/((12Ø.Ø+RG)**3)
L.ØØ44          BR=-(EBG(I)*12Ø.Ø)/((12Ø.Ø+RG)**2)
L.ØØ45          CR=DEG
L.ØØ46          RADR=SQRT(BR**2-4.Ø*AR*CR)
L.ØØ47          DR=(-BR-RADR)/(2.Ø*AR)
L.ØØ48          C=ROTT-(DR+RG)
```

```
L.ØØ49          RAD=SQRT(B**2-4.Ø*A*C)
L.ØØ5Ø          ET=(-B+RAD)/(2.Ø*A)
L.ØØ51          E(I)=ET-ES
L.ØØ52          SUME=SUME+E(I)
L.ØØ53          AVGE=SUME/EN
L.ØØ54          RT(I)=DRT(I)*GT(I)
L.ØØ55          SUMRT=SUMRT+RT(I)
L.ØØ56          AVGRT=SUMRT/EN
L.ØØ57          EK=(Ø.78539816)
L.ØØ58          EW(I)=DW(I)*GW(I)
L.ØØ59          W(I)=EK*EW(I)/Ø.1
L.ØØ6Ø          SUMW=SUMW+W(I)
L.ØØ61          AVGW=SUMW/EN
L.ØØ62          AVGV=AVGW*1.813
L.ØØ63          V(I)=W(I)*1.813
L.ØØ64      5ØØ CONTINUE
L.ØØ65          DO 55Ø I=1,N
L.ØØ66          DEE=(E(I)-AVGE)**2
L.ØØ67          SSDE=SSDE+DEE
L.ØØ68          SDE=SQRT(SSDE/EN)
L.ØØ69          DERT=(RT(I)-AVGRT)**2
L.ØØ7Ø          SSDRT=SSDRT+DERT
L.ØØ71          SDRT=SQRT(SSDRT/EN)
L.ØØ72          DEV=(V(I)-AVGV)**2
L.ØØ73          SSDV=SSDV+DEV
L.ØØ74          SDV=SQRT(SSDV/EN)
L.ØØ75          SDW=SDV/1.814
L.ØØ76      55Ø CONTINUE
L.ØØ77          WRITE(6,63Ø) TEMP
L.ØØ78      63Ø FORMAT(1X,E13.5)
L.ØØ79          WRITE(6,64Ø) AVGE,SDE,AVGRT,SDRT,AVGW,SDW,AVGV
L.ØØ8Ø      64Ø FORMAT(1X,7E13.5/)
L.ØØ81          GO TO 1Ø
L.ØØ82      999 STOP
L.ØØ83          END
L.ØØ84    /DATA
L.ØØ85      /END
```

```
L.ØØØ1   /JOB GO
L.ØØØ2   C      FOIL BALL-DROP DATA REDUCTION
L.Ø ØØ3          DIMENSION DST(5Ø),GST(5Ø),EBG(5Ø),DPT(5Ø)
L.ØØØ4          1,GT(5Ø),ST(5Ø),RT(5Ø),EW(5Ø),DEG(5Ø)
L.ØØØ5           WRITE(6,6ØØ)
L.ØØØ6     6ØØ FORMAT('TEST TEMPERATURE (DEG F)')
L.ØØØ7           WRITE(6,61Ø)
L.ØØØ8     61Ø FORMAT(1X,'AVG  STRAIN',4X,'ONE SIGMA  AVG',
L.ØØØ9          11X,'RISE TIME  ONE SIGMA')
L.ØØ1Ø           WRITE(6,62Ø)
L.ØØ11     62Ø FORMAT(3X,'(IN/IN)',8X,'STRAIN',6X,'(SEC)',
L.ØØ12          17X,'RISE TIME'//)
L.ØØ13      1Ø READ(5) N,TEMP,GF
L.ØØ14           IF(N)999,999,2Ø
L.ØØ15      2Ø DO 3Ø I=1,N
L.ØØ16           READ(5) DST(I),GST(I),EBG(I),DPT(I),GT(I)
L.ØØ17      3Ø CONTINUE
L.ØØ18           EN=N
L.ØØ19           SUMST=Ø.Ø
L.ØØ2Ø           SUMRT=Ø.Ø
L.ØØ21           SUMW=Ø.Ø
L.ØØ22           SSDS=Ø.Ø
L.ØØ23           SSDRT=Ø.Ø
L.ØØ24           SSDV=Ø.Ø
L.ØØ25            GFT=GF*(-Ø.ØØ54466+Ø.ØØØ11496*TEMP
L.ØØ26           1-Ø.ØØØØØØ44623*TEMP**2)
L.ØØ27            GGFT=GFT+GF
L.ØØ28            DO 5ØØ I=1,N
L.ØØ29           DEG(I)=-DST(I)*GST(I)
L.ØØ3Ø            ST(I)=(4.Ø*DEG(I))/(EBG(I)*GGFT)
L.ØØ31           SUMST=SUMST+ST(I)
L.ØØ32           AVGST=SUMST/EN
L.ØØ33           RT(I)=DRT(I)*GT(I)
L.ØØ34           SUMRT=SUMRT+RT(I)
L.ØØ35           AVGRT=SUMRT/EN
L.ØØ36     5ØØ CONTINUE
L.ØØ37           DO 55Ø I=1,N
L.ØØ38           DES=(ST(I)-AVGST)**2
L.ØØ39           SSDS=SSDS+DES
L.ØØ4Ø           SDST=SQRT(SSDS/EN)
L.ØØ41           DERT=(RT(I)-AVGRT)**2
L.ØØ42           SSDRT=SSDRT+DERT
L.ØØ43           SDRT=SQRT(SSDRT/EN)
L.ØØ44     55Ø CONTINUE
L.ØØ45           WRITE(6,63Ø) TEMP
L.ØØ46     63Ø FORMAT(1X,E13.5)
L.ØØ47           WRITE(6,64Ø) AVGST,SDST,AVGRT,SDRT
L.ØØ48     64Ø FORMAT(1X,4E13.5/)
L.ØØ49            GO TO 1Ø
L.ØØ5Ø     999 STOP
L.ØØ51           END
L.ØØ52   /DATA
L.ØØ53   /END
```

```
L.ØØØ1   /JOB GO
L.ØØØ2   C      FOIL HAMMER-DATA REDUCTION
L.ØØØ3          DIMENSION DST(5Ø),GST(5Ø),EBG(5Ø),DRT(5Ø)
L.ØØØ4         1,GT(5Ø),DW(5Ø),GW(5Ø),DEG(5Ø),ST(5Ø),PT(5Ø)
L.ØØØ5         2,EW(5Ø),W(5Ø),V(5Ø)
L.ØØØ6          WRITE(6,6ØØ)
L.ØØØ7     6ØØ FORMAT('TEST TEMPERATURE (DEG F)')
L.ØØØ8          WRITE(6,61Ø)
L.ØØØ9     61Ø FORMAT(1X,'AVG  STRAIN    ONE SIGMA  AVG RISE'
L.ØØ1Ø        1,1X,'TIME  ONE SIGMA   AVG IMP VEL   ONE',1X,
L.ØØ11        2'SIGMA   MEAN IMP VEL')
L.ØØ12          WRITE(6,62Ø)
L.ØØ13     62Ø FORMAT(3X,'(IN/IN)',8X,'STRAIN',6X,'(SEC)',7X,
L.ØØ14        1'RISE TIME    (RAD/SEC)      IMP VEL',5X,
L.ØØ15        2'(IN/SEC)'//)
L.ØØ16      1Ø READ(5) N,TEMP,GF
L.ØØ17         IF(N)999,999,2Ø
L.ØØ18      2Ø DO 3Ø I=1,N
L.ØØ19         READ(5) DST(I),GST(I),EBG(I),DRT(I),GT(I)
L.ØØ2Ø         READ(5) EBT(I),DW(I),GW(I)
L.ØØ21      3Ø CONTINUE
L.ØØ22         EN=N
L.ØØ23         SUMST=Ø.Ø
L.ØØ24         SUMRT=Ø.Ø
L.ØØ25         SUMW=Ø.Ø
L.ØØ26         SSDS=Ø.Ø
L.ØØ27         SSDRT=Ø.Ø
L.ØØ28         SSDV=Ø.Ø
L.ØØ29          GFT=GF*(-Ø.ØØ54466+Ø.ØØØ11496*TEMP
L.ØØ3Ø        1-Ø.ØØØØØ44623*TEMP**2)
L.ØØ31          GGFT=GFT+GF
L.ØØ32          DO 5ØØ I=1,N
L.ØØ33         DEG(I)=-DST(I)*GST(I)
L.ØØ34          ST(I)=(4.Ø*DEG(I))/(EBG(I)*GGFT)
L.ØØ35         SUMST=SUMST+ST(I)
L.ØØ36         AVGST=SUMST/EN
L.ØØ37         RT(I)=DRT(I)*GT(I)
L.ØØ38         SUMRT=SUMRT+RT(I)
L.ØØ39         AVGRT=SUMRT/EN
L.ØØ4Ø         EK=(Ø.78539816)
L.ØØ41         EW(I)=DW(I)*GW(I)
L.ØØ42         W(I)=EK*EW(I)/Ø.1
L.ØØ43         SUMW=SUMW+W(I)
L.ØØ44         AVGW=SUMW/EN
L.ØØ45         V(I)=W(I)*1.813
L.ØØ46         AVGV=AVGW*1.813
L.ØØ47      5ØØ CONTINUE
L.ØØ48         DO 55Ø I=1,N
L.ØØ49         DES=(ST(I)-AVGST)**2
```

```
L.ØØ5Ø          SSDS=SSDS+DES
L.ØØ51          SDST=SQRT(SSDS/EN)
L.ØØ52          DERT=(RT(I)-AVGRT)**2
L.ØØ53          SSDRT=SSDRT+DERT
L.ØØ54          SDRT=SQRT(SSDRT/EN)
L.ØØ55          DEV=(V(I)-AVGV)**2
L.ØØ56          SSDV=SSDV+DEV
L.ØØ57          SDV=SQRT(SSDV/EN)
L.ØØ58          SDW=SDV/1.813
L.ØØ59     55Ø  CONTINUE
L.ØØ6Ø          WRITE(6,63Ø) TEMP
L.ØØ61     63Ø  FORMAT(1X,E13.5)
L.ØØ62          WRITE(6,64Ø) AVGST,SDST,AVGRT,SDRT
L.ØØ63         1,AVGW,SDW,AVGV
L.ØØ64     64Ø  FORMAT(1X,7E13.5/)
L.ØØ65           GO TO 1Ø
L.ØØ66     999  STOP
L.ØØ67          END
L.ØØ68   /DATA
L.ØØ69   /END
```

BIBLIOGRAPHY

BIBLIOGRAPHY

1. Becker, E. C. H. and Conway, H. H., "Generation and Use of Mechanical Step Transients in Dynamic Measurements," Brit. J. of Appl. Phys., vol. 15, 1964, pp. 1225-1231.

2. Bickle, L. W., "The Response of Strain Gages to Longitudinally Sweeping Strain Pulses," Exp. Mech., vol. 10, no. 8, August, 1970 pp. 333-337.

3. BLH Electronics, Inc., "SR-4 Semi-Conductor Strain Gages," Bulletin 102-2, A Subsidiary of Baldwin-Lima-Hamilton Corporation, Waltham, Mass., May, 1970.

4. Chiddister, J. L., "An Experimental Study of Aluminum at High Strain Rates and Elevated Temperatures," Thesis, Department of Applied Mechanics, Mich. State Univ., 1961, pp. 28.

5. Commerford, G. L. and Whittier, J. S., "Uniaxial-Strain Wave-Propagation Experiments Using Shock-Tube Leading," Exp. Mech., vol. 10 no. 3, March, 1970, pp. 120-126.

6. Crane Packing Company, "Measuring Flatness With Lapmaster," Bulletin No. L-404-6, Lapmaster Division, Morton Grove, Illinois.

7. Cunningham, D. M. and Goldsmith, W., "Short-Time Impulses Produced by Longitudinal Impact," Proc. Soc. Exp. Str. Anal., vol. 16, no. 2, 1959, pp. 153-165.

8. Daniel, I. M. and Marino, R. L., "Wave Propagation in Layered Model Due to Point-Source Loading in Low-Impedance Medium," Exp. Mech., vol. 11, no. 4, May, 1971, pp. 210-216.

9. Davies, R. M., "A Critical Study of the Hopkinson Pressure Bar," Phil. Trans. Roy. Soc. Lond., Ser. A, vol. 240, 1948, pp. 414.

10. DeForest, A. V., "The Measurement of Impact Strains," Proc. Fifth Inter. Cong. Appl. Mech., John Wiley and Sons, Inc., New York, 1939, pp. 673-676.

11. Halpin, W. J. et al., Symposium on "Dynamic Behavior of Materials," ASTM Special Technical Publication, no. 336, Amer. Soc. Test. Mat., Phil., Pa., 1963, pp. 208-218.

12. Hamilton Watch Company, "MET-Data," Sheet #4, Precision Metals Division, Lancaster, Pa., June 1, 1971.

13. Hartman, W. F. et al, "An Experiment on Laser-Generated Stress Waves in a Circular Elastic Ring," J. Appl. Mech., Paper No. 71-APMW-2, August, 1970.

14. International Nickel Company, Inc., "Engineering Properties of Ni-Span-C Alloy 902," Tech. Bull. T-31, Huntington Alloy Products Division, Huntington, W. Va., 1963.

15. Kolsky, H., Stress Waves in Solids, Dover Pub., New York, 1963, pp. 54-57.

16. Love, A. E. H., A Treatise on the Mathematical Theory of Elasticity, Dover Pub., New York, 1934, pp. 201-289.

17. Micro-Measurements, "Gage Listings Section," Cat. 200, A Div. of Vishay Intertechnology, Inc., Romulus, Mich. 1970.

18. Micro-Measurements, "Strain Gage Applications with M-Bond and 610 Adhesives," Instr. Bull. B-130, A Div. of Vishay Intertechnology, Inc., Romulus, Mich., Dec., 1968.

19. Oi, K., "Transient Response of Bonded Strain Gages," Exp. Mech., vol. 6, no. 2, Feb., 1966, pp. 463-469.

20. Peffley, W. M., "A Study of Stress Waved Production by Pulsed High-Energy Radiation," Appl. Phys. Let., Amer. Inst. Phys., vol. 10, no. 6, March 15, 1967, pp. 171-173.

21. Percival, C. M., "Thermally Generated Stress Waves in a Dispersive Elastic Rod," Thesis, Univ. of Calif., Livermore, UCRL - 50252., April, 1967.

22. Percival, C. M. and Cheney, J. A., "Thermally Generated Stress Waves in a Dispersive Elastic Rod," Exp. Mech., vol. 9, no. 2, Feb., 1969, pp. 49-57.

23. Rader, D. and Mao, M., "Amplification of Longitudinal Stress Pulses in Elastic Bars with an Intermediate Tapered Region," Exp. Mech., Feb., 1972, vol. 12, no. 2, pp. 90-94.

24. Sears, J. E., "On the Longitudinal Impact of Metal Rods with Rounded Ends," Proc. Cam. Phil. Soc., vol. 14, 1908, pp. 257-258.

25. Stuetzer, O. M., "Laplace Transform Analysis of Thin Piezoelectric Plate Configurations," Sandia Corp., Albuquerque, N. Mex., SC-RR-67-66, Feb., 1967.

26. Taylor, D. A. W., "Time and Amplitude Errors in the Measurement of Dynamic Strain Pulses by Resistance Strain Gages," Inter. J. Mech. Sci., Pergamon Press, New York, 1966, pp. 193-212.

27. United Detector Technology, Silicon Photodetector Design Manual, Santa Monica, Calif., 1970, pp. 10.

28. Vigness, I., "Magnetostrictive Effects in Wire Strain Gages," Proc. Soc. Exp. Str. Anal., vol. 14, no. 2, Nov. 1956, pp. 139-148.